



University Potsdam
Faculty of Mathematics and Natural Sciences
Institute of Biochemistry and Biology

The influence of environmental parameters
on the distribution of Dolly Varden in the Beaufort Sea
A remote sensing approach, using Landsat 8 and Sentinel 2 data
from 2013 to 2019

Master thesis

To attain the academic degree of
Master Ecology Evolution and Conservation (M. sc.)

First tutor:

Herr Prof. Dr. Hugues Lantuit

Second tutor:

Herr Prof. Dr. Hans-Peter Grossart

Date of Submission: 01.11.2021

Winter term 2021/ 22

Author:

Name: Niklaas Schmidt

Matriculation number: 798969

Study program: Ecology, Evolution and Conservation

Acknowledgements

First, I would like to thank Prof. Dr. Hugues Lantuit and Colin P. Gallagher. Both accompanied me extensively during the whole period of my master thesis and provided me with all supporting measures within the possibilities of the AWI as well as the DFO to achieve meaningful results.

Furthermore, I would like to express my sincere and heartfelt gratitude to the involved indigenous communities on site Herschel Island and Shingle Point. Without the cooperation and in situ data collection, this study would not have been possible.

In addition, I would like to thank the Alfred Wegener Institute for Marine and Polar Research in Potsdam, which gave me the opportunity to conduct this study. In particular, I would like to thank the COPER working group members who worked with me during this time.

Finally, I would like to thank Prof. Dr. Hans-Peter Grossart and all those who, with the help of their collective guidance and support, in the form of advice and feedback, have contributed to making this master's thesis "The influence of environmental parameters on the distribution of Dolly Varden in the Beaufort Sea", comprehensively possible through their individual and professional skills.

Abstract

The spatial and temporal heterogeneity of ecosystems plays an important role in species distribution and ecosystem dynamics (Kovalenko et al., 2012). The physical and biochemical properties of the waters of the Mackenzie Shelf in the Beaufort Sea are strongly influenced by the eponymous river and its discharge plume, occasionally causing strong salinity, temperature, and turbidity gradients (Brenkman et al., 2007; Swanson & Kidd, 2009; Jensen et al., 2014), thus affecting the distribution of economically and culturally important organisms, among others. Clarifying how the physical characteristics of marine habitats influence the relative abundance and demographic characteristics of anadromous fishes has an important bearing on management and conservation objectives. The objective of this study was to examine how the timing and catch of Dolly Varden in the nearshore summer subsistence fishery are affected by environmental conditions in the Beaufort Sea. In addition, we examined whether there is a relationship between environmental parameters and the demographic and somatic characteristics of the Dolly Varden caught.

The study analysed fisheries-dependent data from two different study sites (Herschel Island and Shingle Point, Yukon Territory, Canada) from 2013 to 2019. Remotely sensed environmental parameters of *temperature*, *chlorophyll-a*, *turbidity*, and *sea ice* were derived from Landsat-8 and Sentinel-2 imagery and examined along with wind vectors. To provide information on how Dolly Varden abundances respond to stochastic environmental events in marine waters.

Measured environmental parameters show that aggregation of Dolly Varden on Herschel Island is spatially correlated with increased chlorophyll-a as well as SST. Stochastic turbidity events showed a negative influence, causing specimens to seek spatial refuge in better water conditions. Results showed similar correlations for SPT, although the parameters here are much more difficult to differentiate due to the high suspended sediment concentration (CDOM).

Data obtained from this study indicate that the geographic distribution of Dolly Varden in the Beaufort Sea is dependent on condition and osmoregulation (age/length). In marine waters, adult individuals are clearly influenced by stochastic environmental events (temperature and turbidity), opportunistically seeking out production hotspots for feeding (sea ice and chlorophyll-a).

Zusammenfassung

Die räumliche und zeitliche Heterogenität von Ökosystemen spielt eine wichtige Rolle für die Verbreitung von Arten und die Dynamik von Ökosystemen (Kovalenko et al., 2012). Die physikalischen und biochemischen Eigenschaften des Wassers des Mackenzie-Schelfs in der Beaufortsee werden durch den gleichnamigen Fluss und dessen Abflussfahne stark beeinflusst, wodurch gelegentlich starke Salz-, Temperatur- und Trübungsgradienten auftreten (Brenkman et al., 2007; Swanson & Kidd, 2009; Jensen et al., 2014), und somit die Verbreitung von u. a. wirtschaftlich und kulturell wichtigen Organismen beeinflussen. Die Klärung der Frage, wie die physikalischen Eigenschaften mariner Lebensräume die relative Abundanz und die demografischen Eigenschaften anadromer Fische beeinflussen, hat einen wichtigen Einfluss auf die Bewirtschaftungs- und Erhaltungsziele. Ziel dieser Studie war es, zu untersuchen, wie der Zeitpunkt und die Fänge von Dolly Varden in der küstennahen Sommer-Subsistenzfischerei von den Umweltbedingungen in der Beaufortsee beeinflusst werden. Außerdem wurde untersucht, ob es einen Zusammenhang zwischen Umweltparametern und den demografischen und somatischen Eigenschaften der gefangenen Dolly Varden gibt.

Im Rahmen der Studie wurden fischereiabhängige Daten von zwei verschiedenen Untersuchungsstandorten (Herschel Island und Shingle Point, Yukon Territory, Kanada) von 2013 bis 2019 analysiert. Die fernerkundeten Umweltparameter *Temperatur*, *Chlorophyll-a*, *Trübung* und *Meereis* wurden aus Landsat-8- und Sentinel-2-Bildern abgeleitet und zusammen mit Windvektoren untersucht, um Informationen darüber zu erhalten, wie Dolly Varden Abundanzen auf stochastische Umweltereignisse in marinen Gewässern reagieren.

Die gemessenen Umweltparameter zeigen, dass die Aggregation Dolly Varden auf Herschel Island räumlich mit erhöhtem Chlorophyll-a sowie SST korreliert. Stochastische Trübungsereignisse zeigten einen negativen Einfluss, wodurch die Exemplare räumliche Zuflucht in besseren Wasserbedingungen suchten. Die Ergebnisse zeigten ähnliche Zusammenhänge für SPT, wobei die Parameter hier aufgrund der hohen Schwebstoffkonzentration (CDOM) deutlich schwerer zu differenzieren sind.

Die aus der Studie gewonnenen Daten zeigen, dass die geographische Verbreitung von Dolly Varden in der Beaufortsee abhängig von der Kondition und Osmoregulation (Alter/Länge) ist. In marinen Gewässern sind erwachsene Exemplare deutlich durch stochastische Umweltereignisse (Temperatur und Trübheit) beeinflusst, wobei diese opportunistisch Produktionshotspots zur Nahrungsaufnahme aufsuchen (Meereis und Chlorophyll-a).

Table of Contents

I.	List of Figures	VII
II.	List of Tables.....	XI
III.	List of Abbreviations.....	XII
1	Introduction	14
1.1	Aims and objective.....	18
2	Scientific background.....	19
2.1	Research area.....	19
2.1.1	Beaufort Sea	19
2.2	Dolly Varden, <i>Salvelinus malma</i>	23
2.2.1	Morphological description.....	23
2.2.2	Life history and migratory behaviour.....	24
2.2.3	Cultural value and trend	25
2.3	Remote sensing.....	26
2.3.1	Satellite platforms.....	27
3	Methods.....	29
3.1	Dolly Varden catches and biological sampling	29
3.1.1	Fork length and weight.....	30
3.1.2	Condition factor.....	30
3.2	Wind speed and - direction.....	31
3.2.1	Sea ice coverage	32
3.3	Remote sensing.....	33
3.3.1	Image selection.....	33
3.3.2	Radiometric Calibration and Atmospheric Correction	33
3.3.3	Retrieval of Chlorophyll- a.....	35
3.3.4	Turbidity.....	35
3.3.5	Retrieval of suspended particulate matter (SPM).....	36
3.3.6	Retrieval of brightness Temperature	37
3.3.7	Sample design at study site.....	38

3.4	Data transformation and statistical analysis	41
3.4.1	Testing Dolly Varden parameters.....	41
3.4.2	Regression Analysis (Wind and Ice).....	41
3.4.3	Environmental remote sensing parameters.....	41
3.4.4	Redundancy Analysis (RDA).....	42
4	Results	43
4.1	Harvesting numbers.....	43
4.1.1	Herschel Island	43
4.1.2	Shingle Point	44
4.2	Fork length	45
4.2.1	Herschel Island	45
4.2.2	Shingle Point	46
4.3	Condition factor.....	47
4.3.1	Herschel Island	47
4.3.2	Shingle Point	48
4.4	Wind directions and speed for HIQ and SPT	49
4.4.1	Herschel Island	50
4.4.2	Shingle Point	51
4.5	Sea ice.....	52
4.6	Remote sensing (Sentinel 2 and Landsat 8)	53
4.6.1	Herschel Island	53
4.6.2	Shingle Point	61
4.6.3	Overview of remote sensing Parameters	69
4.7	Redundancy Analysis	70
4.7.1	Herschel Island	70
4.7.2	Shingle Point	73
4.7.3	Redundancy Analysis on selected parameters.....	74
5	Discussion	76
5.1	Dolly Varden Parameters	76
5.1.1	Harvesting Rate	76

5.1.2	Fork length and Condition factor	78
5.1.3	Limitations.....	79
5.2	Environmental Parameters.....	80
5.2.1	Wind speed and direction	80
5.2.2	Sea Ice Concentration.....	81
5.3	Environmental parameters (L8 and S2).....	82
5.3.1	Limitations.....	83
5.4	Redundancy Analysis and Synopsis	84
5.4.1	Limitations.....	86
6	Conclusion and Recommendation.....	87
7	Bibliography	89
	Appendix I, Date acquisition and sensors of images obtained	i
	Eidesstattliche Erklärung.....	iv

I. List of Figures

FIG. 1, SATELLITE VIEW OF THE LOWER MACKENZIE RIVER AND DISCHARGE PLUME TAKEN. ...	15
FIG. 2, MAP OF THE BEAUFORT SEA IN THE SOUTHWESTERN CANADIAN ARCTIC, ILLUSTRATING THE BATHYMETRY, COASTLINE, AND PLACE NAMES, SPANNING FROM INUPIAQ TO BANKS ISLAND. BASE MAP PROVIDED BY ESRI, GARMIN, GEBCO, NOAA, NGDC AND OTHER CONTRIBUTORS, RETRIEVED FROM ARCGIS ONLINE.	20
FIG. 3, MAP OF THE STUDY AREA IN THE SOUTHWESTERN CANADIAN ARCTIC OF THE BEAUFORT SEA AT THE BORDER OF THE YUKON TERRITORY. ILLUSTRATING THE MACKENZIE RIVER DELTA AND THE TWO RESPECTIVE SAMPLING SITES A) HERSCHEL ISLAND QIQTARUK AND B) SHINGLE POINT TAPQAQ. BASE MAP PROVIDED BY ESRI, GARMIN, GEBCO, NOAA, NGDC AND OTHER CONTRIBUTORS, RETRIEVED FROM ARCGIS ONLINE.	22
FIG. 4, MATURE ANADROMOUS MALE OF <i>S. MALMA MALMA</i> (COSEWIC. 2010)	23
FIG. 5, MATURE ANADROMOUS FEMALE OF <i>S. MALMA MALMA</i> (COSEWIC, 2010)	24
FIG. 6, MAP OF HARVESTING AREAS AT BOTH STUDY SITES A) HERSCHEL ISLAND QIQTARUK, B) SHINGLE POINT TAPQAQ. RED RECTANGLES REPRESENT THE HARVESTING AREAS BOTH RESPECTIVE STUDY SITES. BASE MAP PROVIDED BY ESRI, GARMIN, GEBCO, NOAA, NGDC AND OTHER CONTRIBUTORS, RETRIEVED FROM ARCGIS ONLINE.	29
FIG. 7, SAMPLING AREAS ON SEA ICE ABUNDANCE (%) AT THE TWO-HARVESTING SITES A) HERSCHEL ISLAND QIQTARUK AND B) SHINGLE POINT TAPQAQ.	32
FIG. 8, AREAS OF INTEREST (AOIS) DIVIDED INTO NEAR (N-AREA) AND FAR (F-AREA) SUBCLASSES FOR BOTH RESEARCH LOCATIONS WHEREAS A) AND B) ILLUSTRATE THE THE F-AREA SUBCLASSES (F1 – F5) FOR BOTH RESEARCH AREAS C) AND D) DEPICT THE N-AREA (N1 – N4 PLUS PC/ SPT) SUBCLASSES OF HIQ AND SPT RESPECTIVELY	39
FIG. 9, SEASONAL HARVESTING NUMBERS OF DOLLY VARDEN (<i>S. MALMA MALMA</i>) AT HERSCHEL ISLAND QIQTARUK (HIQ) IN DEPENDENCE OF THE CALENDAR DAY (STARTING 1 ST OF JUNE) THROUGHOUT SAMPLING YEARS (2013 – 2019).	43
FIG. 10, SEASONAL HARVESTING NUMBERS OF DOLLY VARDEN (<i>S. MALMA MALMA</i>) AT SHINGLE POINT TAPQAQ (SPT) IN DEPENDENCE OF THE CALENDAR DAY (STARTING 1 ST OF JUNE) THROUGHOUT SAMPLING YEARS (2013 – 2019).	44
FIG. 11, AVERAGE FORK LENGTH (MM) OF DOLLY VARDEN (<i>S. MALMA MALMA</i>) THROUGHOUT THE SUMMER SEASON AMONG SAMPLING YEARS AT HERSCHEL ISLAND QIQTARUK (HIQ). THE DOTS REPRESENT INDIVIDUAL SAMPLES, WHEREAS THE COLOURED LINE REPRESENTS THE MEAN VALUE TREND THROUGHOUT THE SEASON.....	45
FIG. 12, AVERAGE FORK LENGTH (MM) OF DOLLY VARDEN (<i>S. MALMA MALMA</i>) THROUGHOUT THE SUMMER SEASON AT SHINGLE POINT TAPQAQ (SPT) PER SAMPLING YEAR (2013 – 2019). THE DOTS REPRESENT THE LENGTH OF INDIVIDUAL FISH, WHEREAS THE COLOURED LINE REPRESENTS THE MEAN VALUE TREND THROUGHOUT THE FISHING SEASON.	46
FIG. 13, AVERAGE CONDITION FACTOR OF DOLLY VARDEN (<i>S. MALMA MALMA</i>) THROUGHOUT THE SUMMER SEASON AMONG SAMPLING YEARS AT HERSCHEL ISLAND QIQTARUK (HIQ). THE DOTS REPRESENT TAKEN SAMPLES, WHEREAS THE COLOURED LINE REPRESENTS THE MEAN VALUE TREND THROUGHOUT THE SEASON.....	47
FIG. 14, AVERAGE CONDITION FACTOR OF DOLLY VARDEN (<i>S. MALMA MALMA</i>) THROUGHOUT THE SUMMER SEASON AROUND SHINGLE POINT TAPQAQ (SPT). THE DOTS REPRESENT INDIVIDUAL FISH, WHEREAS THE COLOURED LINE REPRESENTS THE MEAN VALUE TREND THROUGHOUT THE FISHING SEASON. THE SEASONAL TRENDS IN THE FORK LENGTH ARE SORTED BY THE INDIVIDUAL SAMPLING YEARS (2013 - 2019).	48

FIG. 15, WINDROSE DIAGRAM SHOWING WIND DIRECTION AND SPEED FREQUENCY FOR THE SUMMER MONTHS JUNE, JULY AND AUGUST. DATA WAS ACQUIRED FOR 2013 - 2019 FROM THE WEATHER STATION AT SIMPSON POINT, HIQ. DIAGRAM IS BASED ON ACQUIRED SATELLITE DATA IN SCOPE OF THE THESIS AND DOES NOT COVER WIND DATA OF THE WHOLE RESPECTIVE MONTH.	49
FIG. 16, NUMBER OF HARVESTED DOLLY VARDEN AT HERSCHEL ISLAND QIQTARUK (HIQ), DEPENDING ON WIND DIRECTION (RADIAN). WITH THE DIFFERENT SYMBOLS REPRESENTING THE MONTH OF THE ANNUAL SAMPLE PERIOD WHILE THE SYMBOLS SIZE ILLUSTRATES THE MAGNITUDE OF WIND SPEED AT THE DATA POINT.	50
FIG. 17, NUMBER OF HARVESTED DOLLY VARDEN AT SHINGLE POINT TAPQAQ (SPT) DEPENDING ON WIND DIRECTION (RADIAN). WITH THE DIFFERENT SYMBOLS REPRESENTING THE MONTH OF THE ANNUAL SAMPLE PERIOD WHILE THE SYMBOLS SIZE ILLUSTRATES THE MAGNITUDE OF WIND SPEED AT THE DATA POINT.	51
FIG. 18, NUMBER OF HARVESTED DOLLY VARDEN SPECIMENS AT HERSCHEL ISLAND QIQTARUK (HIQ), IN DEPENDENCE TO SEA ICE COVERAGE (%) OF THE RESPECTIVE SAMPLING. WHEREAS THE BLACK POINT REPRESENT THE SAMPLE SIZE AT THE RESPECTIVE ICE COVERAGE, LINEAR REGRESSION IS REPRESENTED BY THE RED LINE.	52
FIG. 19, AVERAGE MONTHLY BRIGHTNESS TEMPERATURE (BT) VALUES FOR HERSCHEL ISLAND QIQTARUK (HIQ) REPRESENTING THE SAMPLING PERIOD 2013 - 2019. DATA WAS DERIVED FROM LANDSAT 8 THERMAL INFRARED CHANNELS (BAND 10). VALUES WERE MEASURED IN KELVIN (K).....	53
FIG. 20 MONTHLY (JUNE – AUGUST) MEAN BRIGHTNESS TEMPERATURES (BT) VALUES AROUND HERSCHEL ISLAND QIQTARUK IN DEPENDENCE OF THE SAMPLING YEAR (2013 – 2019). WHEREAS A) ILLUSTRATES MEAN VALUES FOR THE N-AREAS, B) SHOWS MEAN VALUES FOR THE F-AREAS. VALUES WERE MEASURED IN KELVIN (K).....	54
FIG. 21, MEAN MONTHLY CHLOROPHYLL-A (CHL-A) VALUES FOR HERSCHEL ISLAND QIQTARUK (HIQ) REPRESENTING THE SAMPLING PERIOD 2013 - 2019. DATA WAS DERIVED LANDSAT 8 AND SENTINEL 2 SATELLITE IMAGERY. VALUES WERE MEASURED IN MICROGRAM PER LITRE (MG/L)	55
FIG. 22, MONTHLY (JUNE – AUGUST) MEAN LOGARITHMIC CHLOROPHYLL-A (CHL-A) CONCENTRATION AROUND HERSCHEL ISLAND QIQTARUK IN DEPENDENCE OF THE SAMPLING YEAR (2013 – 2019). WHEREAS A) ILLUSTRATES MEAN VALUES FOR THE N-AREAS, B) SHOWS MEAN VALUES FOR THE F-AREAS. VALUES WERE MEASURED IN MICROGRAM PER LITRE (MG/L).....	56
FIG. 23, AVERAGE MONTHLY SUSPENDED PARTICULATE MATTER (SPM) VALUES FOR HERSCHEL ISLAND QIQTARUK (HIQ), REPRESENTING THE SAMPLING PERIOD 2013 - 2019. DATA WAS DERIVED LANDSAT 8 AND SENTINEL 2 SATELLITE IMAGERY. VALUES WERE MEASURED IN GRAMS PER CUBIC METRE (G/M ³).....	57
FIG. 24 MONTHLY (JUNE – AUGUST) MEAN LOGARITHMIC SUSPENDED PARTICULATE MATTER (SPM) CONCENTRATION AROUND HERSCHEL ISLAND QIQTARUK IN DEPENDENCE OF THE SAMPLING YEAR (2013 – 2019). WHEREAS A) ILLUSTRATES MEAN VALUES FOR THE N-AREAS, B) SHOWS MEAN VALUES FOR THE F-AREAS. VALUES WERE MEASURED IN GRAMS PER CUBIC METRE (G/ M ³)	58
FIG. 25, AVERAGE MONTHLY TURBIDITY (FNU) VALUES FOR HERSCHEL ISLAND QIQTARUK (HIQ), REPRESENTING THE SAMPLING PERIOD 2013 - 2019. DATA WAS DERIVED FROM LANDSAT 8 AND SENTINEL 2 SATELLITE IMAGERY. VALUES WERE MEASURED IN FORMAZIN NEPHELOMETRIC UNITS (FNU)	59

FIG. 26, MONTHLY (JUNE – AUGUST) MEAN LOGARITHMIC TURBIDITY (FNU) CONCENTRATION AROUND HERSCHEL ISLAND QIQTARUK IN DEPENDENCE OF THE SAMPLING YEAR (2013 – 2019). WHEREAS A) ILLUSTRATES MEAN VALUES FOR THE N-AREAS, B) SHOWS MEAN VALUES FOR THE F-AREAS. FORMAZIN NEPHELOMETRIC UNITS (FNU) 60

FIG. 27, AVERAGE MONTHLY BRIGHTNESS TEMPERATURE (BT) VALUES FOR SHINGLE POINT TAPQAQ, REPRESENTING THE SAMPLING PERIOD 2013 - 2019. DATA WAS DERIVED FROM LANDSAT 8 THERMAL INFRARED CHANNELS (BAND 10). VALUES WERE MEASURED IN KELVIN (K)..... 61

FIG. 28, MONTHLY (JULY – AUGUST) MEAN BRIGHTNESS TEMPERATURE (BT) VALUES AROUND HERSCHEL ISLAND QIQTARUK IN DEPENDENCE OF THE SAMPLING YEAR (2013 – 2019). WHEREAS A) ILLUSTRATES MEAN VALUES FOR THE N-AREAS, B) SHOWS MEAN VALUES FOR THE F-AREAS. VALUES WERE MEASURED IN KELVIN (K)..... 62

FIG. 29, AVERAGE MONTHLY CHLOROPHYLL-A (CHL-A) VALUES FOR SHINGLE POINT TAPQAQ, REPRESENTING THE SAMPLING PERIOD 2013 - 2019. DATA WAS DERIVED FROM LANDSAT 8 AND SENTINEL 2 SATELLITE IMAGERY. VALUES WERE MEASURED IN MICROGRAM PER LITRE (MG/L)..... 63

FIG. 30, MONTHLY (JULY – AUGUST) MEAN CHLOROPHYLL-A (CHL-A) CONCENTRATION AROUND SHINGLE POINT TAPQAQ (SPT) IN DEPENDENCE OF THE SAMPLING YEAR (2013 – 2019). WHEREAS A) ILLUSTRATES MEAN VALUES FOR THE N-AREAS, B) SHOWS MEAN VALUES FOR THE F-AREAS. VALUES WERE MEASURED IN MICROGRAM PER LITRE (MG/L). 64

FIG. 31, AVERAGE MONTHLY SUSPENDED PARTICULATE MATTER (SPM) VALUES FOR SHINGLE POINT TAPQAQ, REPRESENTING THE SAMPLING PERIOD 2013 - 2019. DATA WAS DERIVED FROM LANDSAT 8 AND SENTINEL 2 SATELLITE IMAGERY. VALUES WERE MEASURED IN GRAMS PER CUBIC METRE (G/M³)..... 65

FIG. 32, MONTHLY (JULY – AUGUST) MEAN SUSPENDED PARTICULATE MATTER (SPM) CONCENTRATION AROUND SHINGLE POINT TAPQAQ (SPT) IN DEPENDENCE OF THE SAMPLING YEAR (2013 – 2019). WHEREAS A) ILLUSTRATES MEAN VALUES FOR THE N-AREAS, B) SHOWS MEAN VALUES FOR THE F-AREAS. VALUES WERE MEASURED IN MICROGRAM GRAMS PER CUBIC METER (G/M³)..... 66

FIG. 33, AVERAGE MONTHLY TURBIDITY VALUES FOR SHINGLE POINT TAPQAQ, REPRESENTING THE SAMPLING PERIOD 2013 - 2019. DATA WAS DERIVED FROM LANDSAT 8 AND SENTINEL 2 SATELLITE IMAGERY. VALUES WERE MEASURED IN FORMAZIN NEPHELOMETRIC UNITS (FNU)..... 67

FIG. 34, MONTHLY (JULY – AUGUST) MEAN TURBIDITY CONCENTRATION AROUND SHINGLE POINT TAPQAQ (SPT) IN DEPENDENCE OF THE SAMPLING YEAR (2013 – 2019). WHEREAS A) ILLUSTRATES MEAN VALUES FOR THE N-AREAS, B) SHOWS MEAN VALUES FOR THE F-AREAS. VALUES WERE MEASURED IN FORMAZIN NEPHELOMETRIC UNITS (FNU)..... 68

FIG. 35, REDUNDANCY ANALYSIS (RDA) OF THE BIOLOGICAL PARAMETERS OF DOLLY VARDEN (*S. MALMA MALMA*). RDA 1 (40.1 %) AND RDA2 (30.13 %) SHOW THE RELATION OF THE RESPONSE VARIABLES (RED ARROWS) ON THE ENVIRONMENTAL PARAMETERS OF THE DIFFERENT AOIS AS EXPLANATORY VARIABLES (BLUE ARROWS). THE LENGTH OF AN ARROW REFLECTS THE CONTRIBUTION TO EXPLAIN THE TOTAL VARIANCE WHILE A SMALL ANGLE BETWEEN TWO ARROWS REPRESENTS THE STRENGTH OF THE CORRELATION BETWEEN THE TWO CORRESPONDING PARAMETERS. THE RDA WAS SIGNIFICANT ($p < 0.05$) AND REVEALED AN ADJUSTED COEFFICIENT OF DETERMINATION OF 0.51..... 71

FIG. 36, REDUNDANCY ANALYSIS (RDA) OF THE BIOLOGICAL PARAMETERS OF DOLLY VARDEN (*S. MALMA MALMA*). RDA 1 (44.3 %) AND RDA2 (29.42 %) SHOW THE RELATION OF THE

RESPONSE VARIABLES (RED ARROWS) ON THE ENVIRONMENTAL PARAMETERS OF THE DIFFERENT AOIS AS EXPLANATORY VARIABLES (BLUE ARROWS). THE LENGTH OF AN ARROW REFLECTS THE CONTRIBUTION TO EXPLAIN THE TOTAL VARIANCE WHILE A SMALL ANGLE BETWEEN TWO ARROWS REPRESENTS THE STRENGTH OF THE CORRELATION BETWEEN THE TWO CORRESPONDING PARAMETERS. THE RDA WAS SIGNIFICANT ($p < 0.05$) AND REVEALED AN ADJUSTED COEFFICIENT OF DETERMINATION OF 0.49..... 74

II. List of Tables

TABLE 1, LANDSAT 8 SPECTRAL BANDS, WAVELENGTHS, AND SPATIAL RESOLUTION.	27
TABLE 2, SENTINEL -2 SPECTRAL BANDS, WAVELENGTHS, AND SPATIAL RESOLUTION	28
TABLE 3, SURFACE SIZE (M ²) OF THE FOUR RESPECTIVE SAMPLING AREAS AT HIQ AND SPT. THE SAMPLING AREAS ARE LISTED IN THE RESPECTIVE TO CLOCKWISE ORDINATION.....	32
TABLE 4, AREAS OF INTEREST SIZE (M ²) OF HIQ AND SPT (NEAR VS. FAR). THE SUBAREAS ARE LISTED IN THE RESPECTIVE CATEGORY IN THE NUMBERS FROM 1 TO 5, ADDITIONALLY THE NUMBER OF EXTRACTION POINTS PER AREA IS LISTED.	40
TABLE 5, MULTIPLE REGRESSION PREDICTING DOLLY VARDEN PARAMETERS BY EXPLANATORY WIND VARIABLES.	50
TABLE 6, MULTIPLE REGRESSION PREDICTING DOLLY VARDEN PARAMETERS BY EXPLANATORY WIND VARIABLES.	51
TABLE 7, OVERVIEW OF SATELLITE IMAGERY DERIVED ENVIRONMENTAL PARAMETERS ACCORDING TO BOTH RESPECTIVE SAMPLING POINTS HIQ AND SPT). FOR EACH VALUE THE MEAN VALUE (MEAN) AND STANDARD DEVIATION (SD) ARE GIVEN ACCORDING TO N- AND F-AREAS AT BOTH RESPECTIVE SAMPLING SATES. BOTH SAMPLING SITES WERE TESTED WITH AN INDEPENDENT SAMPLES T-TEST. RESULTS ARE SHOWN ON LAST COLUMN	69
TABLE 8, RDA RESULT FOR EACH RESPONSE VARIABLE (HARVEST NUMBER, BODY WEIGHT, FORK LENGTH) IN RELATION TO THE EXPLANATORY VARIABLES INCLUDED IN THE MODEL. PARAMETERS TO EXPLAIN THE RESPONSE VARIABLE WERE CHOSEN BASED ON THE STEPWISE SELECTION. ASTERISKS SYMBOLISE THE DEGREE OF SIGNIFICANT LINEAR CORRELATION. .	70
TABLE 9, RDA RESULT FOR EACH RESPONSE VARIABLE (HARVEST NUMBER, BODY WEIGHT, FORK LENGTH) IN RELATION TO THE EXPLANATORY VARIABLES INCLUDED IN THE MODEL. PARAMETERS TO EXPLAIN THE RESPONSE VARIABLE WERE CHOSEN BASED ON THE STEPWISE SELECTION. ASTERISKS SYMBOLISE THE DEGREE OF SIGNIFICANT LINEAR CORRELATION. .	73

III. List of Abbreviations

AC	atmospheric correction
AOI	areas of interest
BT	brightness temperature
CDOM	Chromophoric dissolved organic matter
Chl-a	Chlorophyll- <i>a</i>
DN	digital number
DSF	Dark Spectrum Fitting
F-area	Far Area
FNU	Formazin Nephelometric Unit
HIQ	Herschel Island Qiqiktaruk
K	condition factor
MSI	Multispectral Instrument
N-area	Near Area
NIR	near infrared radiation
OLI	Operational Land Imager
PC	Pauline Cove
RDA	Redundancy analysis
SD	standard deviation
SIC	sea-ice concentration
SPM	suspended particulate matter
SPT	Shingle Point Tapqaq
SWIR	short-wave infrared
TIRS	Thermal Infrared Radiometer Sensor
TOA	top of atmosphere
USGS	United States Geological Survey

1 Introduction

Elucidating how the physical properties of marine habitats influence the relative abundance and demographic properties of anadromous fishes targeted in marine fisheries is relevant to assess the productivity of fisheries and has an important bearing on management and conservation objectives. Habitat complexity is an important driver of faunal abundance and richness, biotic structure, and ecosystem functioning (Kovalenko et al., 2012). Physical substrate (e.g., coral, rock formation) or even physiochemical environmental properties and events (e.g. temperature, salinity, turbidity) (Gouveia et al., 2019) shape a complex three-dimensional environmental structure by which numerous spatial- and temporal niches arise with which organisms can directly interact. (Kovalenko et al., 2012).

River deltas are dynamic environments linking freshwater and marine ecosystems, whose physical, chemical, and biological properties are influenced by seasonal freshwater run off and high loads of sediments and nutrients and saline sea water (e.g., Carmack et al., 2004; Gouveia et al., 2019). These environmental systems are known to harbour a great variety of biological diversity with multiple interlinked trophic connections leading to complex food webs (Sheaves, 2009). Riverine discharges into the coastal ocean often create a thin buoyant plume of fresh, nutrient rich water over the dense oceanic water (Carmack & Macdonald, 2002). These emerging, highly productive, and relatively persistent boundaries of estuary areas are rich in phytoplankton biomass and therefore provide a predictable food source for planktivorous fishes and the higher trophic levels that rely on them (MacGregor & Houde, 1996).

The Mackenzie River is the largest river draining into the Arctic Ocean in North America and has a major influence on surface water properties and environmental characteristics of the Beaufort Sea in the western Canadian Arctic (Carmack & Macdonald, 2002) (Fig. 1). The physical properties of the coastal waters along the south-eastern Beaufort Sea integrate both the cooler marine waters of the Beaufort Sea and the warmer freshwater inputs of river systems (Craig, 1984). The Mackenzie Delta is particularly important as a contributor to estuarine habitat, functioning as a migration corridor for anadromous fishes (i.e., fish that perform seasonal migrations between freshwater and marine feeding; Gallagher et al., 2021) during the summer months. With the Mackenzie Plume extending along 750 km of Beaufort Sea shoreline, the relatively warm, brackish water band provides habitat for numerous anadromous (e.g., Arctic cisco *Coregonus autumnalis*, Dolly Varden *Salvelinus malma*) and marine (e.g., Arctic cod *Boreogadus saida*) fishes that are not only prey for marine mammal species but also provide subsistence for Indigenous communities (Craig, 1984).

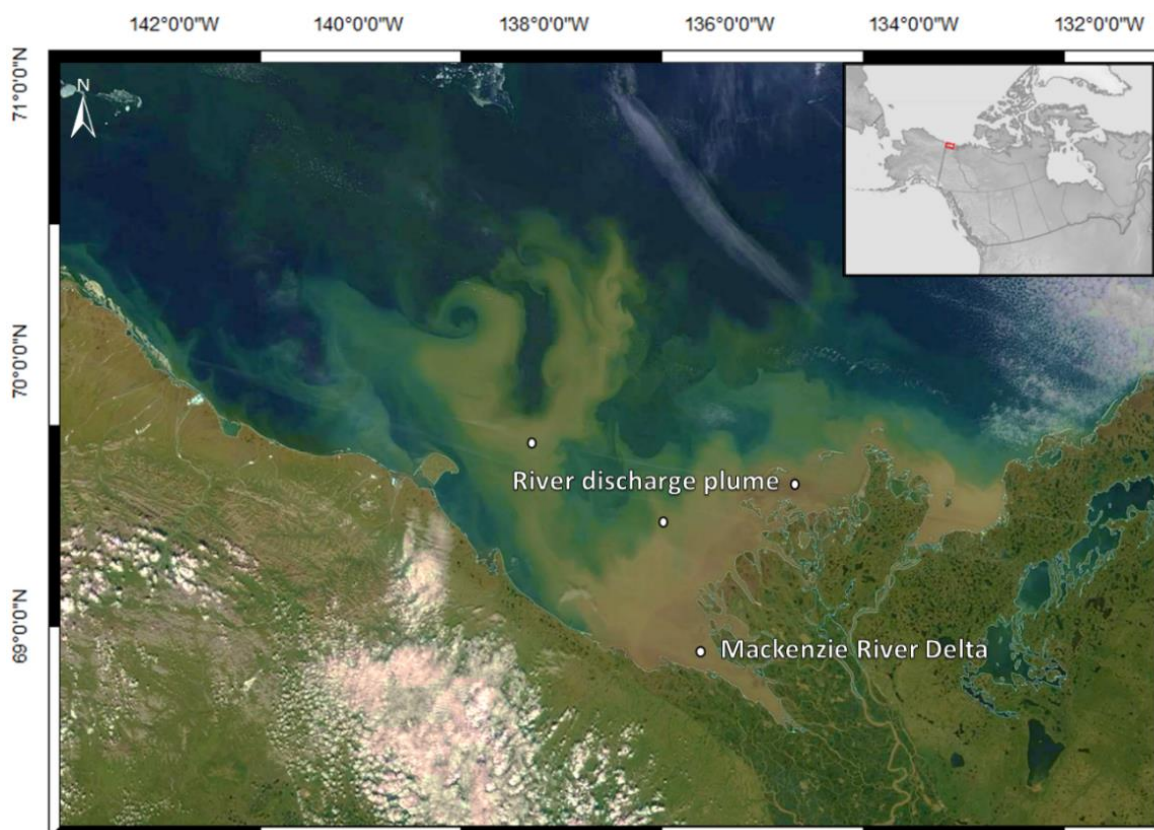


Fig. 1, Satellite view of the lower Mackenzie River and discharge plume taken. Image taken by MODIS, (01/07/2014)

The highly productive Mackenzie Delta is situated in the boundaries of both the Inuvialuit Settlement Region and the Gwich'in Settlement Area (Gwich'in Tribal Council and Indian and Northern Affairs Canada 1992). Both communities have occupied the region for centuries by relying on subsistence fishing, whaling, hunting, and food gathering (Pearce et al., 2010). As a result, the Gwich'in and Inuvialuit have developed a cultural and socio-economic reliance on the Mackenzie Delta and Beaufort Sea (Heine et al., 2007; Turner & Lanz, 2018). In Arctic communities, there is concern regarding changes in the distribution and abundance of the aquatic species harvested. It is shown that a combination of environmental factors related to the increases in water temperatures and decreases in sea ice has led to a shift in marine sympagic fauna (Logerwell et al., 2018). Consequently, this led to a shift in faunal migration routes, which has resulted in a shift of species composition and harvest timing (AMAP, 2017). For some coastal communities, subsistence species availability is shifting or is beyond the geographical reach of harvesters (Loseto et al., 2018).

Marine fishes are widely recognized to play an important role in energy transfer from lower (e.g., zooplankton, epibenthic invertebrates) to upper trophic levels (e.g., predators) (Loseto et al., 2009). For many fishes of the Beaufort Sea, drivers of spatial distribution and their

associated habitat requirements are poorly understood, which can impact conservation and management of species that important to fisheries. In the Beaufort Sea, an important species harvested in Indigenous subsistence fisheries is the northern form of Dolly Varden (*Salvelinus malma malma*) (Pedersen & Linn, 2005; Magdanz et al., 2010; Lea et al., 2021). In the Canadian Arctic, subsistence fisheries for Dolly Varden occur along the coast in summer and in the Mackenzie Delta, Peel River, and Rat River during late summer and fall during the return migration. Harvesters typically use relatively short single mesh gill nets set perpendicular to shore. Some aspects of the life history of northern Dolly Varden are described (e.g., McCart, 1980; DeCicco, 1997) However, while it had been assumed that Dolly Varden exclusively inhabited the warmer, brackish nearshore waters recent satellite telemetry studies demonstrated they can also reside in more offshore habitat up to 150 km from shore in thermal conditions of 5 - 10°C (Gallagher et al., 2021). Although, Dolly Varden are known to occupy nearshore marine habitat, the biotic and abiotic factors that influence their use of this habitat have not been thoroughly investigated. According to Indigenous harvesters, several populations have experienced declines in abundance, while the geographically limited number of critical habitats, particularly in freshwater, make the species particularly vulnerable to local (e.g., overexploitation, stochastic events) and larger-scale events (e.g., climate change) that can threaten long-term viability of populations. Dolly Varden is designated as "Special Concern" under Species at Risk legislation in Canada. Sustainable fisheries and environmental drivers are of interest to Canadian co-management stakeholders (DFO, 2019).

Research infrastructure in the Arctic however remains sparse and challenging in comparison to temperate regions. This makes it challenging to detect rapidly occurring environmental changes and to infer potential impacts on fish population. Remote sensing bears great potential in overcoming some of these issues. It provides the opportunity to capture a wide range of surface parameters with a high temporal repeatability and good availability (Braga et al., 2017). It has been shown in the past to be an important tool for understanding coastal hydrodynamics and processes and is commonly used for coastal zone management strategies (Giardino et al., 2019). Challenges in using remote sensing exist. Oscillations in the hydrology or biochemistry can alter the spectral properties of components in the water column. The spectral properties of water constituents can be affected by any hydrological, physical, or biochemical change, with noticeable impacts on chlorophyll-a (Poddar et al., 2019) and turbidity values (Dogliotti, 2015), as well as brightness temperature (Wukelic et al., 1989). Yet, recent technological progress in remote sensing, algorithm development and its connection to biological and physical

monitoring at high enough spatial and temporal resolution has allowed an examination of the mechanisms of fish distribution (Reese et al., 2011). It is the ambition of this thesis to test remote the capacity of remote sensing to resolve environmental parameters in the southern Beaufort Sea and to link it to fish harvesting strategy in order to better characterize these mechanisms. Over the years, several hypotheses on food availability (Holland et al., 2021), predation (Pellicice et al., 2014), as well as temperature (Reese et al., 2011) have been proposed to explain the main mechanisms that determine the variability of distribution. The approach of this thesis uses new information to test these hypotheses over greater areas using remote sensing.

1.1 Aims and objective

The physical and biochemical properties of the waters from the Mackenzie Shelf in the Beaufort Sea are strongly influenced by the eponymous river through its high loads of freshwater discharge (Carmack & Macdonald, 2002). As a result, strong saline, thermal, and turbidity gradients may occasionally occur on the open water (Brenkman et al., 2007; Swanson & Kidd, 2009; Jensen et al., 2014). With the ability to provide broad-scale, real-time data on aquatic environmental parameters, remote sensing has widely been used in the past for fisheries exploitation and management strategies (e.g., Andrade, 2003; Zainuddin et al., 2008). Therefore, approaches provide information on specific spatiotemporal environmental conditions and processes that are known to affect habitat use fish populations (e.g., temperature, turbidity, etc.) (Klemas, 2013).

The aim of this study was to investigate how the timing and catches of Dolly Varden in coastal summer subsistence fisheries were influenced by environmental conditions in the Beaufort Sea. Furthermore, it was examined whether there was an association between environmental parameters and the demographic and somatic properties of harvested Dolly Varden. For this study, fisheries-dependent data from two different study sites (Herschel Island and Shingle Point, Yukon Territory, Canada) were analysed from 2013 to 2019. Remotely sensed environmental parameters temperature, chlorophyll-a, turbidity and sea ice were derived from Landsat-8 and Sentinel-2 images and examined along with wind vectors were also included. The following specific hypotheses were tested in the thesis:

H1 = Habitat use of anadromous Dolly Varden in terms of spatial distribution, is influenced by changing environmental drivers in the Beaufort Sea

H2 = Habitat use of anadromous Dolly Varden in terms of somatic fitness is influenced by changing environmental drivers in the Beaufort Sea.

This thesis is the product of a collaboration between the Alfred Wegener Institute for Polar and Marine Research in Potsdam, Germany and the Department of Fisheries and Oceans in Winnipeg, Canada.

2 Scientific background

2.1 Research area

The study was conducted in the south-eastern Beaufort Sea at two different locations west of the Mackenzie Delta. The areas of interest, namely Herschel Island Qiqiktaruk (69°36'N; 139°04'W) and Shingle Point Tapqaq (68°59'N; 137°22'W), are located on the coast of the Yukon Territory, Canada. Both are within the Inuvialuit Settlement Region (Burn, 2012) and are the traditional hunting and fishing areas principally used by the Inuvialuit from the hamlet of Aklavik, Northwest Territories.

2.1.1 Beaufort Sea

Being a marginal sea of the Arctic Ocean, the Beaufort Seas coast and shelf extend from Banks Island (Canada) to Inupiaq (Alaska) and encompasses three distinct shelf environments and two significant river systems (Harper, 1990). Along the coast (~ <80 km from shore) the waters of the Beaufort Sea are relatively shallow and rarely exceed 60 m in depth. The depth increases rapidly northwards (Canada Basin) up to ~3700 m and turn into a massive plateau (Alberta Society of Petroleum Geologists, 1951). The nearshore bathymetry is an extension of the Yukon Coastal Plain and is gently sloping towards the North except for a several cross-shelf troughs and plateaus (Harper, 1990). Several long and narrow barrier-islands are situated along the coast of the Yukon Coastal Plain. The largest island along the coast is Herschel Island Qiqiktaruk (4 km offshore) (Fig 2) (Harper, 1990). The climatic condition in the region is generally characterized by long and cold winters (October – May), and short moderate temperate summers (June – September). For the Mackenzie Shelf, strong temperature gradients are associated with the large extent of the Mackenzie River discharge waters, leading to a general decrease in thermal properties towards offshore. To the outer parts of the shelf, the water column exhibits a relatively narrow range of temperature and salinity values as typical of the Arctic Ocean water mass. Under the surface layer, which is generally limited to depths of 50 m or less, thermal values range within 1 °C of freezing point and salinity ranges from 31 to 33.5 psu. There is a relatively wide span of temperature-salinity properties at the surface, which is primarily influenced by the seasonal driven heat exchange at the surface. Over the winter, surface temperatures drop to a few tenths of a degree below freezing as a result of heat loss to the atmosphere and the resulting ice formation, with surface salinity rising to levels above 31 psu. During early summer, temperatures are generally high, typically ranging from 5 to 16 °C because of the Mackenzie River discharge's warm waters and strong solar radiation at this time of year. The high level of solar radiation in summer, combined with the extensive open water areas, may results in surfaces temperatures of up to 6 °C and a salinity of up to 25 psu. (Fissel-

Birch, 1984). With the onset of rising temperatures between mid-May and beginning of June, the discharge of the river reaches peak values, whereby the estuary is quickly flooded.

The surface waters of the Yukon coastal plain and Mackenzie Shelf have a distinct estuarine character as they are strongly influenced by the Mackenzie River, which large freshwater discharge into the Arctic Ocean ($330 \text{ km}^3 \text{ y}^{-1}$) (Dunton & Carmack, 2006), visually affecting the physical water properties of the Beaufort Shelf (Macdonald et al., 1998).

The discharge waters characteristically disperse along the nearshore zone, whereas, according to Giovando and Herlinveaux (1981), the dispersion within the shelf is strongly dependent on winds and the extent of the surface water. Under the absence of winds, the effluent plume propagates eastwards along the Tuktoyaktuk Peninsula, with easterly winds carrying the turbid effluent plume into deep waters. The riverine freshwater mixes with the salty marine water, resulting in nutrient-rich oceanographic fronts, forming rich feeding grounds for organisms of different trophic levels, such as anadromous coastal- and euryhaline marine fishes, and marine ichthyoplankton and zooplankton (Bost et al., 2009). The highly productive Mackenzie Delta is situated in the boundaries of both the Inuvialuit Settlement Region and the Gwich'in Settlement Area (Gwich'in Tribal Council and Indian and Northern Affairs Canada 1992). Both communities have occupied the region for centuries by relying on subsistence fishing, whaling, hunting, and food gathering. (Turner & Lantz, 2018).

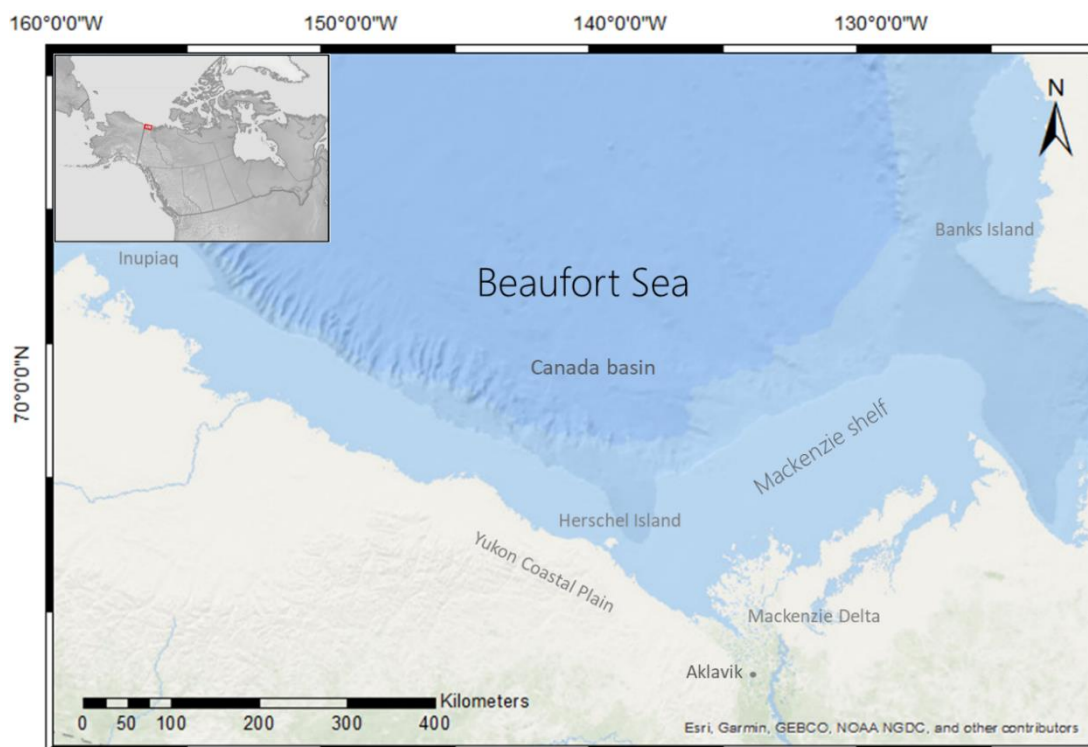


Fig. 2, Map of the Beaufort Sea in the southwestern Canadian Arctic, illustrating the bathymetry, coastline, and place names, spanning from Inupiaq to Banks Island. Base map provided by Esri, Garmin, GEBCO, NOAA, NGDC and other contributors, retrieved from ArcGIS online.

2.1.1.1 *Herschel Island Qiqiktaruk*

Herschel Island Qiqiktaruk (HIQ) is part of the Yukon Coastal Plain physiographic region, which is a landward extension of the Beaufort Sea shelf (Rampton, 1982). HIQ is located about 70 km east of the Yukon-Alaska border and the southern Beaufort Sea. The island covers an area of approximately 108 km² (8 x 15 km), with a peak elevation of 185 m above sea level (Lantuit & Pollard, 2005) (Fig. 3 a). The topography of the island is characterized by rolling hills and steep cliffs that are up to 50m high (Fritz et al., 2012). Coastal thermokarst can often be observed on the coastal slopes as retrogressive thaw slumps (Lantuit & Pollard, 2008). The island is separated from the mainland by the very shallow Workboat Passage (< 3 m deep, about 2 km wide), where longshore currents frequently cause sediment resuspension (Klein et al., 2018). During the summer months, the north shore is exposed to strong wave energy from the Beaufort Sea while the east side is relatively sheltered (Hill et al., 1991). To the northeast of HIQ there is considerable upwelling, enhanced by the Mackenzie Trough, with sea surface temperatures as low as 1 degree. During westerly winds, down welling is promoted, which forces the surface water toward the coast. Since 1987, the entire island has been part of the Herschel Island Territorial Park, whose mandate is to protect and preserve the lands and waters of the area to sustain Inuvialuit subsistence activities (Burn, 2012). Human presence is generally limited to the settlement area on Simpson Point next to Pauline Cove Ilutaq (PC). This settlement has been historically used by Inuit people and greatly increased in size at the turn of the 19th and 20th century with the rise of the whaling industry (Burn, 2012).

2.1.1.2 *Shingle Point Tapqaq*

Located approximately 40 km off the mouth of the Mackenzie River, Shingle Point Tapqaq (SPT) is a 7-10 km long driftwood covered gravel spit that extends into the Beaufort Sea. (Irrgang et al., 2019) (Fig. 3 b). One side of Shingle Point is shallow and sheltered (harbour sided), while the other side is turbulent and deep (sea sided), while the shape of the island can undergo annual changes due to storms and wave action. Because of the high influence of the Mackenzie River, the water characteristics are distinctly brackish, turbid, and warm. There are about 20 cabins on the gravel bar, some of which are used year-round by Inuvialuit communities, while the area is important primarily to Aklavik residents for cultural and subsistence activities such as camping, fishing, whaling, caribou hunting, travelling and berry picking. The headland of Shingle Point is generally divided into three camps (Down the Hill, Middle Camp and The Point). (Loewen et al., 2013)

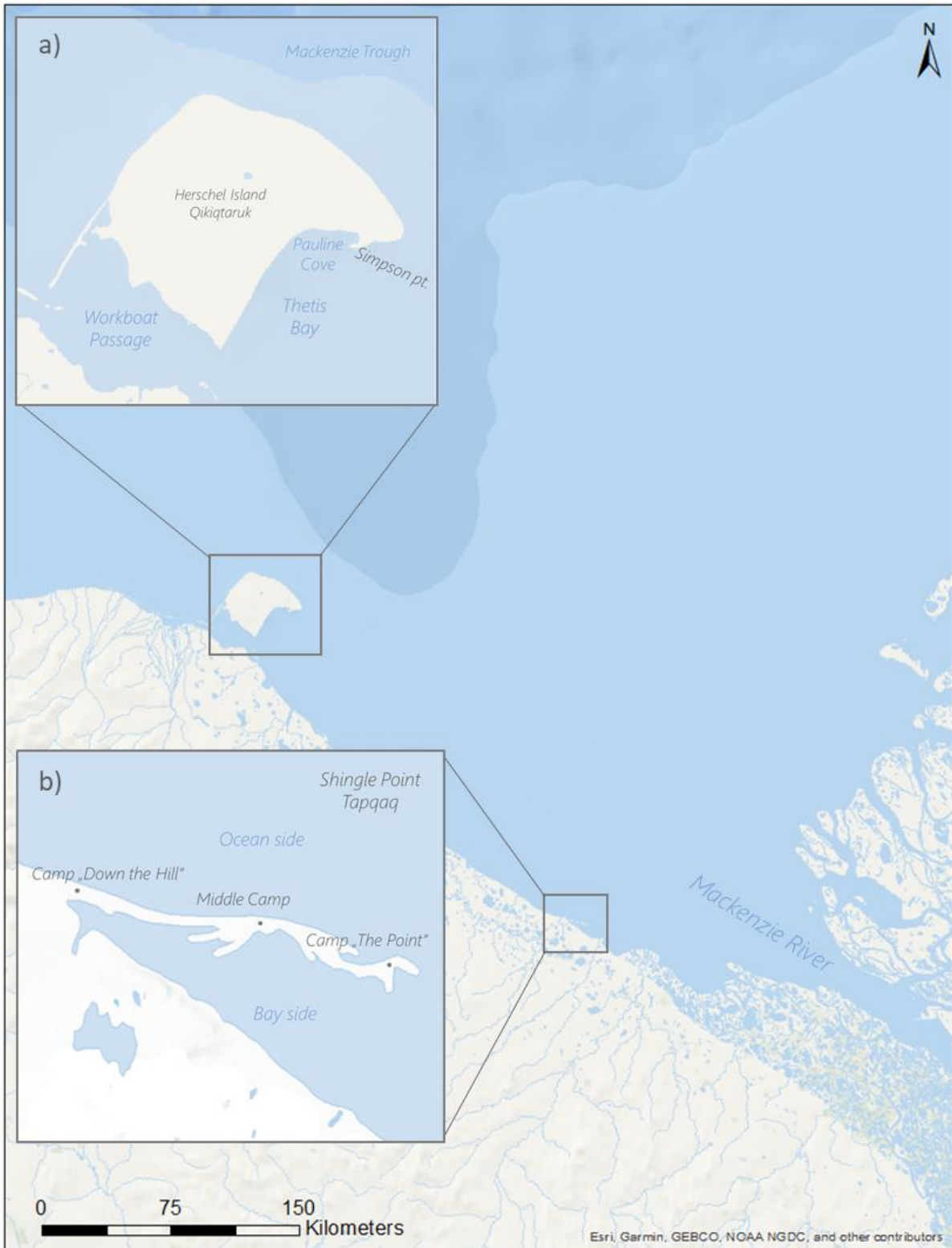


Fig. 3, Map of the study area in the southwestern Canadian Arctic of the Beaufort Sea at the boarder of the Yukon Territory. Illustrating the Mackenzie River Delta and the two respective sampling sites a) Herschel Island Qiqiqtaruk and b) Shingle Point Tapqaq. Base map provided by Esri, Garmin, GEBCO, NOAA, NGDC and other contributors, retrieved from ArcGIS online.

2.2 Dolly Varden, *Salvelinus malma*

The Dolly Varden (*Salvelinus malma*) belongs to the family of the *salmonidae*. The species is distributed in the northern hemisphere and endemic to cold-water streams of the northern Pacific Ocean, Asia, and North America (Mochnacz et al., 2010). *S. malma* consists of four recognized subspecies that are divided into two American and two Asian subspecies. In North America, the "Southern form" of Dolly Varden (*S. m. lordi*) is found in the eastern North Pacific along and south of the Alaska Peninsula. The "northern form" of Dolly Varden (*S. m. malma*) inhabit areas north of the Alaska Peninsula west to the Chukotka Peninsula and east to the Mackenzie River in North America.

2.2.1 Morphological description

The Canadian Dolly Varden, *Salvelinus malma malma* (Walbaum, 1792) populations, hereafter referred as Dolly Varden, populations encompass three different life history strategies, which can be either anadromous, resident, or isolated (Gallagher et al., 2019). Such as other species that undergo partial migration strategies, Dolly Varden are described as polymorphic. Whereas the general morphological traits of the northern form of Dolly Varden have been described in detail by COSEWIC (2010), individuals show different traits regarding their life strategy (i.e., smaller-sized resident and larger-sized migrant) (Harris et al., 2015). Non-spawning, smoltified specimens, also called "silvers", exhibit a silvery ground colour at the base with pale pink to orange spots scattered along the sides (> 100 mm). Mature, anadromous individuals can range in size from approximately 350 to 850 mm and show similar vivid colouration for both sexes. The species is characterized by a brownish-black dorsal fin and an orange-reddish ventral surface. The sides and tip of the male's snout are orange while white leading edges are seen on the maxilla and pectoral fins (COSEWIC, 2010). Males also exhibit secondary sexual characteristics such as a pronounced dorsal ridge, a *kype* on the lower jaw, a notch on the upper jaw, and enlarged teeth (Fig. 4 & 5).



Fig. 4, mature anadromous male of *S. malma malma* (COSEWIC. 2010)

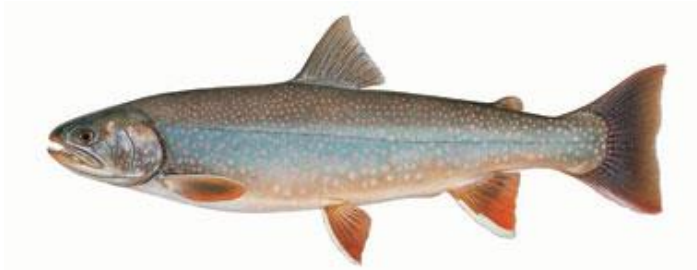


Fig. 5, mature anadromous female of *S. malma malma* (COSEWIC, 2010)

2.2.2 Life history and migratory behaviour

Anadromous Dolly Varden populations have been documented for six river systems in the North Slope (Yukon Territory) as well as in the areas west of the Mackenzie River and Peel River (Northwest Territories) (Gallagher et al., 2013). Gallagher et al. (2012) emphasized the different biological characteristics of the various anadromous populations in the area. The individuals in the Firth River were observed to be larger and older than in other systems, with males in the Babbage River being larger than females. In all systems, individuals of both sexes were found to mature at the same age, with the proportion of female fish in the populations clearly outweighing the males. Life history strategies of individuals often vary between and within populations. Generally, with warming temperatures and ice cover break up (mid-June), smoltified (first emergence into the sea), anadromous Dolly Varden migrate annually on a seasonal basis from freshwater (spawning and overwintering) grounds to marine feeding habitats (typically at 2-5 years of age) (Gallagher et al., 2018). Freshwater salmonid migratory behaviour enables animals to exploit the energy resources of highly productive coastal waters, resulting in pronounced growth and larger body size of animals compared to non-migratory animals (Jonsson & Jonsson, 1993). Although marine migration has a positive effect on reproductive performance through size and increased energy reserves, reproductive maturity is considerably later than in non-migratory conspecifics. Still, migration tactics can vary strongly between and within populations (Hendry et al., 2004). In previous studies, adult Dolly Varden were found to spend an average of 6 to 7 weeks in marine waters during the summer. In that time, they attempted to acquire sufficient energy reserves to survive the winter with little or no additional feeding (Armstrong & Morrow, 1980). Brown et al. (2018) found that time at sea for post-spawning was on average 3 weeks longer than for non-spawners, presumably because they required more time feeding in response to the increased energy demands associated with spawning (Dutil, 1986).

Younger individuals tend to inhabit the nearshore, less saline waters given the less developed osmoregulation (McCormick & Saunders, 1987). Mature individuals on the other hand, occupy warm, brackish waters in the coastal zone (Bond & Erickson, 1989) along with open waters up to 100 km offshore, where they inhabit the warmer (2° - 8° C) upper layers (0.1 - 2.2 m) (Courtney et al., 2018).

Because anadromous individuals rarely feed during spawning and overwintering seasons, the bulk of energy accumulation for growth and reproduction occurs primarily during the summer months (Glova & McCart, 1974). In coastal waters, the species mainly feeds on smaller fish, insects (aquatic and terrestrial; larvae, pupae, adults), crustaceans, molluscs, or annelids (Stewart et al., 2010). Spawning occurs as early as late August to late October when individuals have generally returned to overwintering locations upstream. Anadromous adult and juvenile individuals show marked natal philopatry, with recruitment from other populations rarely documented. In addition, several studies report that individuals were observed overwintering in marine waters. Nevertheless, these individuals are believed to be non-spawning specimens (McCart, 1980).

2.2.3 Cultural value and trend

In Inuvialuit and Gwich'in culture, subsistence economy (i.e., hunting and fishing) plays an essential role in their cultural identity and domestic food security (Pearce et al., 2010). In the coastal and inland sites of Inuvialuit and Gwich'in settlement areas, the Dolly Varden harvest (2009 - 2014) showed an annual average harvest of between 654 and 1086 fish (Lea et al., 2021), making the species an essential subsistence fishery resource for indigenous traditional lifestyle (Magdanz et al., 2010). For many generations, the Inuvialuit have fished Dolly Varden along the coast at Herschel Island, Ptarmigan Bay, King Point, and Shingle Point. Generally, larger fish are caught at Herschel Island, an observation attributed to the less turbid water with higher salinity (Burn, 2012). Scientific observations (e.g., Bouchard et al., 2017; Ehrlich et al., 2020) and Indigenous knowledge (e.g., Steiner et al., 2019) found that a combination of warming temperatures and decreasing sea ice have led to shifts in terrestrial and aquatic migratory pathways, whose effects led to shifts in the species composition and harvesting season. According to the Inuvialuit, changing environmental conditions have led to shifts in marine species distribution and abundance in the coastal zone as well as increasing effort to access harvesting grounds (Loseto et al., 2018; Steiner et al., 2019). However, geographically limited number of critical habitats, particularly in freshwater, make the species particularly

vulnerable to local (e.g., overexploitation, stochastic events) and larger-scale events (e.g., climate change) that can threaten long-term viability of populations. Dolly Varden is designated as "Special Concern" under Species at Risk legislation in Canada. Sustainable fisheries and environmental drivers are of interest to Canadian co-management stakeholders (DFO, 2019).

2.3 Remote sensing

Since the 1960s, remote sensing has been increasingly used to collect environmental information using satellites. The acquisition of data is based on the reflectance and/or electromagnetic radiation (EMR), which is emitted and/or reflected by a certain object. The measured radiance results from the flux of electromagnetic energy, which is transmitted from a surface in direction by a unit angle (α) and is given as ($\text{W}/\text{m}^2 \text{ sr}$). Consequently, the radiant energy and target objects can interact in three different ways: 1) Absorption by internal conversion of rays into energy; 2) Scattering/deflection by particles and molecules; 3) Transmission by radiation passing through the object or is emitted. (Deschamps et al., 1985)

The characteristics of water in remotely sensed products are determined by complex optical properties and energy-object interactions. The colour properties of water bodies are strongly influenced by the particulate and dissolved matter (Dassenakis et al., 2011). Pure water appears to be colourless because of the low reflectance properties and the high transmission in the visible spectrum (400 - 760 nm). The reflectance decreases significantly at higher wavelengths in the visible range. The penetration of blue wavelengths (450 - 495 nm) is highest in pure water, whereas near infrared radiation (NIR) is completely absorbed by it. A yellow-brown colouration of the water body can be attributed to the presence of dissolved organic and/or particulate matter (SPM) as well as chlorophyll-a (Chl-a), which absorb the blue rays in the visible spectrum. (Mather & Koch, 2011).

Chl-a absorbs waves of different length spectra, which are mostly below 500 nm, between 640 and 690 nm and can even reach peak values around 560 and 710 nm. For this reason, sensors with a high spectral resolution are required for its detection (Ruddick et al., 2016). The reflection of wavelengths in the green range can be relatively high due to absorption and backscattering of dissolved organic and particulate matter in the water body. At high concentration, the signals in longer wavelengths increase due to the scattering of light. (Chen et al., 2014).

2.3.1 Satellite platforms

In this thesis, remotely sensed imagery from the Landsat 8 and Sentinel-2 platforms was used. The current generation of multispectral sensors aboard these satellites offers opportunities for synoptic and detailed surveillance applications in aquatic environments. Due to the improved (i) radiometric sensitivity (ii) spatial resolution (iii) overflight cycles as well as (iv) improved spectral configuration in the NIR range, satellites have been shown to be a particularly suitable tool for water resources surveillance (Gernez et al., 2017; Pahlevan et al., 2019).

Landsat 8 (L8) was launched on 11 February 2013, with normal operations starting on 30 May 2013. The repeat cycle of the ground orbit of L8 spans 16 days with an equatorial crossing time at 10:00 a.m. Scenes with three paths (66; 67; 68) cover the study area, with a repetition time of seven to nine days. The platform has two sensors: 1) Operational Land Imager (OLI) that measures eight multispectral bands in the visible, NIR and short-wave infrared (SWIR), which have a resolution of 30 m, and a panchromatic band with a resolution of 15 m; and 2) Thermal Infrared Radiometer Sensor (TIRS) that measures two bands with a spatial resolution of 100 m (Table 1) (USGS 2016). TIRS is sensitive to thermal infrared wavelengths and allows the separation of atmospheric and land surface temperature.

Table 1, Landsat 8 spectral bands, wavelengths, and spatial resolution.

Landsat-8 Bands	Spectral resolution (Micrometers)	Spatial resolution (Meters)
Band 1 - Ultra Blue (coastal / aerosol)	0.435 - 0.451	30
Band 2 - Blue	0.452 - 0.512	30
Band 3 - Green	0.533 - 0.590	30
Band 4 - Red	0.636 - 0.673	30
Band 5 - NIR	0.851 - 0.879	30
Band 6 - Shortwave Infrared (SWIR)1	1.566 - 1.651	30
Band 7 - Shortwave Infrared (SWIR)2	2.107 - 2.294	30
Band 8 - Panchromatic	0.503 - 0.676	15
Band 9 - Cirrus	1.363 - 1.384	30
Band 10 - Thermal Infrared (TIRS) 1	10.60 - 11.19	100
Band 11 - Thermal Infrared (TIRS) 2	11.50 - 12.51	100

Sentinel 2 satellites (S2) encompass Sentinel 2A and 2B, which move in a sun-synchronous orbit. The satellites support the monitoring of various environmental parameters. Sentinel-2A and 2B were launched in 2015 and 2017, respectively by the European Space Agency (ESA). Both satellites have a 10-day repetition cycle and are equipped with a Multispectral Instrument (MSI) sensor, which covers 13 spectral bands from blue to shortwave infrared and thus complements Landsat-8's OLI data (Table 2). Sentinel-2A and 2B include three bands in the visible- and one in the near infrared (NIR) spectrum with a spatial resolution of 10 m. The Red-Edge and SWIR bands have a resolution of 20 m. Water vapour, cirrus bands and aerosol have a spatial resolution of 60 m (USGS, 2017).

Table 2, Sentinel -2 spectral bands, wavelengths, and spatial resolution

Sentinel-2 Bands	Spectral resolution (Micrometers)	Spatial resolution (Meters)
Band 1 - Coastal / aerosol	0.0443	60
Band 2 - Blue	0.490	10
Band 3 - Green	0.560	10
Band 4 - Red	0.665	10
Band 5 - Vegetation Red Edge	0.705	20
Band 6 - Vegetation Red Edge	0.740	20
Band 7 - Vegetation Red Edge2	0.783	20
Band 8 - NIR	0.842	10
Band 8A - Vegetation Red Edge	0.865	20
Band 9 - Water vapor	0.945	60
Band 10 - SWIR- Cirrus	1.375	60
Band 11 - SWIR	1.610	20

3 Methods

Harvest and biological data were collected from Dolly Varden subsistence fisheries along the Yukon coast (HIQ and SPT). Parameters derived from satellite imagery and climatic records on temperature, turbidity, chl-a concentration, and wind were then combined with harvesting data to explore statistical relationships.

3.1 Dolly Varden catches and biological sampling

Data on the Dolly Varden harvest and biology were collected during the summer season from 2013 to 2019 (see Gallagher et al., 2013). Both harvest locations differed in the length of summer fishing seasons, with June – August on HIQ; and July to August on SPT respectively. On HIQ, the total harvest of Dolly Varden was conducted by rangers from Herschel Island Territorial Park located in Pauline Cove, (PC). On SPT, members from the Aklavik community spent the summer at the site to record the number of harvested Dolly Varden. Daily harvest numbers (count) as well as fork length (mm) and body weight (gram) per specimen were recorded by the harvesters at PC on HIQ (Fig. 6 a) and SPT (Fig. 6 b) respectively. (Fig. 6 b).

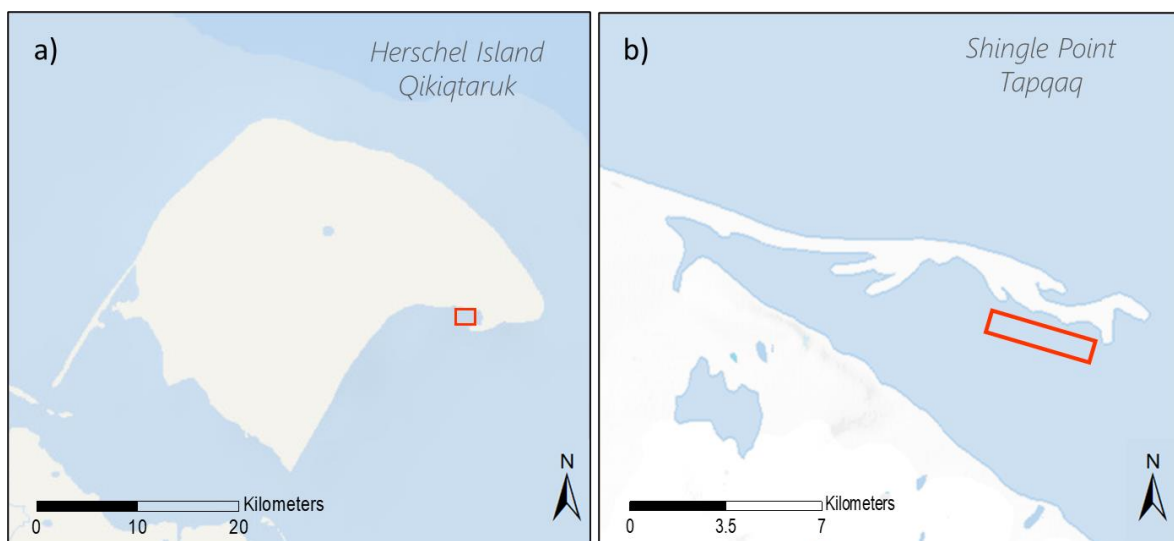


Fig. 6, Map of harvesting areas at both study sites a) Herschel Island Qiqiqtaruk, b) Shingle Point Tapqaq. Red rectangles represent the harvesting areas both respective study sites. Base map provided by Esri, Garmin, GEBCO, NOAA, NGDC and other contributors, retrieved from ArcGIS online.

To capture Dolly Varden, the harvesters used 25 m long gillnets with a mesh size of 3.5 - 4 inches (8.89 - 10.16 cm) for HIQ and 3 – 3.5 inches (7.62 – 8.89 cm) for SPT. Yet, as harvesting fell under the scope of the subsistence fishing culture of the rangers, it was primarily opportunistic and did not follow a systematic sampling strategy. This resulted in sampling times changing substantially from one day to the other. This also meant that harvesting did not occur on some days or that the duration of the net deployment could vary substantially from one day to another.

3.1.1 Fork length and weight

Subsistence fishers of the Inuvialuit communities in the region, have a great interest in understanding how environmental conditions affect the prevalence of large or small catches. The spatial distribution of Dolly Varden in marine waters strongly depends on the body size of the specimens, since a minimum size is required to cope with certain environmental fluctuations (i.e., salinity through osmoregulation, predation). To provide information on how environmental conditions might influence the size related distribution of Dolly Varden in the Beaufort Sea, the information on the fork length of harvested individuals was measured from the tip of the snout to the end of the middle caudal fin ray. Length was measured to the nearest mm (± 5 mm), round weight to the nearest 1 g. In situ, all biological measurements and samples were obtained from dead fish.

3.1.2 Condition factor

In fish, the relative fitness of a specimen can be described using the condition factor (K), as it reflects the extent of sexual maturity and the degree of nutrition (Sarkar et al., 2017). Being derived from the body weight of a fish specimen, K is a non-lethal morphometric index for estimating the physical fitness of fish specimens. Therefore, K assumes that larger individuals with higher body weights have better condition (Robinson et al., 2008), whereas male and female individuals peak at the onset of the spawning stage (Sarkar et al., 2017). In fact, a variety of factors can influence K values, including stress, sex, time of year, nutritional resource availability, and water quality (Ferdaushy & Alam, 2015). Being a quantitative parameter of ontogenetic well-being, it can provide insight into reproduction and survival, with the potential to be used to determine the current and future success of a population (Hossain et al., 2012). According to Anderson and Gutreuter (1983), the K value of a fish is determined as follows (Eq. 1):

$$K = \frac{W \cdot 10^5}{L^3} \quad (1)$$

where W equals to weight and L is length

3.2 Wind speed and - direction

Wind data was gathered from two different weather stations (Herschel Island; Komakuk Beach) and were acquired from the climate archive of the Canadian government (<http://climate.weather.gc.ca>). Data from Komakuk Beach were used when the station on Herschel Island failed (July 2013 and 2015). The weather is monitored on an hourly basis at both stations, thereby providing 24 data points per day. Hourly wind speed and direction were acquired for the entire summer (June – August) 2013 – 2019 apart from July 2018, as for that time no data was retrievable. Since wind direction, unlike wind speed, is not continuous data, a vector function was used to average the daily direction. Each data point is then transformed into a sine (Equ. 2 & 3) and cosine (Equ. 4 & 5) vector value, according to Grange (2014):

$$\vec{u}_i = -u_i * \sin \left[2 \pi * \frac{\theta_i}{360} \right] \quad (2)$$

$$\vec{u} = \frac{1}{n} \sum_{i=1}^n \vec{u}_i \quad (3)$$

$$\vec{v}_i = -u_i * \cos \left[2 \pi * \frac{\theta_i}{360} \right] \quad (4)$$

$$\vec{v} = \frac{1}{n} \sum_{i=1}^n \vec{v}_i \quad (5)$$

Where \vec{u}_i and \vec{v}_i are the respective wind components for the x and y axis, u_i is the point specific wind speed while the negative sign negates the direction from where the wind is blowing. θ_i account for the point specific wind direction in degrees, being transformed into radians. \vec{u} and \vec{v} are the respective mean values of the 24 daily data point.

To calculate the resultant vector average wind speed ($|\vec{V}|$) and meteorological -direction angle (Φ) Equ. 6 and Equ. 7 were applied:

$$|\vec{V}| = \sqrt{\vec{u}^2 + \vec{v}^2} \quad (6)$$

$$\Phi = \arctan \left(\frac{\vec{u}}{\vec{v}} \right) + \text{windflow} \quad (7)$$

$$\text{windflow} = +180 \text{ for } \arctan \left(\frac{\vec{u}}{\vec{v}} \right) < 180$$

$$\text{windflow} = -180 \text{ for } \arctan \left(\frac{\vec{u}}{\vec{v}} \right) > 180$$

3.2.1 Sea ice coverage

Both, traditional knowledge of the Inuvialuit and previous studies document a correlation between sea ice and fish harvest (Byers et al., 2019; Gallagher et al., 2021). The interest was focused on the effect of drifting sea ice on the summer distribution of marine fish. After the breakup of the ice cover in spring, the sea remained ice-free in summer, except for singular events of drift ice in July and August. Accordingly June was neglected from the analysis. The sea-ice concentration (SIC) estimates were derived from satellite images. As ice cover varied between locations, areas were divided into four subareas (SIC-N, SIC-E, SIC-S, and SIC-W). Each of the respective subareas had different marine surface areas given differences in their overlap with the land (Table 3). To determine the average abundance of sea ice cover, a circular area of interest with a radius of 20 km was drawn around HIQ and SPT (Fig. 7).

Table 3, Surface size (m^2) of the four respective sampling areas at HIQ and SPT. The sampling areas are listed in the respective to clockwise ordination.

Area	Shingle Point	Herschel Island
	size (km^2)	size (km^2)
SIC-N	302	258
SIC-E	123	331
SIC-S	1.7	142
SIC-W	214	153

The percent coverage of ice was determined visually for each of the four subareas according to the methods of Timco and Johnston (2003). In contrast to a relatively temporally homogeneous ice cover in June among sampling years, notable differences were apparent for the months of July and August.

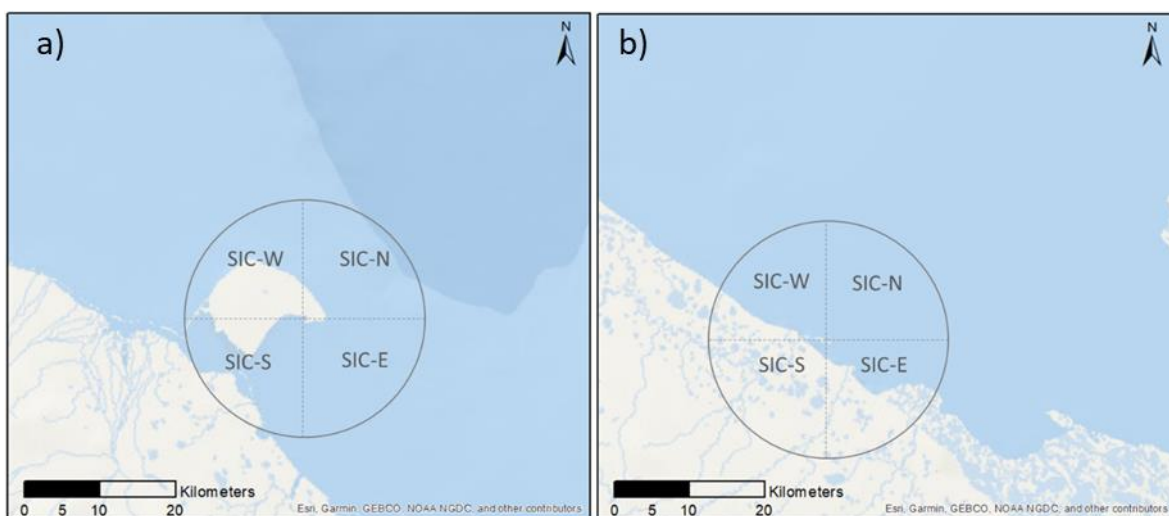


Fig. 7, Sampling areas on sea ice abundance (%) at the two-harvesting sites a) Herschel Island Qikitaruk and b) Shingle Point Tapqaq. .

3.3 Remote sensing

3.3.1 Image selection

Orthorectified OLI data (Level1) were retrieved from Earth Explorer (<https://earthexplorer.usgs.gov/>) provided by the United States Geological Survey USGS and MSI data (Level-1C) were retrieved from the Copernicus Open Access Hub (<https://scihub.copernicus.eu>) provided by the European Space Agency (ESA) Copernicus. The imagery was obtained in the Level 1 Product Generation and provided in Georeferenced Tagged Image File Format (GeoTIFF) with UTM projection and WGS84 datum. For the summer season (2013 – 2019), a total of 94 scenes were available with a cloud cover $\leq 30\%$ (Appendix I). It is important to note that based on the harvest months, satellite images for HIQ span the months of June - August whereas SPT only covers the months of July and August.

3.3.2 Radiometric Calibration and Atmospheric Correction

Satellite products (L8 and S2) were provided as calibrated top-of-atmosphere reflectance. As satellite sensors record the electromagnetic radiation of every pixel as a digital number (DN), these numbers are converted into units such as radiance, reflectance, or brightness temperature. The calibration is executed regarding factors such as sensor noise, brightness of pixels and geometric features (view- and zenith angle). According to Nazeer et al. (2014) the conversion is expressed as the following (Equ. 8):

$$p\lambda = \frac{M_p Q_{cal} + A_p}{\cos(\theta_{sz})} \quad (8)$$

Where $p\lambda$ is the top of atmosphere (TOA)-reflectance, θ_{sz} is the local zenith angle; $\theta_{sz} = 90^\circ - \theta_{SE}$, θ_{SE} is the local sun elevation (given in the metadata), M_p stands for the Band-specific multiplicative rescaling factor while A_p is the Band-specific additive rescaling factor which both are taken from the metadata. Q_{cal} is the quantized and calibrated standard product pixel value.

Spectral remote sensing reflectance ($R_{rs}(\lambda)$) is primarily used to generate higher level products over open water and can be derived from TOA and water leaving reflectance (p_w). Measurements in the ocean colour spectrum can be used to characterize water quality such as turbidity and chl-*a* (Chl-*a*) concentration (O'Reilly et al., 1998). Reflectance in the blue and green wavelength spectrum are used to estimate the Chl-*a* concentration (Franz et al., 2015) while reflectance in the red wavelength estimates suspended particulate matter (Vanhellemont & Ruddick, 2014). Therefore, according to Mobley (1999), $R_{rs}(\lambda)$ can be defined as $p_w(\lambda)$, which is corrected for bidirectional effects and normalized by downwelling solar irradiance ($E_d(\lambda)$) above the sea surface (Equ. 9).

$$R_{rs}(0, \Phi, \lambda) = \frac{p_w(0, \Phi, \lambda)}{E_d(\lambda)} = \frac{p_w(\lambda)}{\pi} \quad (9)$$

Where $R_{rs}(\lambda)$ is the remote sensing reflectance (sr^{-1}), $p_w(\lambda)$ accounts to the water leaving reflectance; $E_d(\lambda)$ is the downwelling irradiance occurring on the sea surface and $\pi = 3.142$. 0 and Φ specify the polar and azimuthal directions.

The satellite sensors that record the electromagnetic radiation also measure the reflection of the object of interest as well as the effects of the atmosphere. Therefore, to measure the surface reflectance of an object of interest, atmospheric correction (AC) is necessary as it removes the effects of scattering and absorption.

ACOLITE is a freely available software which was developed by the Royal Belgian Institute of Natural Sciences (RBINS). It was designed to process Landsat (5/7/8) and Sentinel-2 (A/B) imagery data primarily. The software encompasses preconfigured atmospheric correction algorithms. It was designed for the purpose of quantifying inland and marine water properties, making it applicable to study sediment fluxes or algal blooms in the water body (Davis et al., 2016). The downloaded files were the acquired Level 1 L8/S2 images that included the calibrated TOA reflectance of all spectral bands (Pahlevan et al., 2017).

AC for remote sensing reflectance ($R_{rs} \lambda$) was performed with the ACOLITE software (version 20190326.0). In this thesis, Dark Spectrum Fitting (DSF) was executed as a standard AC-method in Acolite. DSF is specifically developed for aquatic applications of Landsat and Sentinel-2 imagery (Vanhellemont & Ruddick, 2018). The DSF method on L8 and S2 imagery is an adapted method for aquatic applications, which encompasses an automated tiled procession for the complete satellite scene and an optional scene-based glint correction (Vanhellemont, 2019). The approach of the AC is that it uses various dark targets in the subscene to create a "dark spectrum" that is then used to derive the atmospheric path reflectance (ρ_{path}) according to the best-fitting aerosol model. The best-fitting band which yields the lowest ρ_{path} is then chosen automatically (Vanhellemont, 2019).

3.3.3 Retrieval of Chlorophyll- a

Chl-a concentration ($\mu\text{g/l}$) was retrieved by applying the widely tested Ocean Chlorophyll algorithm at three $R_{rs}(\lambda)$ (OC 3) by O'Reilly et al. (1998). The ratios of the maximum of the two blue bands ($R_{rs} \lambda$ 443 or 490 nm) and the green bands ($R_{rs} \lambda$ 560 nm) are related to Chl-a concentration ($\mu\text{g/l}$) with a fourth-order polynomial relationship. Alternatively, the red and NIR bands are applied over highly turbid waters to estimate Chlorophyll (Franz et al., 2014) (Equ. 10):

$$\log_{10}(\text{chl } a) = a_0 \sum_{i=1}^4 a_i \left(\log_{10} \left(\frac{R_{rs}(\lambda \text{ blue})}{R_{rs}(\lambda \text{ green})} \right) \right)^i \quad (10)$$

Where a_0 and a_i are sensor specific coefficients, and $R_{rs}(\lambda \text{ blue})$ and $R_{rs}(\lambda \text{ green})$ are the greatest of values from 443 > 483 and 555 nm, respectively, on the OLI/ MSI sensors aboard Landsat 8 and Sentinel-2

3.3.4 Turbidity

The atmospheric corrected water-leaving reflectance (p_w) was transformed into turbidity as Formazin Nephelometric Unit (FNU) by ACOLITE using the algorithm of Dogliotti et al. (2015). Being an inherent optical property, with no response to the ambient light field, FNU is better attributed to the bio-optical models that underlie many remote sensing approaches (Dogliotti et al., 2015) whereby it is measured with an infrared light source. Since the algorithm is primarily based on the approach that water surface reflectance increases with greater particle load in the water column which shifts to the red or near-infrared range (Giardino et al., 2017) so the purpose particle load can be estimated (Ruddick et al., 2006).

The algorithm assumes that particulate backscattering is equivalent to turbidity. Turbidity is the measure of the proportion of the scattered light at a 90° angle to forward transmitted light at 860 nm in comparison to the equivalent proportion of the Formazin suspension (Nechad et al., 2010). The p_w is associated with optical properties such as the reflection and refraction of the water surface, and the proportion between the water-leaving and down welling radiance. These properties are related to absorption and backscattering of radiation, which are expressed by particulate and non-particulate contribution. Since the non-particulate backscatter in turbid water is negligible, the turbidity specific absorption and backscatter results in the ratio between particulate contribution and turbidity (Nechad et al., 2009). The relationship between turbidity (T) and water reflectance (w_p) is established according to Dogliotti et al. (2015) (Equ. 11):

$$T = \frac{A_T \rho_w(\lambda)}{(1 - \rho_w(\lambda) / C^\lambda)} \text{ [FNU]} \quad (11)$$

Where the A_T and C are two wavelengths that are dependent to calibration coefficients, C is determined by applying inherent optical properties, and A_T is in situ measurements of turbidity derived from a non-linear regression. When the reflectance ρ_w is less than 0.05, which equals a turbidity < 15 FNU, the red band is used. For reflectance > 0.07 and turbidity > 45 FNU, the NIR band is applied (Dogliotti et al., 2015).

3.3.5 Retrieval of suspended particulate matter (SPM)

To convert $p_w(\lambda)$ into suspended particulate matter (SPM), ACOLITE applies bio-optical algorithms that are subject to the NIR spectral range according to Nechad et al. (2010). As the reflectance increases with growing SPM concentration, longer wavelengths are applied for high concentrations and shorter wavelengths for low or moderate concentrations (Nechad et al., 2010). The particulate backscattering is predicted to be equivalent to the SPM aggregation with an additional fixed specific particulate backscattering coefficient. The coefficients demonstrate a spectral magnitude of variation that is subject to the size and composition of the particles. Therefore, backscattering in the green, red, and NIR spectrum is influenced by particulates (Nechad et al., 2010). Two wavelengths depending on calibration (Equation 12 and 13) coefficients are part of the formula, which are derived from inherent optical properties:

$$A = \frac{a_{np}}{b_{bp}^*} \quad (12)$$

Where A is the ratio of non-particulate absorption (a_{np}) to the particulate backscattering (b_{bp}^*) coefficient

$$C = \frac{b_{bp}^*}{a_p^*} \quad (13)$$

C is the ratio of particulate backscattering coefficient (b_{bp}^*) to the particulate absorption coefficient (a_p^*).

SPM concentration (g/m^3) can then be calculated according to the following equation of Nechad et al. (2010) (Equ. 14):

$$SPM = \frac{A^p * \rho_w(\lambda_0)}{(1 - \rho_w(670)) / C^p} + B^p \quad (14)$$

Where $\rho_w(\lambda_0)$ is the water leaving reflectance and A^p is the ratio of non-algal particulate absorption to the specific particulate backscattering coefficient (b_{bp}/SPM). C is the ratio of b_{bp}/SPM to the specific particulate absorption, (a_p/SPM) A^p (g/m^3) and C^p (dimensionless) are related to the inherent optical property (IOP). B^p describes uncertainties in the measurements.

3.3.6 Retrieval of brightness Temperature

There is a strong positive correlation between the extent of radiant flux radiated by an object and its true kinetic temperature. Accordingly, the radiant temperature of an object can easily be determined by remotely placed radiometers. Yet, there are stray light issues associated with the two TIRS bands (Band 10 and Band 11) due to the curvature of the optical lens (Montanaro et al., 2014). Thermal Infrared Sensor (TIRS) Band 10 was used given its higher accuracy compared to band 11 (Barsi et al., 2014). Thermal infrared image data from Landsat satellites are only available as L1T data product, as they are not provided with AC by USGS. Therefore, according to Wukelic et al. (1989), the conversion from digital numbers (DN) to spectral radiance (L_λ) (Equ. 15) was computed beforehand executing the calculation of brightness temperature (BT, [K]) (Equ. 16):

$$L_\lambda = L_M * DN + L_A \quad (15)$$

$$BT[^\circ C] = K_2 * \left[\ln \left(\frac{K_1}{L_\lambda} \right) + 1 \right] - 273,15 \quad (16)$$

Where L_M and L_A are the radiance multiplier and radiance add, $K_2 = 774.89$ [$W / (m^2 * sr * \mu m)$] and $K_1 = 1321.08^\circ K$ are thermal constants provided by Landsat Metafile (MTL), and L_λ is the spectral radiance exiting the top of the atmosphere. To retrieve brightness temperature as $^\circ C$, 273.15 units were subtracted.

3.3.7 Sample design at study site

The remote sensing images were obtained from the area where harvesting occurred. To examine the influence of marine habitat properties on Dolly Varden (e.g., influence of the Mackenzie River plume and upwelling areas), areas of interest (AOI) were delineated in the vicinity of the harvesting locations.

For both study sites, the AOIs were divided into Near (N-area) and Far (F-area) subclasses, with the subclasses distinguished in their surface area and distance from the sampling site. There is evidence from previous studies that hydrodynamic variability is greater in the coastal zone than in open waters, (e.g., Klein et al., 2019; Asplin et al., 2020), thus the N- and F-areas differed in shape and size in order to be able to record the best possible signal in the coastal- and offshore areas. In total, 10 AOIs (1 harvesting site; 4 N-area; 5 F-Area) were selected randomly location-based around HIQ and SPT (Fig. 8). The AOIs varied in their area size and distance from shore, respective to their subclass. Regarding the resolution of Landsat 8 (30 m) and Sentinel 2 (10 m), the AOIs were drawn at a distance of at least 7 (L8) and 20 (S2) pixels (200 m) off the coastline to avoid mixing of terrestrial and aquatic pixels (Klein et al., 2019). Overall, N- areas were drawn in distance to coast of at least 150 - 500 m (HIQ) and 500 - 1500 m (SPT), while the F-areas were drawn to extract offshore information (distance ≥ 10 km; ≤ 30 km).

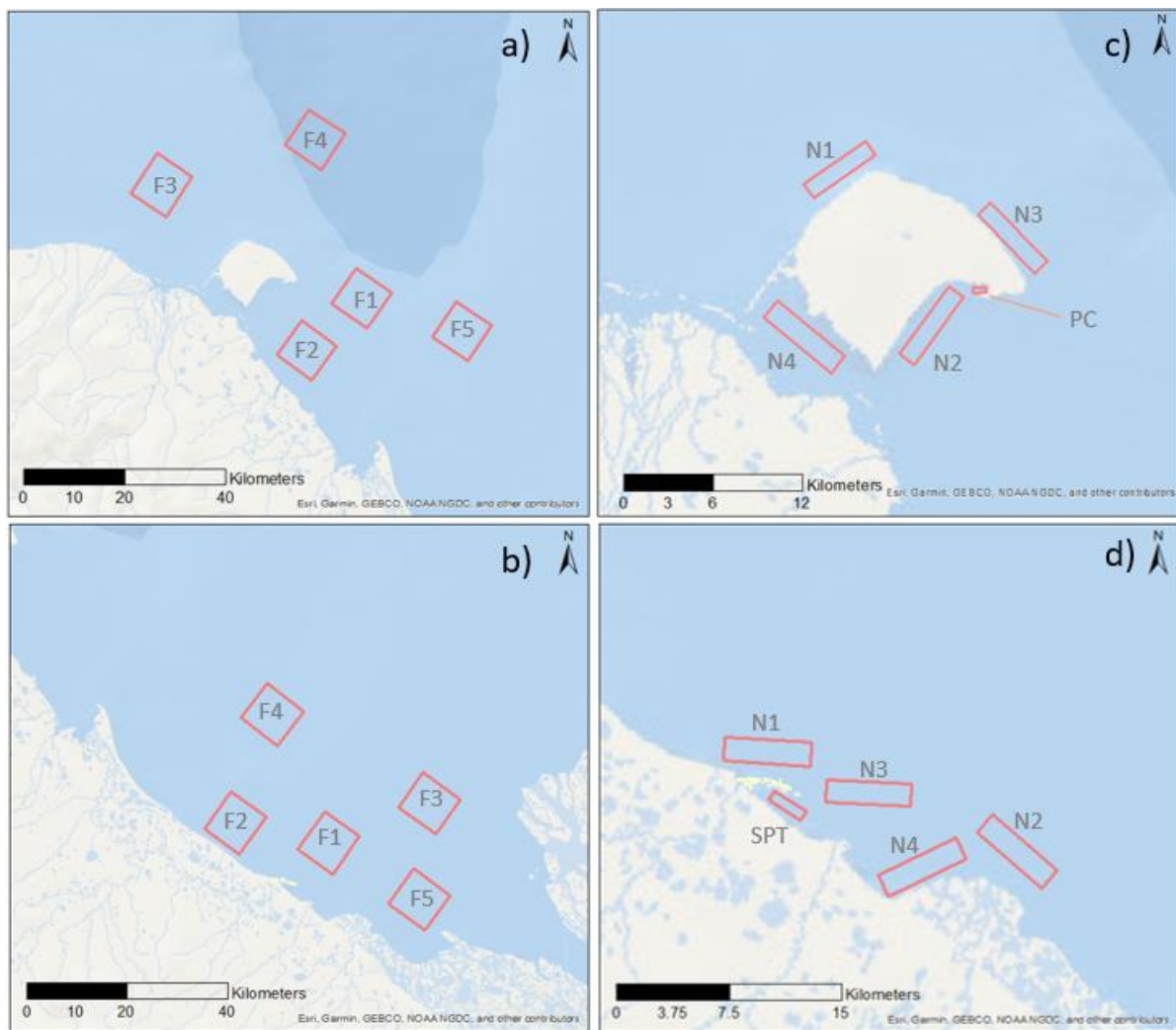


Fig. 8, Areas of interest (AOIs) divided into Near (N-area) and Far (F-area) subclasses for both research locations Whereas a) and b) illustrate the the F-Area subclasses (F1 – F5) for both research areas c) and d) depict the N-Area (N1 – N4 plus PC/SPT) subclasses of HIQ and SPT respectively

Each AOI contained randomly distributed sampling points to extract pixel values of environmental parameters (Table 4). The random point function in the spatial analyst toolbox in ArcMap 10.7.1 was used to draw random sampling points within the areas of interest. To ensure that the sampling points were homogeneously distributed in the respective AOIs, a minimum distance (F-areas (200 m), N-areas (100 m) and harvesting area (50 m)) was set for the sub-categorical areas between the individual points.

Subsequently, the multi-value to point function in ArcMap was used to extract parameter values at each sampling point. The attribute tables were then exported as .txt and processed in RStudio (1.4.1103) for statistical analysis.

Table 4, Areas of interest size (m²) of HIQ and SPT (Near vs. Far). The subareas are listed in the respective category in the numbers from 1 to 5, additionally the number of extraction points per area is listed.

Area		Shingle Point	Herschel Island	No. of sampled points
		size (km ²)	size (km ²)	
Near	1	8.25	8.25	100
	2	8.25	8.25	100
	3	8.25	8.25	100
	4	8.25	8.25	100
	Harvest site	1.75	0.27	75
Far	1	76.5	76.5	250
	2	76.5	76.5	250
	3	76.5	76.5	250
	4	76.5	76.5	250
	5	76.5	76.5	250

3.4 Data transformation and statistical analysis

Dolly Varden harvest, condition, and length were examined for inter-annual variation among months (June - August) and between sampling sites. In addition, factors were analysed for relationships with environmental parameters wind and ice cover and remote sensing data BT, Chl-a, turbidity, and SPM.

Data were tested for deviation from normality using a Shapiro-Wilk test and variance of homogeneity using Levene's test. Differences were accepted as statistically significant on an α level of 0.05. The results were reported as mean \pm standard deviation (SD). All statistical analyses and tests were performed according to (Zar, 1999) and using Microsoft Office Excel 365 and RStudio (1.4.1103).

3.4.1 Testing Dolly Varden parameters

Given the residuals were normally distributed, Dolly Varden variables condition factor and fork length were tested on statistical inter-annual differences using a One Factorial Variance Analysis (ANOVA). In case where the assumption of normal distribution was violated, a Kruskal-Wallis test was used instead. The temporal scale uses the number of calendar days in the summer season from June to August where the 1st of June corresponds to "day 1" and the 31st of August corresponds to "day 92".

3.4.2 Regression Analysis (Wind and Ice)

A multiple linear regression (MLR) analyses was applied to test the assumption that Dolly Varden harvest, fork length and condition at both harvesting sites were affected by wind vectors (direction and speed) and ice coverage. All variables were range-transformed to normalize the data. To remove wind-days that did not significantly explain residuals of the response variables, an automatic stepwise selection procedure was applied. This procedure yielded an analysis encompassing wind speed and direction 0, 24 and 48 hours prior to harvest day at both points (HIQ and SPT). Selection of explanatory variables was based on an α level of 0.05 (two-sided tests). Non-significant interaction terms were removed before testing.

3.4.3 Environmental remote sensing parameters

The values of the environmental parameters of the satellite images were extracted for each AOI. The centred and scaled environmental variables of each AOI were compared then intra- and inter-annually. Additionally, environmental parameters were tested on the area subclasses between geographical harvest site locations (HIQ vs. SPT) by applying an independent samples

T-test. In cases when the assumption of normal distribution was violated, a Mann-Whitney-U-Test was used.

3.4.4 Redundancy Analysis (RDA)

A redundancy analysis (RDA) was performed for both harvesting sites (HIQ and SPT) separately to assess which environmental factors significantly explained variations in Dolly Varden harvesting numbers, somatic condition, and size. Prior to the analysis, all variables were range-transformed to normalize the data. The main axes (components) were constrained to be linear for the best combinations of the environmental variables (Ramette & Tiedje, 2007), and multiple regressions were used to model variations between environmental- (explanatory) and Dolly Varden (response) variables. The statistical significance of the RDA was tested with 1000 permutations (α level 0.05). The environmental data used for the RDA were a combination of wind, sea ice cover as well as AOI respective remote sensing derived parameters (BT, Chl-a, turbidity, and SPM). To remove environmental variables that did not significantly explain residuals variations of the response variables, an automatic stepwise selection procedure was applied (Legendre & Legendre, 2012). This approach resulted in a reduced RDA, containing of the environmental variables with the strongest statistical influence on the variance of the Dolly Varden parameters. Statistical analyses were executed using the vegan packages of the RStudio (1.4.1103).

4 Results

The results for HIQ and SPT are presented separately where I report on sampling areas first, followed by the results of the fish parameters and the influence of wind and ice cover. Finally, the environmental parameters derived from the remote sensing presented.

4.1 Harvesting numbers

4.1.1 Herschel Island

A total of 2107 Dolly Varden were caught among 644 harvesting days over the summers of 2013 - 2019 (210 days in June; 217 days each in July and August). The numbers were highly variable among summer months. A peak in harvest numbers was observed between mid- and end of July (day 30 – 60) with a total number of 1168 fish harvested during this month. The total numbers for June and August were 344 and 605 Dolly Varden, respectively (Fig. 9). The annual harvest numbers were highest in 2018 (n = 619 fish) and lowest in 2013 (n = 188 fish) and 2014 (n = 189 fish).

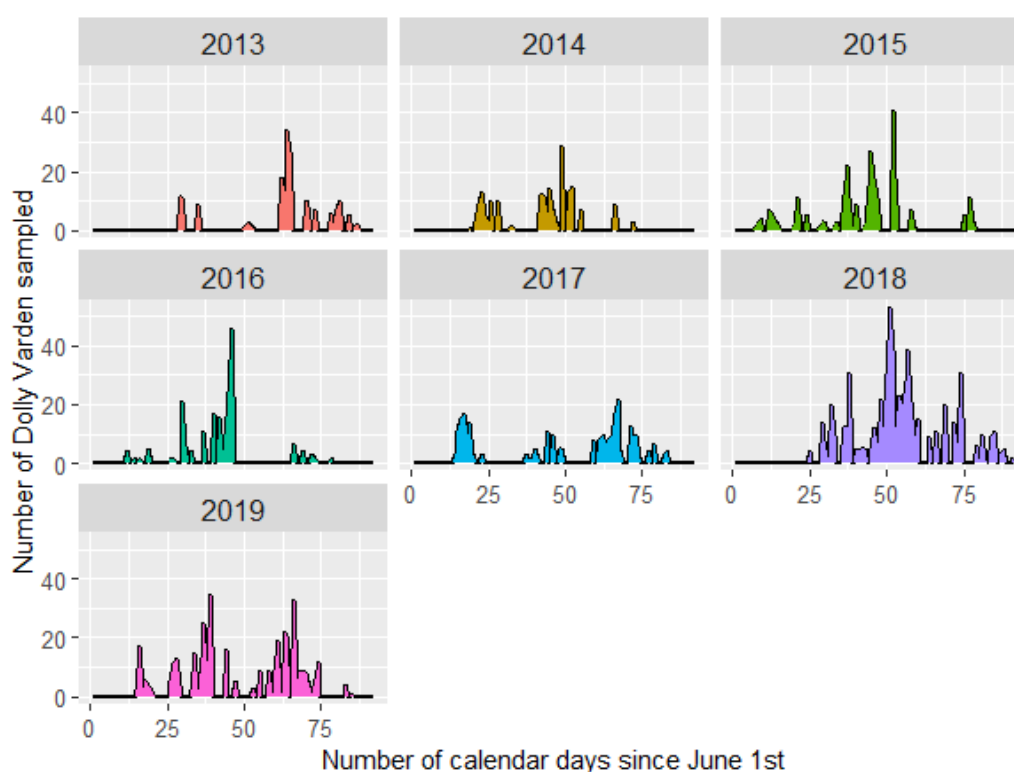


Fig. 9, Seasonal harvesting numbers of Dolly Varden (*S. malma malma*) at Herschel Island Qiqiktaruk (HIQ) in dependence of the calendar day (starting 1st of June) throughout sampling years (2013 – 2019.)

4.1.2 Shingle Point

A total 1433 Dolly Varden were caught on 109 harvesting days among the summers of 2013 - 2019 (82 days in July and 27 days in August). The numbers were highly variable between months. A peak in harvesting numbers was typical between mid- and late-July (day 30 – 60) with a total number of 1207 fish harvested during this month. The harvest in August was 226 fish (Fig. 10).

The annual harvest was highest in 2014 ($n = 419$) whereas the lowest was in 2018 ($n = 47$). Years 2017 and 2019 had a total reported harvest of 147 Dolly Varden.

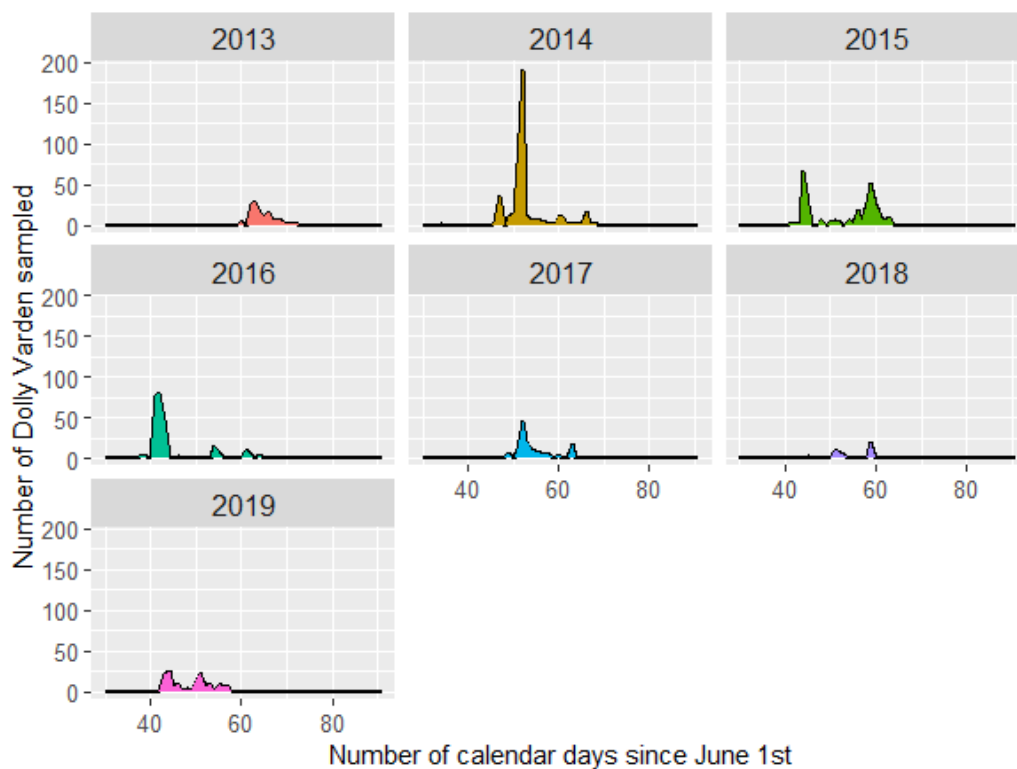


Fig. 10, Seasonal harvesting numbers of Dolly Varden (*S. malma malma*) at Shingle Point Tapqaq (SPT) in dependence of the calendar day (starting 1st of June) throughout sampling years (2013 – 2019).

4.2 Fork length

4.2.1 Herschel Island

The size of Dolly Varden at HIQ was highly variable over the summer. On average, greater lengths were recorded in June (579.56 ± 83.66 mm), followed by August (565.34 ± 90.79 mm) and July (559.05 ± 86.01 mm). The average fork length was significantly different among months ($F_{2,1433} = 4.49$, $p = 0.01$). The Tukey HSD post-hoc test showed a statistically significant difference between June and July. Annually, the greatest length observed in June (day 1 – 30) was in 2018 (609.55 ± 42.65 mm) whereas the lowest values were in 2019 (565.49 ± 100.18 mm). However, no statistically significant difference was found among the sampling years ($F_{6,183} = 1.36$, $p = 0.232$) (Fig. 11).

In July (day 31 - 62), the greatest lengths were in 2013 (586.67 ± 59.9 mm) and 2017 (584.14 ± 74.81 mm) while 2014 had the lowest mean values for July (525.16 ± 89 mm). The Tukey HSD post-hoc test revealed that the year 2013 and 2017 were statistically significant different to 2014 ($F_{6,822} = 4.71$, $p < 0.001$).

In August (day 63 – 94), the highest mean value was in 2017 (584.54 ± 89.37 mm) and 2019 (582.61 ± 81.88 mm) whereas the lowest mean values were in 2014 (510 ± 79.29 mm) and 2013 (512.89 ± 78.6 mm).

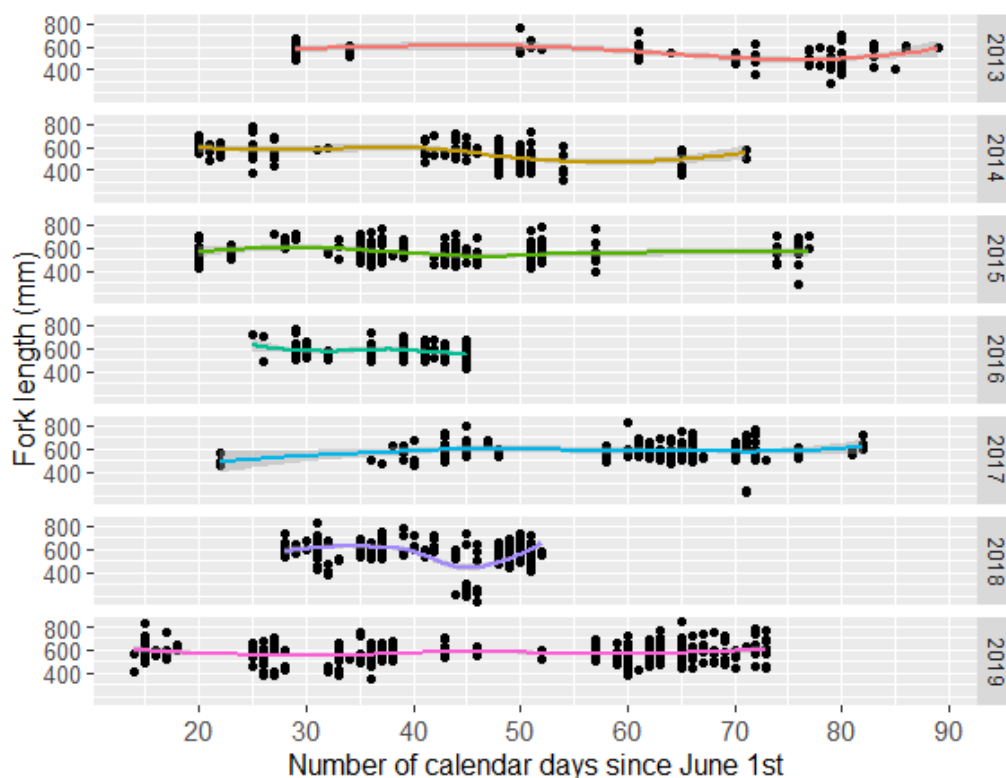


Fig. 11, Average fork length (mm) of Dolly Varden (*S. malma malma*) throughout the summer season among sampling years at Herschel Island Qiqiktaruk (HIQ). The dots represent individual samples, whereas the coloured line represents the mean value trend throughout the season.

4.2.2 Shingle Point

Similar to HIQ, the fork length of Dolly Varden harvested at SPT fluctuated over the sampling months. Dolly Varden harvested in July (497.52 ± 70.93 mm) had a greater average length than the ones harvested in August (475.87 ± 68.89). Accordingly, a statistically significant difference was found in the fork length between both sampling months ($t_{(1411)} = 4.32, p < 0.001$).

A peak in distribution of fork length is typically reached in mid-July (day 40 – 50), with a decreasing trend towards the end of the season (day 65 - 70) (Fig. 12).

In July (day 31 - 62), the highest length values were in 2013 (586.67 ± 59.9 mm) and 2017 (584.14 ± 74.81 mm) while 2014 had the lowest mean values for July (525.16 ± 89 mm). The Tukey post-hoc test revealed that the year 2013 and 2017 were statistically significant different compared to 2014 ($F_{6,822} = 4.71, p < 0.001$).

In August (day 63 – 94), the highest mean length value was in 2017 (584.54 ± 89.37 mm) and 2019 (582.61 ± 81.88 mm) whereas the lowest mean values were in 2014 (510 ± 79.29 mm) and 2013 (512.89 ± 78.6 mm).

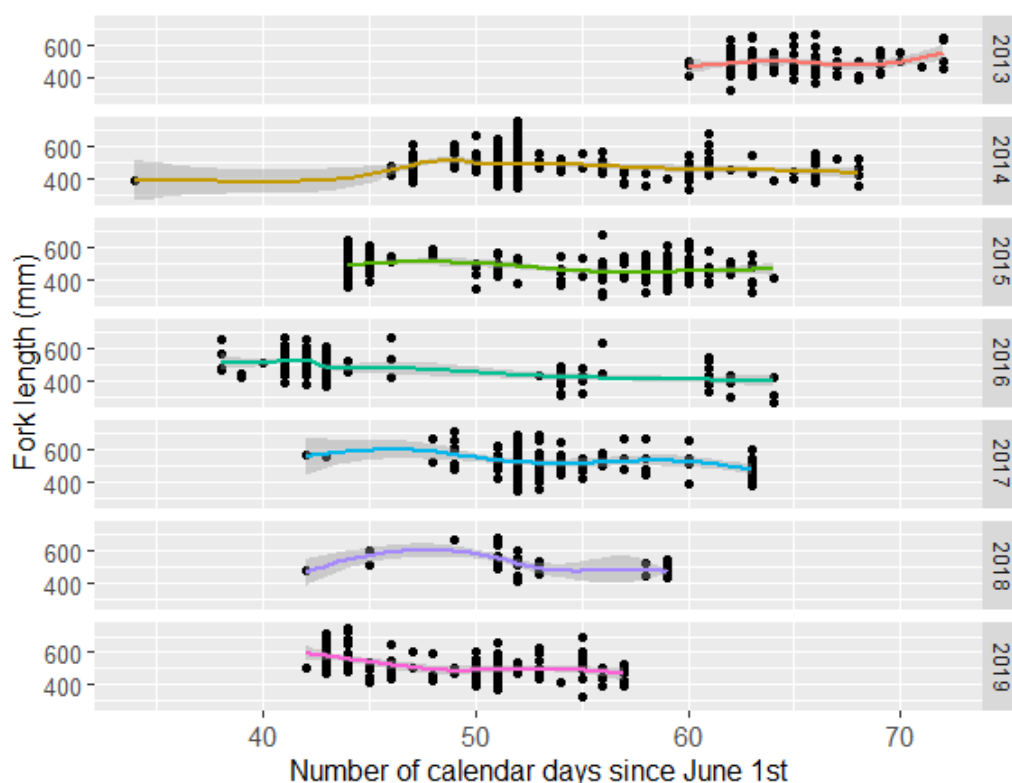


Fig. 12, Average fork length (mm) of Dolly Varden (*S. malma malma*) throughout the summer season at Shingle Point Tapqaq (SPT) per sampling year (2013 – 2019). The dots represent the length of individual fish, whereas the coloured line represents the mean value trend throughout the fishing season.

4.3 Condition factor

4.3.1 Herschel Island

The condition factor of Dolly Varden harvested at HIQ demonstrated a steady increase over the summer. Whereas in June (day 0-30) fishes had an average K of 0.87 ± 0.16 , in July (day 31-62) the K rose to 1.07 ± 0.18 and reached highest recorded values in August (1.17 ± 0.27). However, the different sampling years had differences in their respective monthly average values.

For June, the highest values were recorded in 2016 (1.01 ± 0.12) while 2014 (0.77 ± 0.6) had the lowest K. The Tukey Post-hoc test showed a significant difference between years 2014 and 2016 ($F_{6,183} = 8.95$, $p < 0.001$).

For July, the highest values were recorded in 2015 (1.15 ± 0.18) while 2013 (0.94 ± 0.08) and 2018 (0.99 ± 0.18) had the lowest K values. Comparing the entire sampling years, the post hoc showed a significant difference between the years 2015 as well as 2013 and 2018 ($F_{6,822} = 15.08$, $p < 0.001$).

For August, the highest mean value was in 2015 (1.35 ± 0.16) whereas the lowest was in 2014 (1.14 ± 0.08). Regarding the Tukey Post-hoc the only statistically significant difference between the 2015 and 2014 ($F_{4,346} = 2.68$, $p = 0.03$) (Fig. 13).

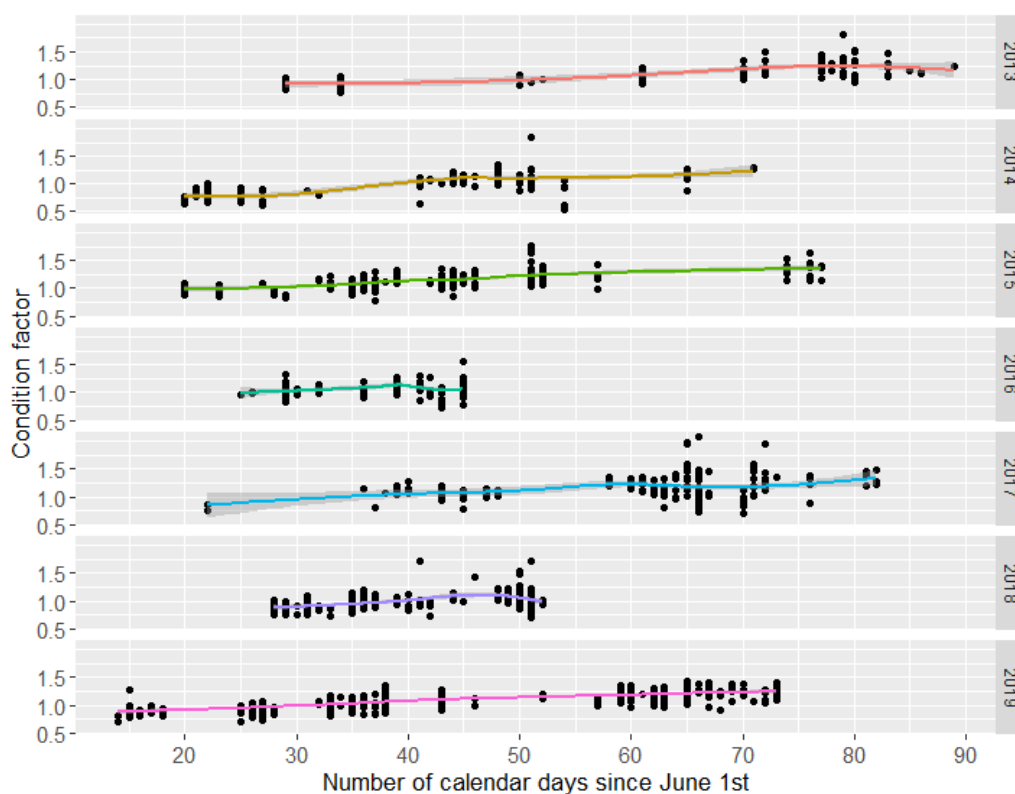


Fig. 13, Average condition factor of Dolly Varden (*S. malma malma*) throughout the summer season among sampling years at Herschel Island Qiqiktaruk (HIQ). The dots represent taken samples, whereas the coloured line represents the mean value trend throughout the season.

4.3.2 Shingle Point

Similar to HIQ, fish condition at SPT increased over the summer season. In July (day 31 - 62) the K had a mean (\pm SD) value of 1.07 ± 0.18 and increased to 1.17 ± 0.27 in August. The sampling years however showed differences in their monthly average values (Fig. 14).

For July, the highest average values were recorded in 2018 (1.07 ± 0.09) while 2014 (0.72 ± 0.27) had the lowest K. Sampling year demonstrated a significant difference in Dolly Varden K. As a result of the strongest deviation from the interannual mean values, the post-hoc test revealed a significant difference in July values between the years 2014 and 2018 ($F_{5, 64} = 3.35$, $p = 0.009$).

For August, the highest mean value was in 2016 (1.19 ± 0.06) whereas the lowest mean value was in 2014 (0.73 ± 0.4). The Tukey Post-hoc Test found no interannual statistically significant difference in the fork length of Dolly Varden caught in August at SPT ($F_{3,19} = 1.98$, $p = 0.15$).

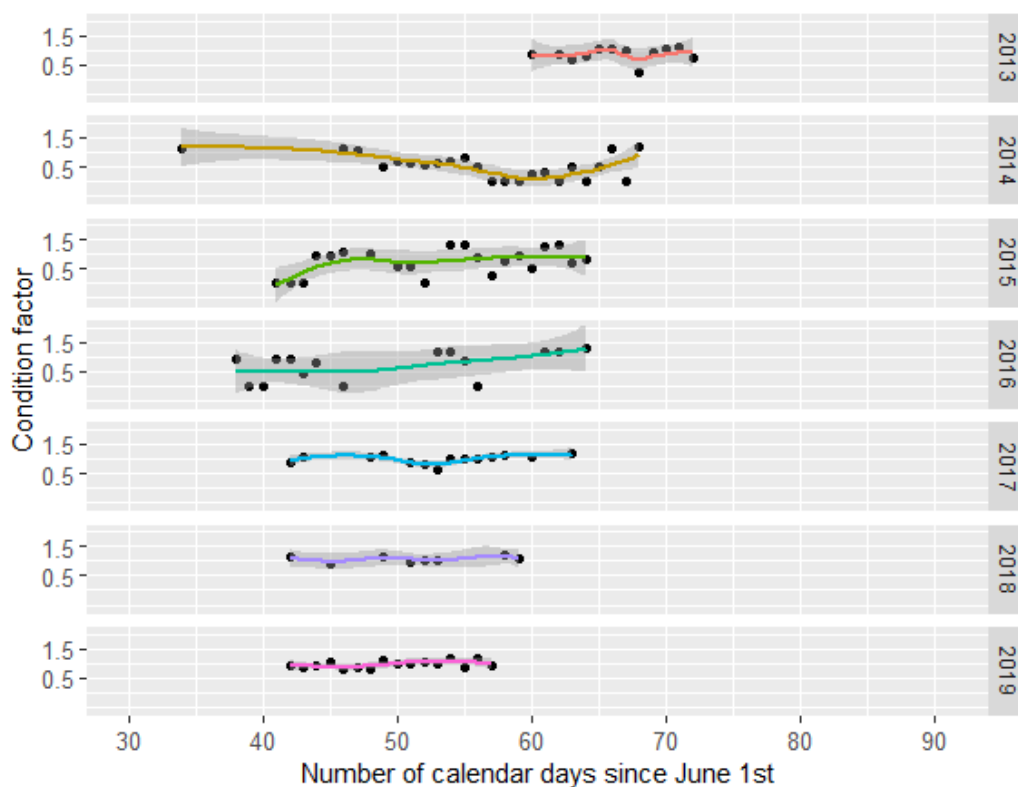


Fig. 14, Average condition factor of Dolly Varden (*S. malma malma*) throughout the summer season around Shingle Point Tapqaaq (SPT). The dots represent individual fish, whereas the coloured line represents the mean value trend throughout the fishing season. The seasonal trends in the fork length are sorted by the individual sampling years (2013 - 2019).

4.4 Wind directions and speed for HIQ and SPT

A total of 610 data points (June n= 207, July n= 187, August n= 216) during the study period (2013 - 2019) was included to the analysis (Fig. 15).

For all three months, winds were primarily blowing from E-SE and W - NWN cardinal direction. The average wind speed was considered moderate (17.02 ± 7.6 km/h). June had an average wind speed of 16.39 ± 7.02 km/h, primarily from the E - ESE cardinal direction. The highest speed values (38.26 km/h) blew from W - NW, with minimum values (3.88 km/h) recorded from all directions. July had an average wind speed of 17.44 ± 7.14 km/h typically from NW and ESE. The maximum speed was 39.16 km/h while the lowest was 4.33 km/h. Like June, the highest speed values blew from the NW in July, with the low values showing no specific direction. August showed an average wind speed of 17.26 ± 8.46 km/h primarily from E - SE, WSW - W and NW. The highest speeds reached values up to 48.42 km/h, which blew from WSW - W direction. The lowest values had speeds up to 5.67 km/h.

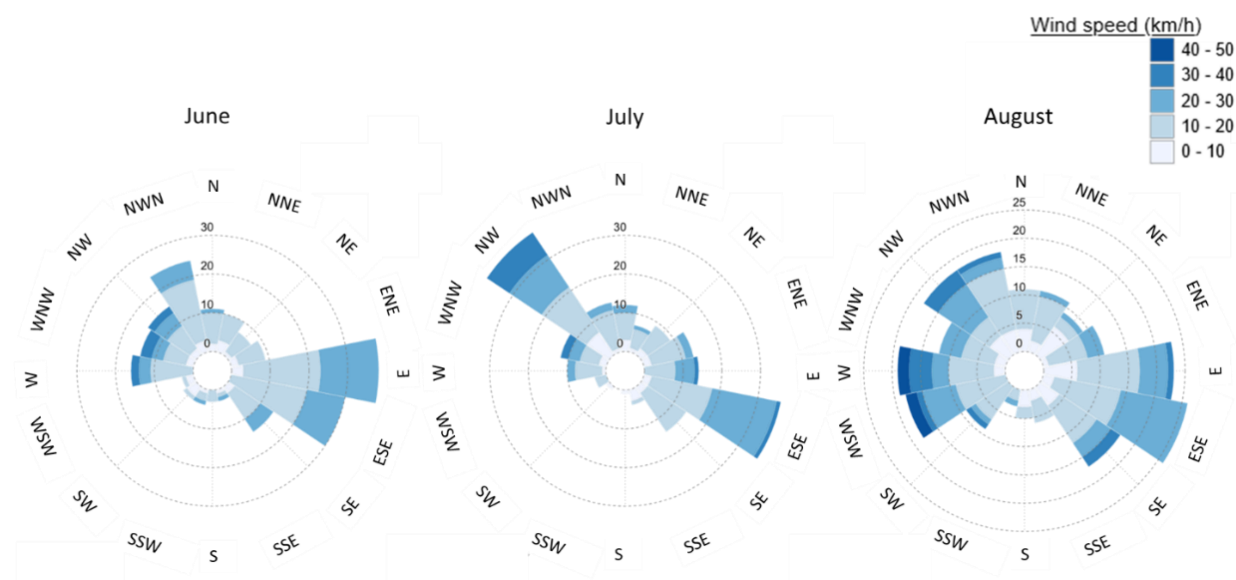


Fig. 15, Windrose diagram showing wind direction and speed frequency for the summer months June, July and August. Data was acquired for 2013 - 2019 from the weather station at Simpson Point, HIQ. Diagram is based on acquired satellite data in scope of the thesis and does not cover wind data of the whole respective month.

4.4.1 Herschel Island

The multiple linear regression used to predict Dolly Varden parameters demonstrated that wind speed and direction were poor explanatory variables based on the very R^2 explained by the wind factors (Table 5). No significant linear correlation was found on dispersal mechanisms in terms of condition and length. Harvest numbers had a significant negative linear relationship with wind speed and direction on harvest day and 48 hours beforehand. The results show that most of the Dolly Varden were caught in moderate wind speed (20 - 28 km/h) in June and July and in fresh breezes (28 - 38 km/h) in August. The wind direction on HIQ was clearly dominated by SE (2 radians) as well as NW (5 - 6 radians) (Fig. 16).

Table 5, Multiple regression predicting Dolly Varden parameters by explanatory wind variables.

Day	Parameter	Wind speed	Wind direction (sin)	Wind direction (cos)
Harvest day	Harvest number	-0.13**	-0.25	-1.55**
	Condition factor	< 0.01	0.02	0.02
	Fork length	1.04	-5.11	-11.55
24 h prior	Harvest number	-0.41	-0.55	-1.09
	Condition factor	< 0.01	-0.1	0.01
	Fork length	1.08	-8.39	-13.17
48 h prior	Harvest number	-0.12 *	-0.99 *	-0.8
	Condition factor	< 0.01	< 0.01	0.03
	Fork length	1.04	-6.59	-0.39

Significant explanatory variables are indicated with the following symbols.

* $P < 0.05$.

** $P < 0.01$.

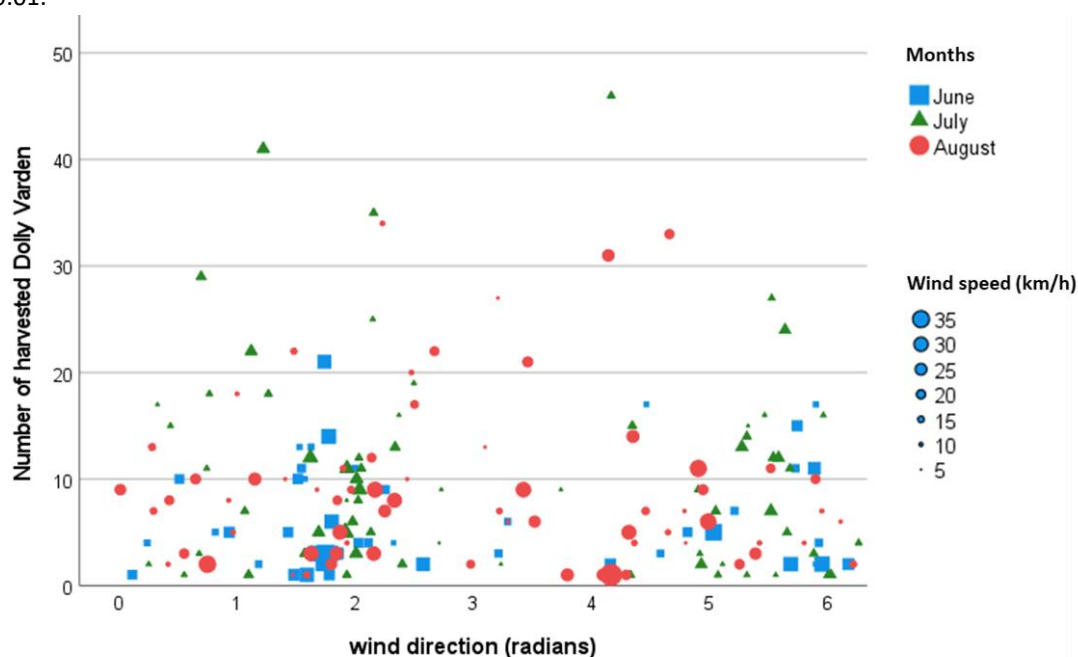


Fig. 16, Number of harvested Dolly Varden at Herschel Island Qikiqtaruk (HIQ), depending on wind direction (radians). With the different symbols representing the month of the annual sample period while the symbols size illustrates the magnitude of wind speed at the data point.

4.4.2 Shingle Point

The models show for all three response variables a very low proportion of variance (adj R²) that is explained by both wind factors (Table 6). The regression analysis found no statistically significant linear relationship between the windspeed, direction and Dolly Varden parameters. Nevertheless, harvest numbers were highest at SE and NW cardinal directions (Fig. 17). Whereas the highest rates were obtained at wind speeds of 10 - 20 km/h on the day of harvest.

Table 6, Multiple regression predicting Dolly Varden parameters by explanatory wind variables.

Day	Parameter	Wind speed	Wind direction (sin)	Wind direction (cos)	Adj. R ²
Harvest day	Harvest number	-0.79	-1.17	-1.97	0.03
	Condition factor	0.05	0.01	< 0.01	0.02
	Fork length	0.51	1.35	3.227	0.01
24 h prior	Harvest number	-0.66	-0.23	-1.55	0.01
	Condition factor	< 0.01	0.02	0.03	< 0.01
	Fork length	0.26	-0.53	-1.46	0.02
48 h prior	Harvest number	-0.24	0.22	-1.08	0.01
	Condition factor	< 0.01	-0.01	< 0.01	0.01
	Fork length	0.36	-1.71	--6.23	0.02

Significant explanatory variables are indicated with the following symbols.

*P < 0.05.

**P < 0.01.

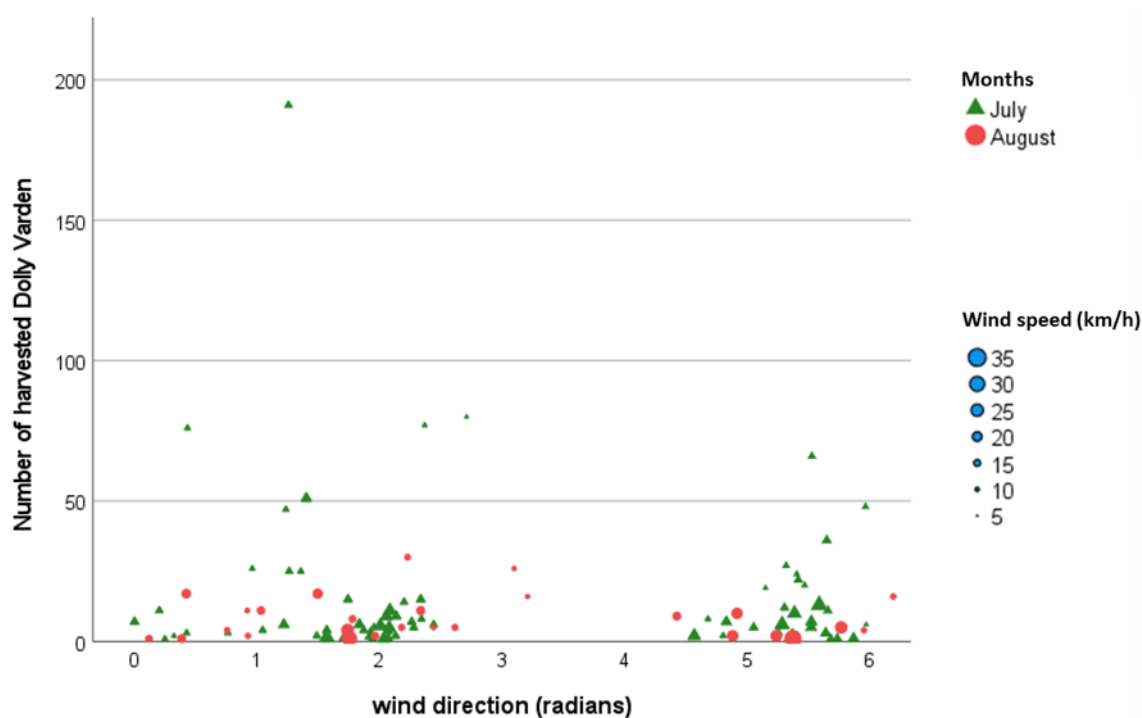


Fig. 17, Number of harvested Dolly Varden at Shingle Point Tapqaq (SPT) depending on wind direction (radians). With the different symbols representing the month of the annual sample period while the symbols size illustrates the magnitude of wind speed at the data point

4.5 Sea ice

Among study years there was no ice cover within a 2 km radius from PC. Within the 20 km radius, ice cover was present in 4 scenes in 2013, with an overall average (mean \pm SD) of 6.87 ± 6.88 % cover, and in 2018 (6 scenes) with 34.58 ± 22.77 % cover. A significant albeit weak relationship (R^2 of 0.18) was found ($F_{1, 30} = 6.65$, $p = 0.01$) between ice cover and harvest numbers. No significant relationship was found between ice and condition factor ($F_{1, 19} = 0.447$, $p = 0.51$) and fork length ($F_{1, 19} = 0.163$, $p = 0.69$) with an R^2 of 0.02 and 0.01 respectively.

The four areas demonstrated different percentage of ice cover. The western area (SIC-W) showed the highest values on average (12.5 ± 27.71 %) whereas the southern area recorded the lowest values (3.44 ± 12.6 %). The northern (SIC-N) and eastern (SIC-E) areas showed an average sea ice coverage of 9.69 ± 22.84 % and 5 ± 12.75 % respectively (Fig. 18).

A simple linear regression was calculated to predict the harvest number based on the sea ice coverage (%). A significant regression equation was only found for SIC-E ($F_{1, 30} = 4.89$, $p = 0.03$) and SIC-N ($F_{1, 30} = 5.98$, $p = 0.02$) with an R^2 of 0.14 and .012 respectively.

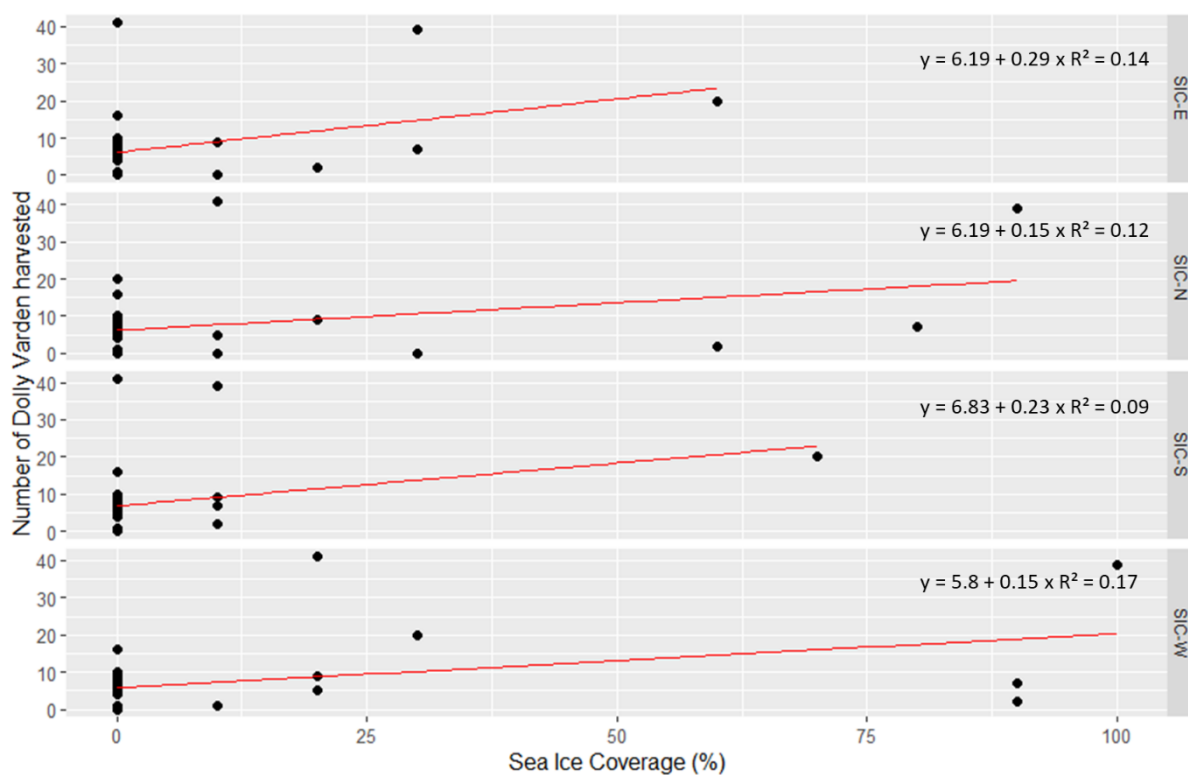


Fig. 18, Number of harvested Dolly Varden specimens at Herschel Island Qiqiktaruk (HIQ), in dependence to Sea ice coverage (%) of the respective sampling. Whereas the black point represent the sample size at the respective ice coverage, linear regression is represented by the red line.

4.6 Remote sensing (Sentinel 2 and Landsat 8)

4.6.1 Herschel Island

4.6.1.1 Brightness Temperature

June displayed the lowest average BT values among the three months (275.97 ± 4.14 K). The highest average values were observed in July (281.82 ± 2.92 K), whereas August was in between June and July with average BT values of 279.89 ± 3.54 K (Fig. 19).

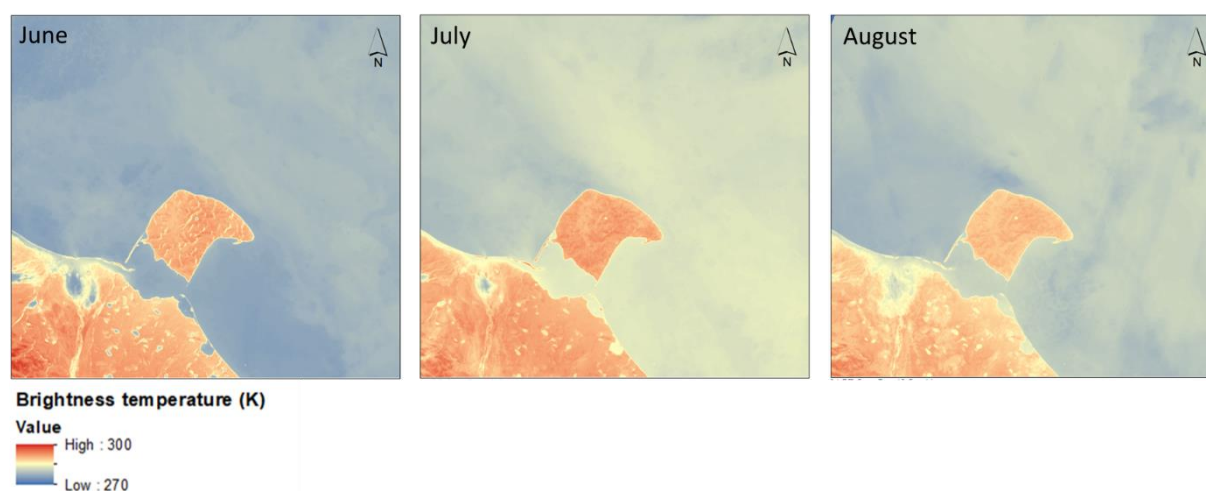


Fig. 19, Average monthly brightness temperature (BT) values for Herschel Island Qiqiktaruk (HIQ) representing the sampling period 2013 - 2019. Data was derived from Landsat 8 thermal infrared channels (Band 10). Values were measured in Kelvin (K)

The mean BT pixel values in June were marginally higher in the F-areas (276.21 ± 4.75 K) than the N-areas (275.74 ± 3.53 K). In July, both F- (281.88 ± 3.05 K) and N-areas (281.77 ± 2.82 K) had similar mean values. In August, higher pixel means were observed in the N-areas (280.3 ± 3.25 K) compared to F-areas (279.48 ± 3.81 K) (Fig. 20 a & b).

The highest annual average BT for the summer months were recorded in 2016 (281.57 ± 4.27 K) while the lowest was in 2015 (278.32 ± 3.87 K). The annual average BT value across all years for the summer months was 279.36 ± 4.04 K. This number, however, was strongly influenced by values in July due to the high amount of data available for that month.

The AOIs displayed different average BT values for the summer months, which appeared related to the geographical proximity to the Mackenzie Delta and influence of the Mackenzie River plume. The highest average BT values were observed in F3 (280.49 ± 3.9 K) and PC (280.38 ± 4.22 K), while the lowest mean values were detected in N1 (277.7 ± 3.79 K) and F4 (278.15 ± 3.64 K).

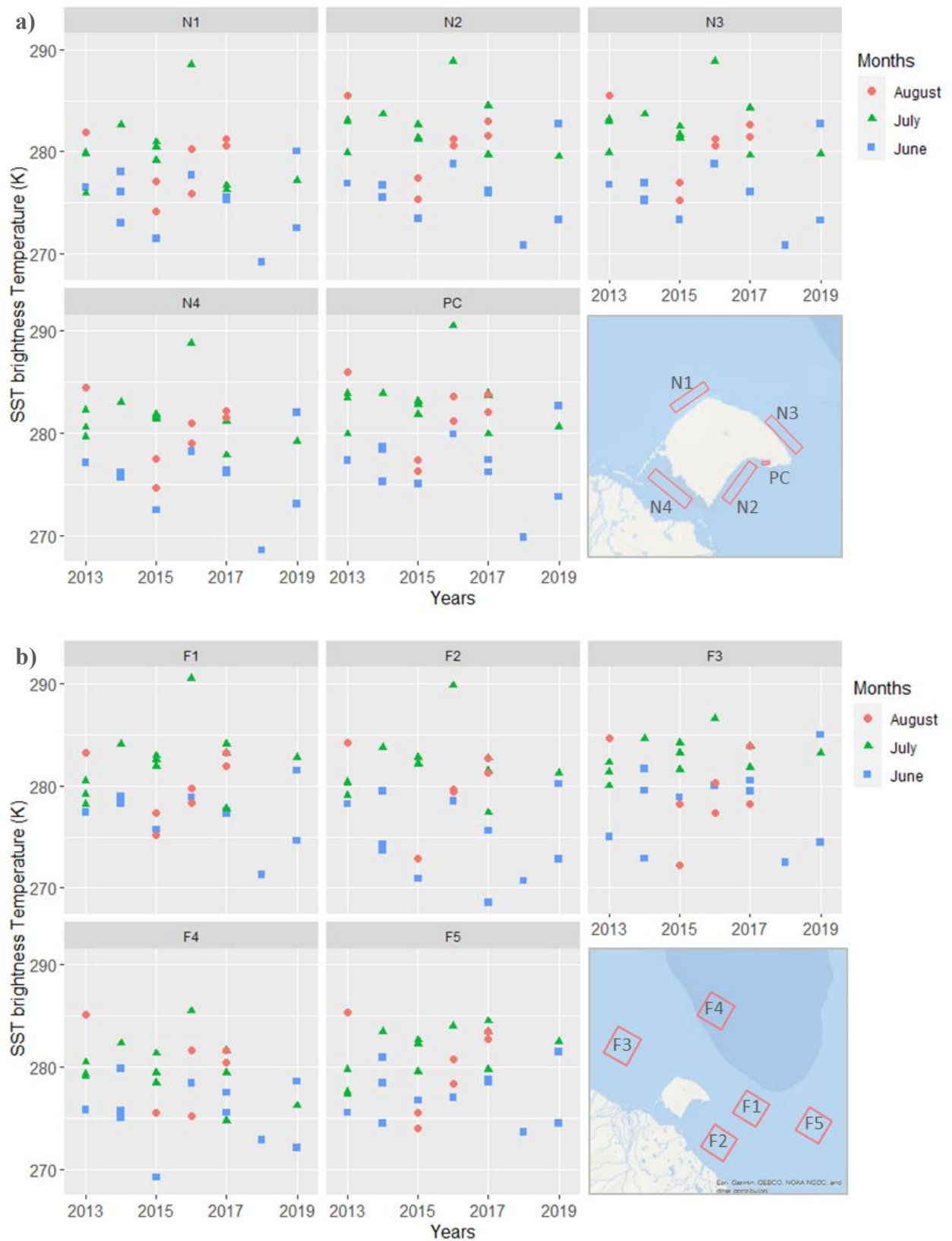


Fig. 20 Monthly (June – August) mean brightness temperatures (BT) values around Herschel Island Qiqiktaruk in dependence of the sampling year (2013 – 2019). Whereas a) illustrates mean values for the N-Areas, b) shows mean values for the F-Areas. Values were measured in Kelvin (K)

4.6.1.2 Chlorophyll-a

The average monthly chl-a concentrations in the upper water column demonstrated similar temporal patterns to BT. The lowest average values were observed in June ($2.83 \pm 1.49 \mu\text{g/l}$) and the highest in July ($5.32 \pm 3.2 \mu\text{g/l}$) with August's average in between ($3.47 \pm 1.23 \mu\text{g/l}$) (Fig. 21).

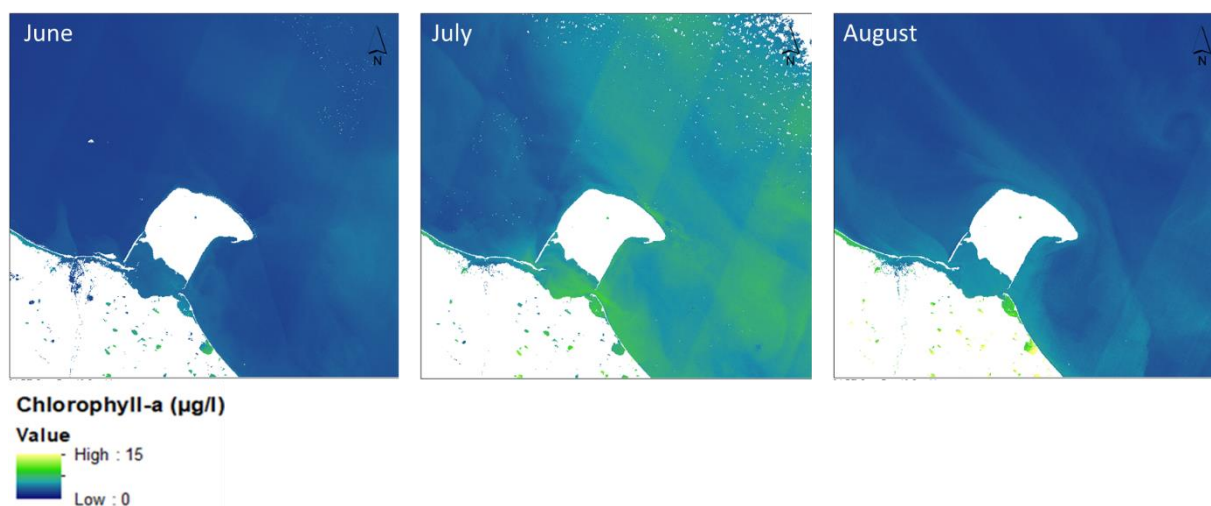


Fig. 21, Mean monthly Chlorophyll-a (Chl-a) values for Herschel Island Qiqiktaruk (HIQ) representing the sampling period 2013 - 2019. Data was derived Landsat 8 and Sentinel 2 satellite imagery. Values were measured in microgram per litre ($\mu\text{g/l}$)

The average ($\pm\text{SD}$) chl-a concentrations in June were marginally higher in the F-areas ($3.06 \pm 1.88 \mu\text{g/l}$) compared to the N-areas ($2.62 \pm 0.94 \mu\text{g/l}$), July had similar average values for both sub-areas with $5.39 \pm 3.3 \mu\text{g/l}$ and $5.25 \pm 3.09 \mu\text{g/l}$ for N- and F-areas respectively. In August, higher concentrations were observed in the N-areas ($4.09 \pm 1.13 \mu\text{g/l}$) than in the F-areas ($2.82 \pm 0.97 \mu\text{g/l}$) (Fig. 22 a & b).

The highest annual chl-a values for the summer months were recorded in 2013 ($6.62 \pm 3.98 \mu\text{g/l}$), whereas the lowest annual average was in 2019 ($2.53 \pm 0.79 \mu\text{g/l}$). The average annual chl-a values for summer months among years was $4.16 \pm 2.69 \mu\text{g/l}$, which was strongly influenced by values in July due to the high data availability for that month.

The AOIs displayed different average chl-a concentrations, which appeared to be related to geographical location and exposure to the Mackenzie River plume. The highest chl-a values were observed in F3 ($5.44 \pm 3.43 \mu\text{g/l}$) and PC ($4.73 \pm 3.17 \mu\text{g/l}$) while the lowest were observed in N1 ($3.63 \pm 1.93 \mu\text{g/l}$) and F4 ($2.95 \pm 2.32 \mu\text{g/l}$).

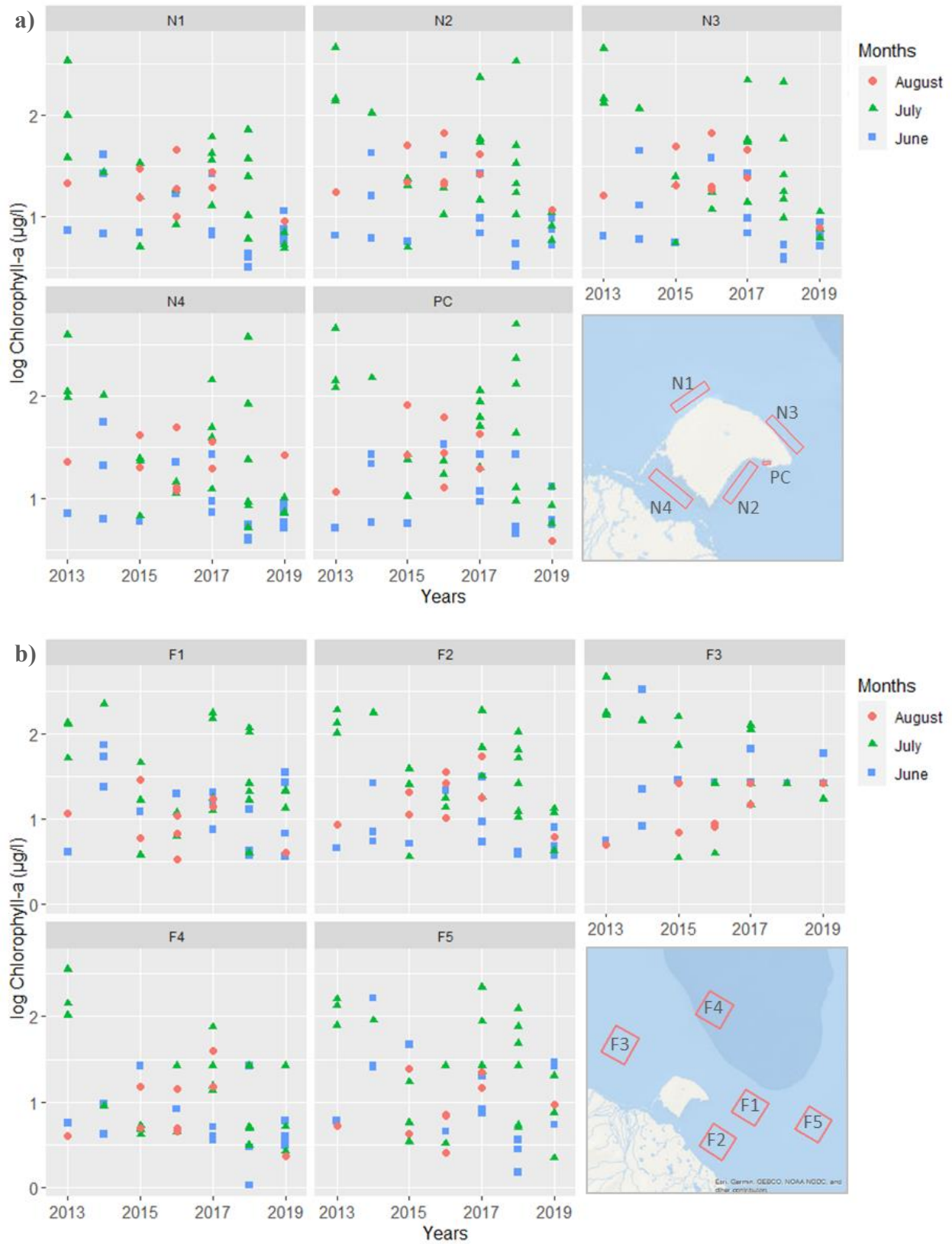


Fig. 22, Monthly (June – August) mean logarithmic chlorophyll-a (Chl-a) concentration around Herschel Island Qiqiktaruk in dependence of the sampling year (2013 – 2019). Whereas a) illustrates mean values for the N-Areas, b) shows mean values for the F-Areas. Values were measured in microgram per litre ($\mu\text{g/l}$)

4.6.1.3 Suspended particulate matter (SPM)

The highest average values of SPM on the sea surface were observed in June ($14.35 \pm 9.87 \text{ g/m}^3$), while the lowest values, unlike the other parameters, were observed in August ($11.81 \pm 7.35 \text{ g/m}^3$). SPM in July were between the other two months and showed an average of $13.34 \pm 7.29 \text{ g/m}^3$ (Fig. 23).

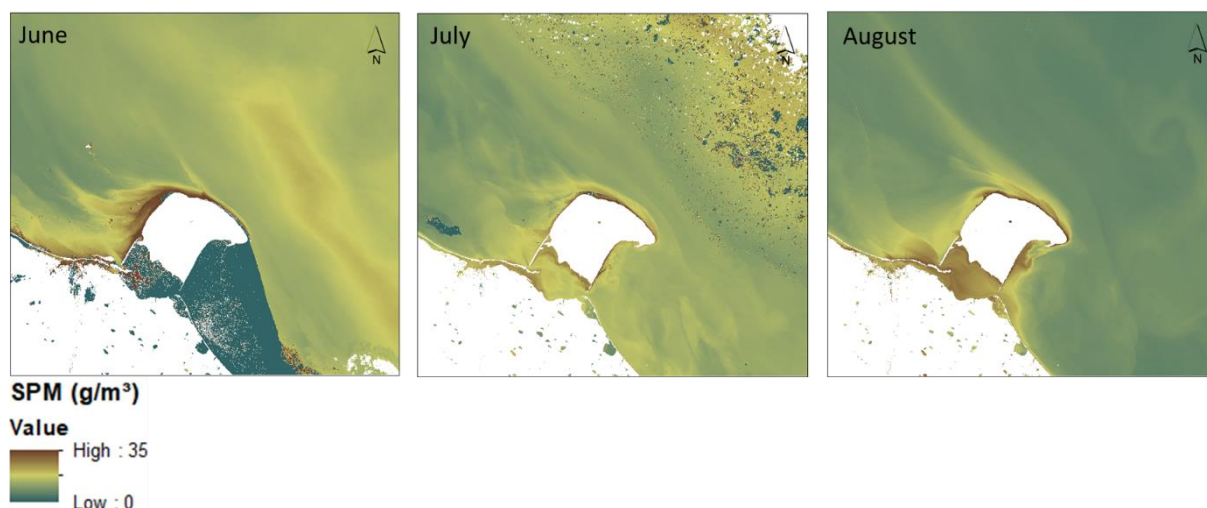


Fig. 23, Average monthly suspended particulate matter (SPM) values for Herschel Island Qiqiktaruk (HIQ), representing the sampling period 2013 - 2019. Data was derived Landsat 8 and Sentinel 2 satellite imagery. Values were measured in grams per cubic metre (g/m^3)

The SPM values in June were higher in the F-areas ($22.11 \pm 29.79 \text{ g/m}^3$) compared to N-areas ($15.58 \pm 14.1 \text{ g/m}^3$). Average July values in N-areas ($14.15 \pm 5.91 \text{ g/m}^3$) were marginally higher than F-areas ($12.36 \pm 8.6 \text{ g/m}^3$). In August, higher concentrations were detected in N-areas ($15.04 \pm 7.17 \text{ g/m}^3$) than F-areas ($8.42 \pm 5.92 \text{ g/m}^3$) (Fig. 24 a & b).

The annual average SPM for the summer months showed minor inter-annual fluctuations with an average value of $12.08 \pm 6.53 \text{ g/m}^3$. An outlier was observed in 2013, which had the highest average value of particulate matter (23.71 ± 12.19). Alternatively, the lowest average values were detected in 2016 (8.64 ± 5.47).

As for BT and Chl-a, the AOIs displayed different average SPM values for the summer months based on their geographical position and proximity to the Mackenzie River plume. Whereas the highest SPM values were observed in F3 ($16.77 \pm 15.55 \text{ g/m}^3$) and PC ($17.94 \pm 13.61 \text{ g/m}^3$), the lowest average values were in N4 ($13.97 \pm 7.28 \text{ g/m}^3$).

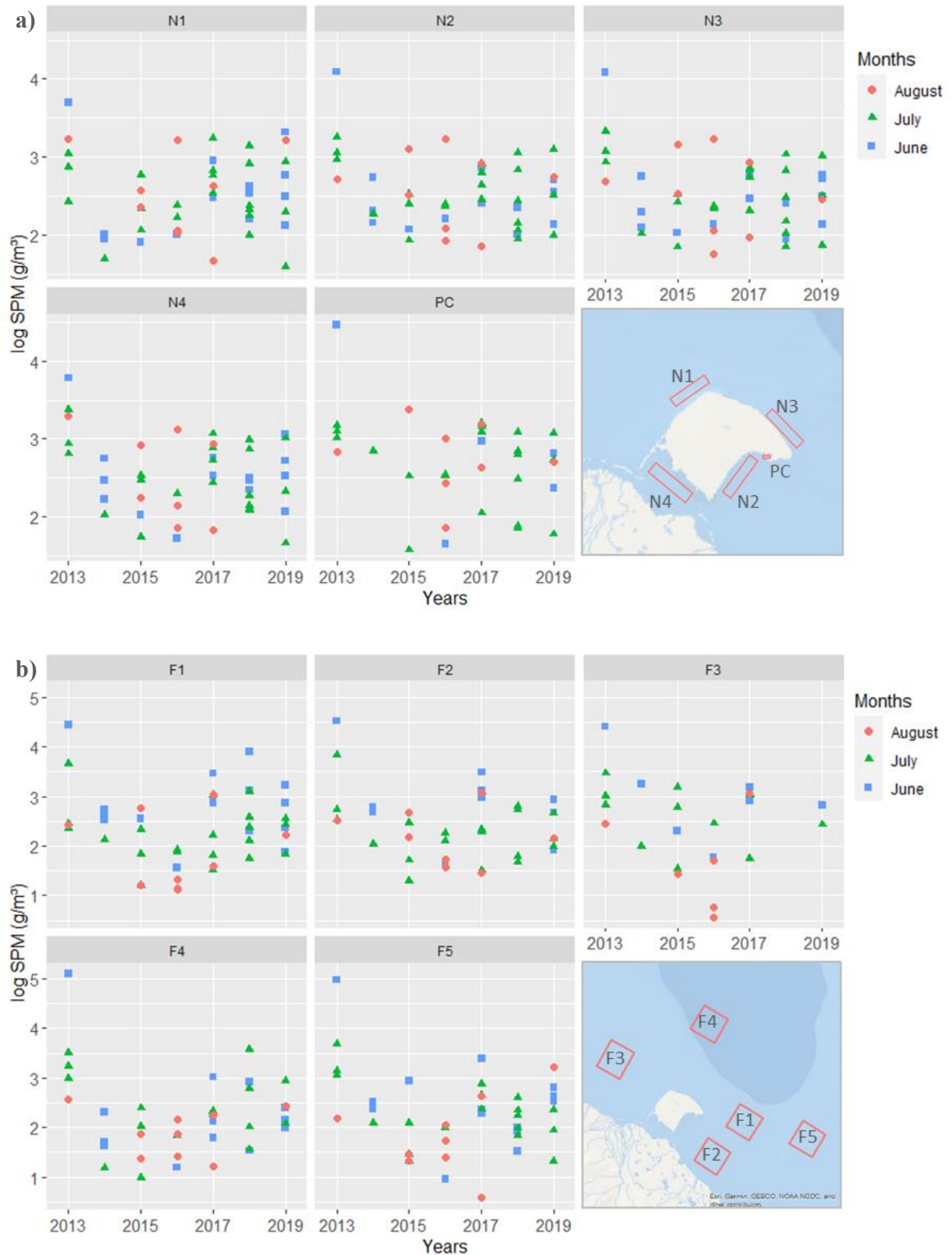


Fig. 24 Monthly (June – August) mean logarithmic suspended particulate matter (SPM) concentration around Herschel Island Qiqiktaruk in dependence of the sampling year (2013 – 2019). Whereas a) illustrates mean values for the N-Areas, b) shows mean values for the F-Areas. Values were measured in grams per cubic meter (g/m^3)

4.6.1.4 Turbidity

The patterns observed for turbidity were similar to those of SPM. In the upper water column, the highest average turbidity values were in June (24.45 ± 49.3 FNU), while the lowest was observed in August (9.32 ± 6.48 FNU). July (12.66 ± 13.39 FNU) was slightly above the general seasonal average and thus between the two other months (Fig. 25).

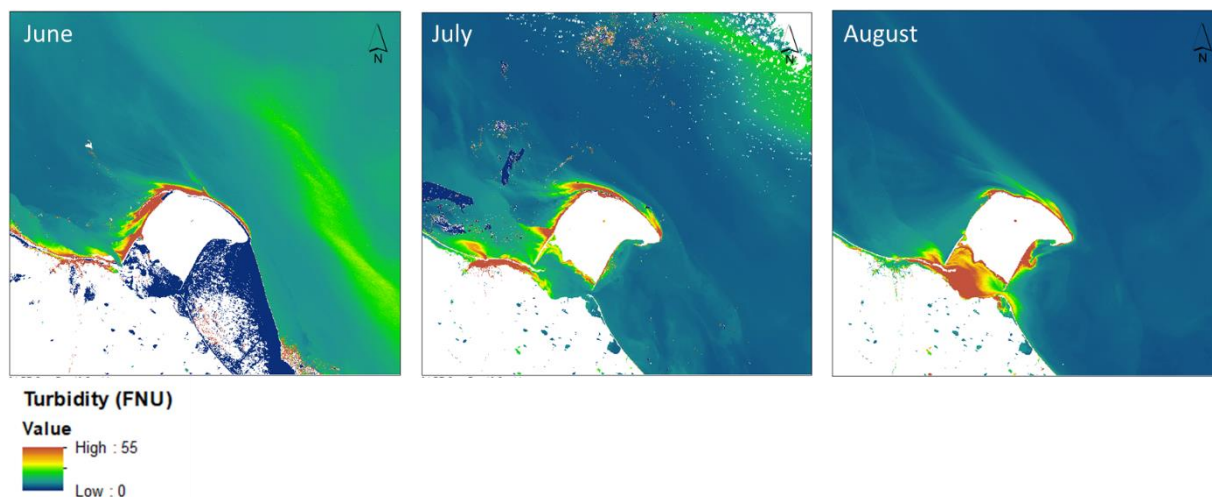


Fig. 25, Average monthly turbidity (FNU) values for Herschel Island Qiqiktaruk (HIQ), representing the sampling period 2013 - 2019. Data was derived from Landsat 8 and Sentinel 2 satellite imagery. Values were measured in Formazin Nephelometric Units (FNU)

The turbidity values in June were higher in F-areas (22.11 ± 29.79 FNU) compared to N-areas (15.58 ± 14.1 FNU). July had similar average values for both sub-areas, although N-areas (11.49 ± 6.56 FNU) were marginally higher than F-areas (11.03 ± 14.86). In August, higher turbidity values were detected in the N-areas (15.04 ± 7.17 FNU) compared to F-areas (8.42 ± 5.92 FNU).

Turbidity displayed similar interannual patterns to SPM, with an average turbidity value for the summer months of 15.95 ± 30.5 FNU and small inter-annual fluctuations. One outlier was the year 2013, which had the highest turbidity concentration (54.47 ± 82.46 FNU). Similar to SPM, this outlier was a result of high readings in June and was considerably different to other years. Alternatively, the lowest values were observed in 2016 (9.74 ± 5.57 FNU).

Like the other parameters, the AOIs displayed different average values based on their geographical position and exposure to the Mackenzie River plume (Fig. 26 a & b). Whereas the highest average turbidity values for the summer months were observed in F3 (18.4 ± 39.37 FNU) and PC (18.5 ± 33.78 FNU), the lowest average values were in N4 (14.49 ± 17.06 FNU).

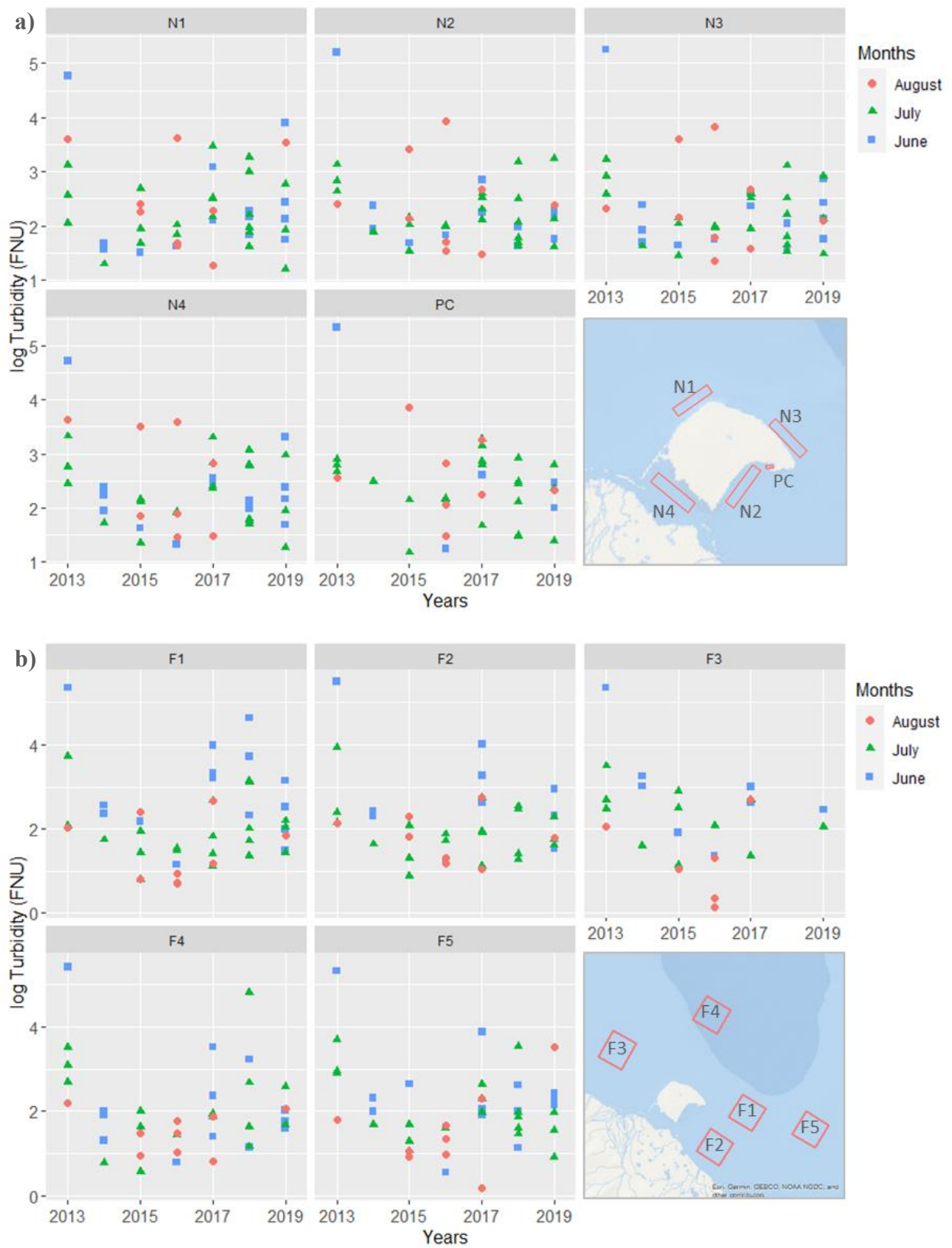


Fig. 26, Monthly (June – August) mean logarithmic turbidity (FNU) concentration around Herschel Island Qiqiktarak in dependence of the sampling year (2013 – 2019). Whereas a) illustrates mean values for the N-Areas, b) shows mean values for the F-Areas. Formazin Nephelometric Units (FNU)

4.6.2 Shingle Point

4.6.2.1 Brightness temperature

With the decreasing ice cover at the beginning of summer, the temperature values for the two sampled summer months at SPT showed little difference in their averages. Nevertheless, the maximum average values were in July (284.73 ± 3.53 K) while August was slightly below (283.74 ± 4.56 K) (Fig. 27).

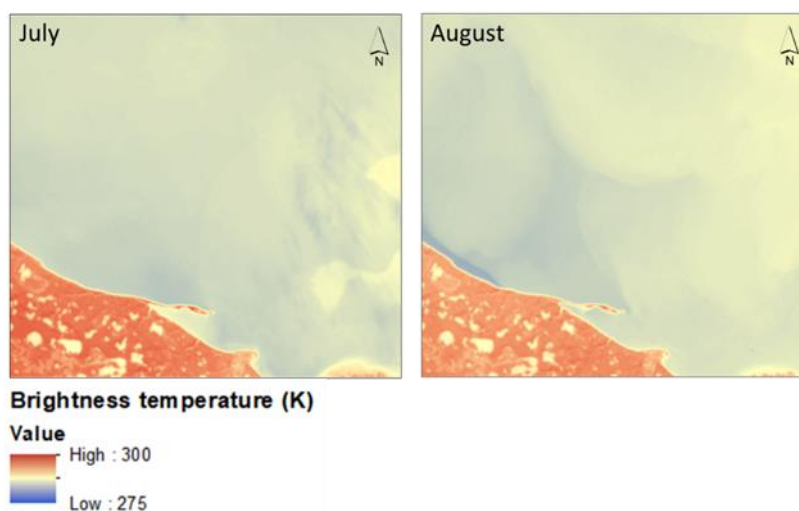


Fig. 27, Average monthly brightness temperature (BT) values for Shingle Point Tapqaq, representing the sampling period 2013 - 2019. Data was derived from Landsat 8 thermal infrared channels (Band 10). Values were measured in Kelvin (K)

The values of BT pixel values in July in F-areas (285.12 ± 3.22 K) were marginally higher than N-areas (284.34 ± 3.8 K) while means in both sub-areas were similar in August (282.51 ± 5.01 K) (Fig. 28 a & b).

The highest annual average BT values among summer months were recorded in 2016 (286.12 ± 3.44 K) while the lowest was in 2019 (280.57 ± 5.1 K). The annual average BT value among all years for the summer months was 286.12 ± 3.44 K. This number, however, was strongly influenced by values in July due to the high data availability during that month.

The AOIs displayed different average BT values for the summer months, which seem to be related to the location and proximity of the Mackenzie River plume. The highest average BT values were observed in F2 (285.37 ± 3.39 K) and F1 (284.45 ± 3.94 K) while the lowest mean values were detected in N4 (281.9 ± 6.99 K).

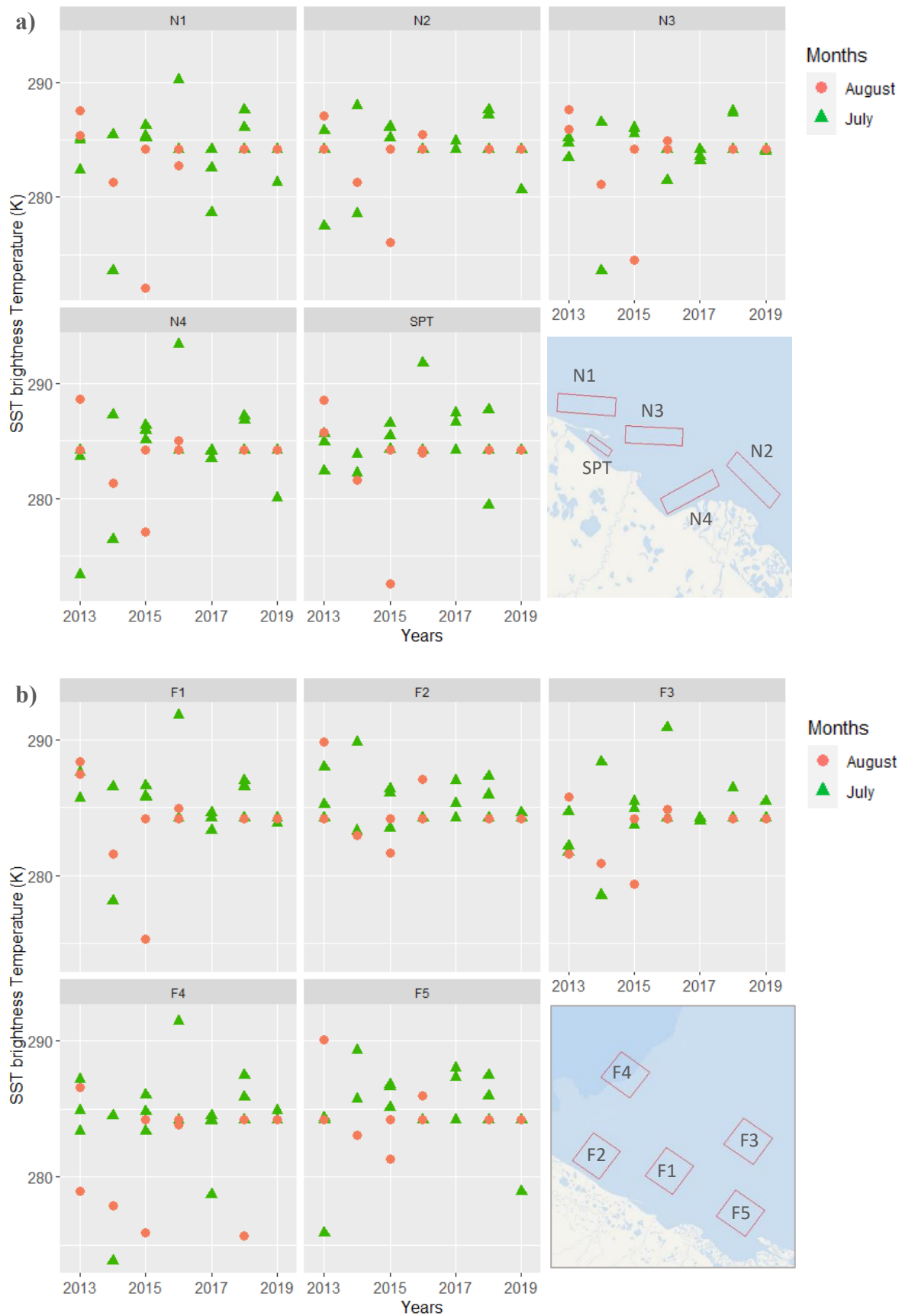


Fig. 28, Monthly (July – August) mean brightness temperature (BT) values around Herschel Island Qiqiktaruk in dependence of the sampling year (2013 – 2019). Whereas a) illustrates mean values for the N-Areas, b) shows mean values for the F-Areas. Values were measured in Kelvin (K)

4.6.2.2 Chlorophyll-a

Similar to HIQ, average monthly chl-a concentrations in the upper water column at SPT demonstrated similar temporal patterns to BT. The highest average values were observed in July ($6.16 \pm 2.77 \mu\text{g/l}$). The values in August were lower than those in July, showing an average of $5.75 \pm 2.72 \mu\text{g/l}$ (Fig. 29).

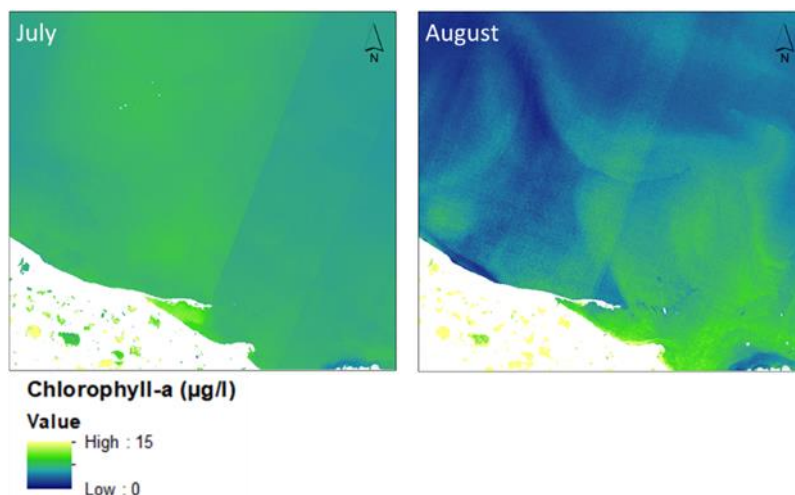


Fig. 29, Average monthly chlorophyll-a (Chl-a) values for Shingle Point Tapqaq, representing the sampling period 2013 - 2019. Data was derived from Landsat 8 and Sentinel 2 satellite imagery. Values were measured in microgram per litre ($\mu\text{g/l}$).

The average chl-a values in July values were $6.59 \pm 3.1 \mu\text{g/l}$ in F-areas and $5.25 \pm 3.09 \mu\text{g/l}$ in the N-areas. Higher pixel values were observed in the N-areas ($6.2 \pm 2.82 \mu\text{g/l}$) than in the F-areas ($5.16 \pm 2.53 \mu\text{g/l}$) in August (Fig. 30 a & b).

The highest annual chl-a values for the summer months were recorded in 2014 ($7.57 \pm 2.4 \mu\text{g/l}$) whereas the year with the lowest average was in 2019 ($3.6 \pm 1.43 \mu\text{g/l}$). The average annual chlorophyll-a values for the summer months across all years was $5.75 \pm 2.69 \mu\text{g/l}$, although this was strongly influenced by values in July due to the high data availability during that month.

The AOIs had different average chl-a values, with the highest observed at SPT ($5.44 \pm 3.43 \mu\text{g/l}$) and N1 ($6.69 \pm 3.72 \mu\text{g/l}$) while the lowest values were recorded in F2 ($4.67 \pm 1.73 \mu\text{g/l}$).



Fig. 30, Monthly (July – August) mean chlorophyll-a (Chl-a) concentration around Shingle Point Tapqaq (SPT) in dependence of the sampling year (2013 – 2019). Whereas a) illustrates mean values for the N-Areas, b) shows mean values for the F-Areas. Values were measured in microgram per litre ($\mu\text{g/l}$).

4.6.2.3 Suspended particulate matter (SPM)

The monthly average values of SPM in the upper water column had higher average values in July ($52.44 \pm 26.56 \text{ g/m}^3$), while the lowest values were recorded in August ($42.09 \pm 23.17 \text{ g/m}^3$) (Fig. 31).

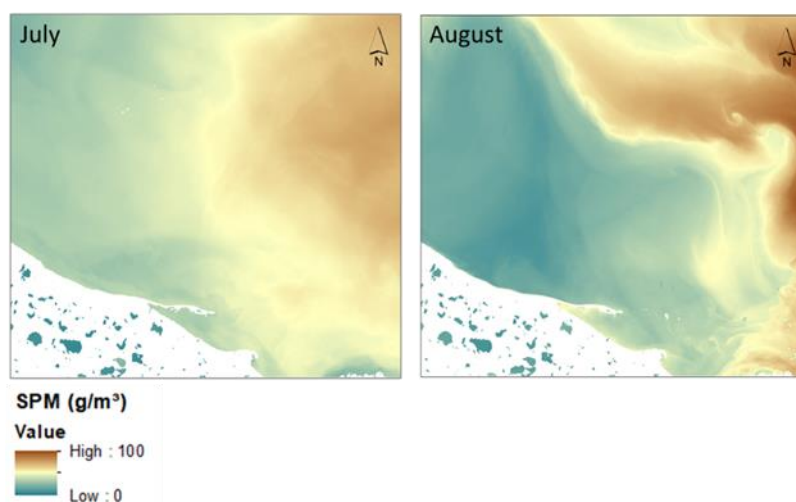


Fig. 31, Average monthly suspended particulate matter (SPM) values for Shingle Point Tapqaq, representing the sampling period 2013 - 2019. Data was derived from Landsat 8 and Sentinel 2 satellite imagery. Values were measured in grams per cubic metre (g/m^3)

The SPM values in July had high concentrations of SPM in the N-areas ($59.88 \pm 31.78 \text{ g/m}^3$), whereas the F-areas during that month had lower concentration ($45.36 \pm 17.82 \text{ g/m}^3$). In August, values decreased although N-areas ($48.43 \pm 28.7 \text{ g/m}^3$) still had a greater SPM accumulation than F-areas ($36.19 \pm 15.98 \text{ g/m}^3$) (Fig. 32 a & b).

The annual average SPM values for the summer months had relatively minor fluctuations with an average of $52.14 \pm 29.65 \text{ g/m}^3$. The year 2019 had the highest particulate matter average ($64 \pm 35.27 \text{ g/m}^3$). The lowest average values were recorded in 2016 ($40 \pm 23.47 \text{ g/m}^3$).

Like the other parameters, the AOIs displayed different average SPM values for the summer months based on their geographical position and proximity to the Mackenzie River plume. The highest average SPM values were in F6 ($16.77 \pm 15.55 \text{ g/m}^3$) and F2 ($17.94 \pm 13.61 \text{ g/m}^3$), while F4 ($36.14 \pm 29.97 \text{ g/m}^3$) and N1 ($36.89 \pm 23.13 \text{ g/m}^3$) had the lowest concentrations.

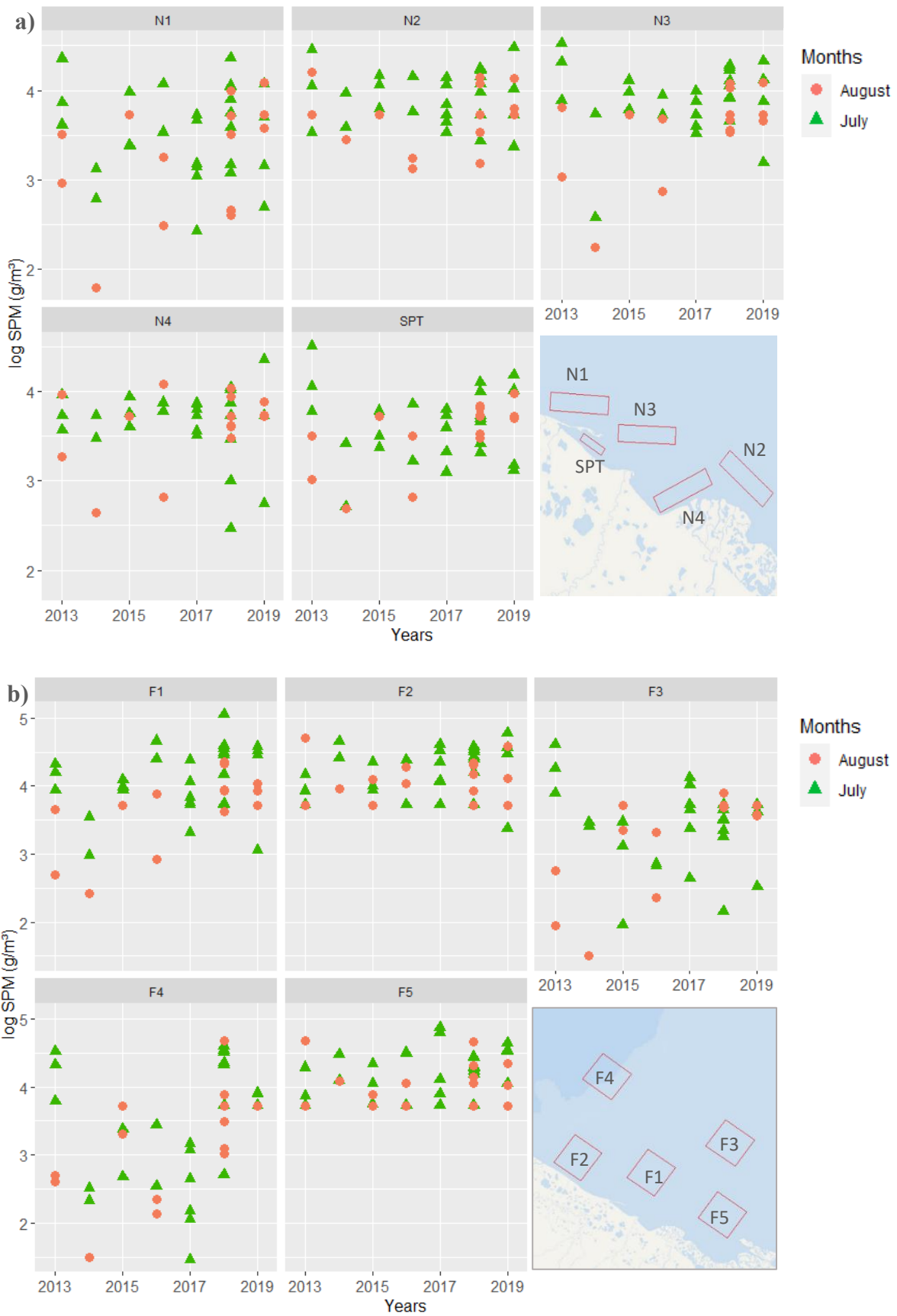


Fig. 32, Monthly (July – August) mean suspended particulate matter (SPM) concentration around Shingle Point Tapqaq (SPT) in dependence of the sampling year (2013 – 2019). Whereas a) illustrates mean values for the N-Areas, b) shows mean values for the F-Areas. Values were measured in microgram grams per cubic meter (g/m³).

4.6.2.4 Turbidity

The patterns of the results for turbidity had strong similarities to SPM. At the sea surface, the highest average turbidity values were in July (156.22 ± 143.08 FNU) while slightly lower values were observed in August (141.8 ± 138.49 FNU) (Fig. 33).

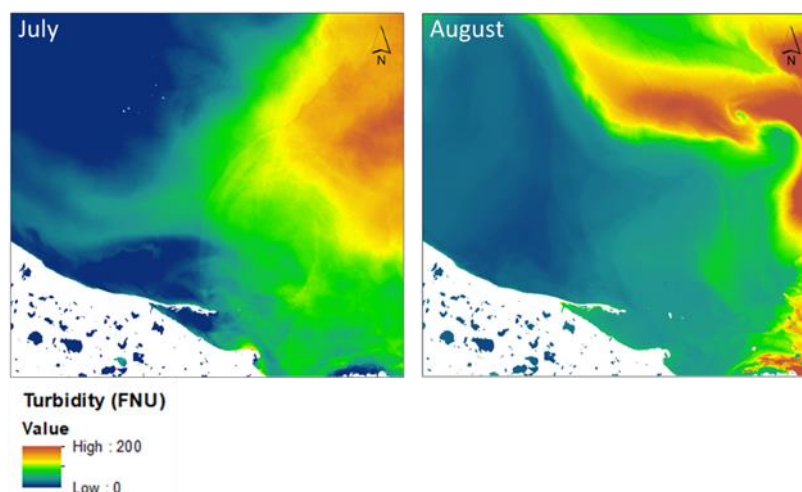


Fig. 33, Average monthly turbidity values for Shingle Point Tapqaq, representing the sampling period 2013 - 2019. Data was derived from Landsat 8 and Sentinel 2 satellite imagery. Values were measured in Formazin Nephelometric Units (FNU)

The average July turbidity values were higher in the N-areas (189.3 ± 169.76 FNU) than the F-areas (124.71 ± 103.14 FNU). In August, average turbidity had decreased although the N-areas (174.6 ± 166.63 FNU) still demonstrated higher average values than the F-areas (109.55 ± 94.57 FNU) (Fig. 34 a & b).

The interannual average turbidity values around SPT had an average of 158.56 ± 147.67 FNU. Similar to SPM, the highest concentration for turbidity was in 2019 (230 ± 189.9 FNU) while the lowest was in 2015 (84.52 ± 52.84 FNU).

Like the other parameters, the AOIs displayed different average values based on their geographical position and exposure to the Mackenzie River plume. The highest average SPM were in F2 (302.15 ± 154.69 FNU) and F6 (294.45 ± 159.37 FNU), while F3 (68.33 ± 95.05 FNU) and F4 (75.58 ± 99.96 FNU) had the lowest turbidity concentration.



Fig. 34, Monthly (July – August) mean turbidity concentration around Shingle Point Tapqaq (SPT) in dependence of the sampling year (2013 – 2019). Whereas a) illustrates mean values for the N-Areas, b) shows mean values for the F-Areas. Values were measured in Formazin Nephelometric Units (FNU)

4.6.3 Overview of remote sensing Parameters

The environmental parameters derived from the satellite imagery demonstrated significant differences between HIQ and SPT (Table 7). All parameters showed significantly higher values in both area groups on SPT. While SPM and turbidity were five and ten times higher than the values at SPT, temperature showed a difference of approximately 3 Kelvin between the two points. Although a difference in chl-a concentration of N-areas of about 2 µg/l was observed, no statistically significant difference in F-areas between locations was detected.

Table 7, Overview of satellite imagery derived environmental parameters according to both respective sampling points HIQ and SPT). For each value the mean value (mean) and standard deviation (SD) are given according to N- and F-Areas at both respective sampling sites. Both sampling sites were tested with an independent samples t-test. Results are shown on last column

Parameters	SPT (n = 45)		HIQ (n = 49)		Lavene's Test		t-test		
	Mean	SD	Mean	SD	F	p	t	df	p
Chl -a									
Near Areas	6.48	3.02	4.52	2.86	0.09	0.76	-5.84	313.00	***
Far Areas	5.54	2.38	5.03	2.93	4.12	0.43	-1.73	331	n.s.
Brightness Temp									
Near Areas	283.87	4.19	280.97	3.37	1.87	0.17	-5.28	188	***
Far Areas	284.55	3.66	281.30	3.20	0.86	0.36	-6.44	183	***
Turbidity									
Near Areas	119.88	100.48	9.57	13.00	137.43	0.07	-12.72	319	***
Far Areas	184.51	168.41	12.89	9.52	270.97	0.13	-12.75	333	***
SPM									
Near Areas	42.43	17.73	11.17	8.07	76.61	0.11	-19.15	319	***
Far Areas	56.28	31.22	14.40	6.27	210.48	0.06	-16.51	330	***

Significant explanatory variables are indicated with the following symbols.

***p = 0.001.

n.s. = not statistically significant

4.7 Redundancy Analysis

4.7.1 Herschel Island

4.7.1.1 Selection of parameters

As an explanation of the response of Dolly Varden parameter on HIQ, the outcome of the step wise selection revealed a number of 19 explanatory environmental variables for best fit model out of the initial 47 (40 remote sensing-, 3 wind- and 4 ice variables) (Table 8).

Table 8, RDA result for each response variable (harvest number, body weight, fork length) in relation to the explanatory variables included in the model. Parameters to explain the response variable were chosen based on the stepwise selection. Asterisks symbolise the degree of significant linear correlation.

Response variable	Parameter	Estimate	p value	Adj R ²	p model
Harvest number	`F2-Chl`	-0.47	**	0.64	***
	Windspd48	-0.43	***		
	`N4-FNU`	-0.23	*		
	`PC-Chl`	0.75	***		
	`N1-Chl`	-0.49	*		
	`F4-FNU`	0.26			
	`SIC-E`	0.17			
Condition factor	Windspd	- 0.2		0.87	***
	`N4-Chl`	1.19	***		
	`F4-Chl`	-0.21	***		
	`F2-Chl`	-0.13			
	`N1-FNU`	-0.53	***		
	`N4-FNU`	0.57	***		
	`PC-FNU`	-0.55	***		
	`N1-Chl`	-0.69	***		
	`F4-BT`	-0.14	*		
	`F1-Chl`	-0.28	*		
Fork length	`F5-Chl`	0.16		0.49	***
	`PC-Chl`	-0.09			
	`SIC-N`	-0.40	***		
	`PC-Chl`	0.41	***		
	`F2-Chl`	-0.41	**		
	`PC-FNU`	-0.57	**		
	`F5-Chl`	0.38	**		
`F3-BT`	-0.59	*			
	`F1-BT`	0.29			

Significant explanatory variables are indicated with the following symbols.

*P < 0.05.

**P < 0.01.

***P = 0.001

4.7.1.2 Redundancy Analysis on selected parameters

The RDA analysis for HIQ (Fig. 35) indicated a statistically significant relationship between selected environmental parameters and the characteristics of Dolly Varden harvesting numbers and somatic factors. According to the permutation test, the ordination of the vectors between the canonical axes in the RDA model was statistically significant ($p < 0.05$) and revealed an adjusted coefficient of determination (adj. R^2) of 0.51.

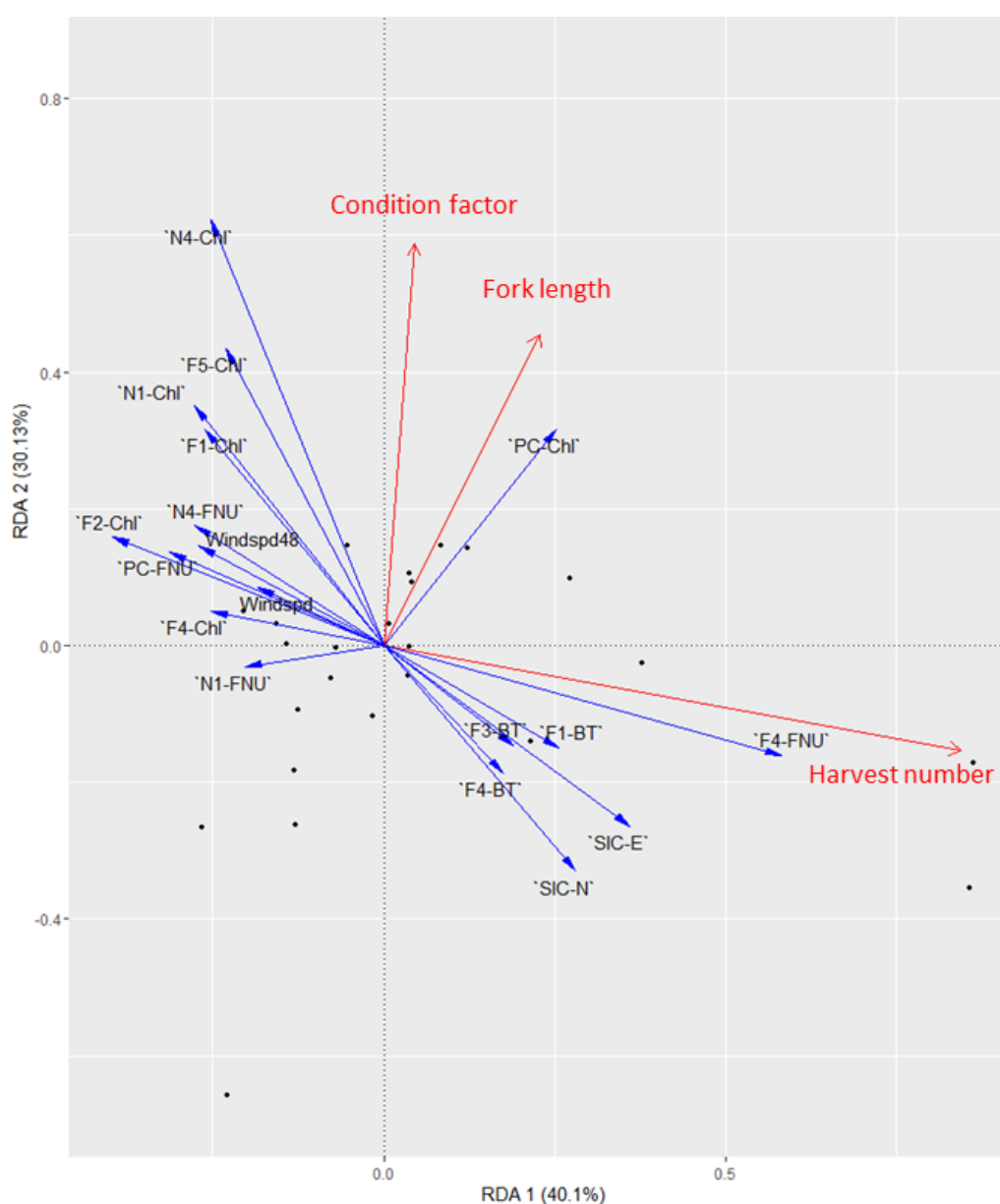


Fig. 35, Redundancy Analysis (RDA) of the biological parameters of Dolly Varden (*S. malma malma*). RDA 1 (40.1 %) and RDA2 (30.13 %) show the relation of the response variables (red arrows) on the environmental parameters of the different AOIS as explanatory variables (blue arrows). The length of an arrow reflects the contribution to explain the total variance while a small angle between two arrows represents the strength of the correlation between the two corresponding parameters. The RDA was significant ($p < 0.05$) and revealed an adjusted coefficient of determination of 0.51.

The first two axes explained 70.23 % of the variance in Dolly Varden indices. The first RDA axis (RDA1; 40.1% of the explained variability) was associated with harvest numbers while the second RDA axis (RDA2; 30,13 % of the explained variability) was correlated with the somatic parameters (Fig. 35). The ordination of the vectors in the RDA can be defined in two groups with each drawing a correlation towards the response variables.

The highest contribution for the explanation on the variance of the response variables (indicated by the arrow length) was provided by sea ice (N and E), FNU (F4) and Chl-a (F2, N4 and PC). The environmental parameter values of east and south facing AOIs, however, showed a stronger influence on the Dolly Varden parameters than the north and west facing AOIs.

The small angle between arrows of the response and explanatory variables in the triplot suggest a positive linear correlation of harvest with BT (F4, F3 and F1), FNU (F4), sea ice coverage (SIC-N and SIC-E) and chl-a concentration in Pauline Cove (PC-Chl). A negative correlation was evident between harvest numbers and increasing concentration of turbidity (PC, N1 and N4), chl-a (F4, F2, F1 and N1) as well as windspeed (harvest day and 48h prior).

Both, fork length and condition factor were strongly correlated with RDA2. The triplot illustrates the two factors are positively correlated with chl-a concentration around HIQ (PC, N4, F5, N1 and F1). Additionally, FNU (N4) and windspeed (48 hours prior) also display an angle $< 90^\circ$ towards both response variables, suggesting a positive correlation towards the response variables. Arrows of the turbidity in AOIs F4 and N1 as well as chl-a of F4 and F2 point both in the opposite direction, indicating a negative relationship with the somatic factors of Dolly Varden harvested at HIQ.

The outcome RDA should be interpreted with caution, as the limited number of data may cause unwanted effects and spurious interactions.

4.7.2 Shingle Point

4.7.2.1 Selection of parameters

As an explanation of the response of Dolly Varden parameter on SPT, the outcome of the step wise selection revealed a number of 17 explanatory environmental variables for best fit model out of the initial 43 (40 remote sensing-, 3 wind variables) (Table 9).

Table 9, RDA result for each response variable (harvest number, body weight, fork length) in relation to the explanatory variables included in the model. Parameters to explain the response variable were chosen based on the stepwise selection. Asterisks symbolise the degree of significant linear correlation.

Response variable	Parameter	Estimate	p value	Adj R ²	p model	
Harvest number	Windspd24	-0.15				
	`N1-SPM`	0.61	***			
	`N3-FNU`	-0.86	**			
	`SPT-SPM`	0.50				
	`N3-BT`	-1.20	**			
	`SPT-BT`	1.08	***			
	`F3-Chl`	-0.21				
	Windspd48	-0.26	**			
	`F4-SPM`	-0.18			0.76	***
	`N2-BT`	0.89	**			
	`F1-BT`	-2.08	***			
	`F4-BT`	0.63	**			
	`F3-SPM`	-1.26				
	`F5-SPM`	0.47	**			
`F2-SPM`	-0.43	*				
`N1-BT`	1.14	*				
`N4-BT`	-0.59					
Condition factor	`F1-BT`	-1.28	***			
	`F2-BT`	0.83	***			
	`N2-FNU`	0.32	**		0.63	***
	`N3-BT`	0.43	*			
	`F1-FNU`	0.22	*			
	`F5-BT`	-0.32				
Fork length	`N4-FNU`	-0.68	***			
	`N1-Chl`	0.46	*			
	`N3-Chl`	-1.01	**		0.46	***
	`N2-Chl`	0.34				
	`F4-Chl`	0.17				

Significant explanatory variables are indicated with the following symbols.

*P < 0.05.

**P < 0.01.

***P = 0.001.

4.7.3 Redundancy Analysis on selected parameters

The RDA analysis for SPT (Fig. 36) indicated a statistically significant relationship between the environmental parameters and the characteristics of Dolly Varden harvesting numbers and somatic factors for SPT. According to the permutation test, the ordination of the vectors between the canonical axes in the RDA model was statistically significant ($p < 0.05$) and revealed an adjusted coefficient of determination (adj. R^2) of 0.49.

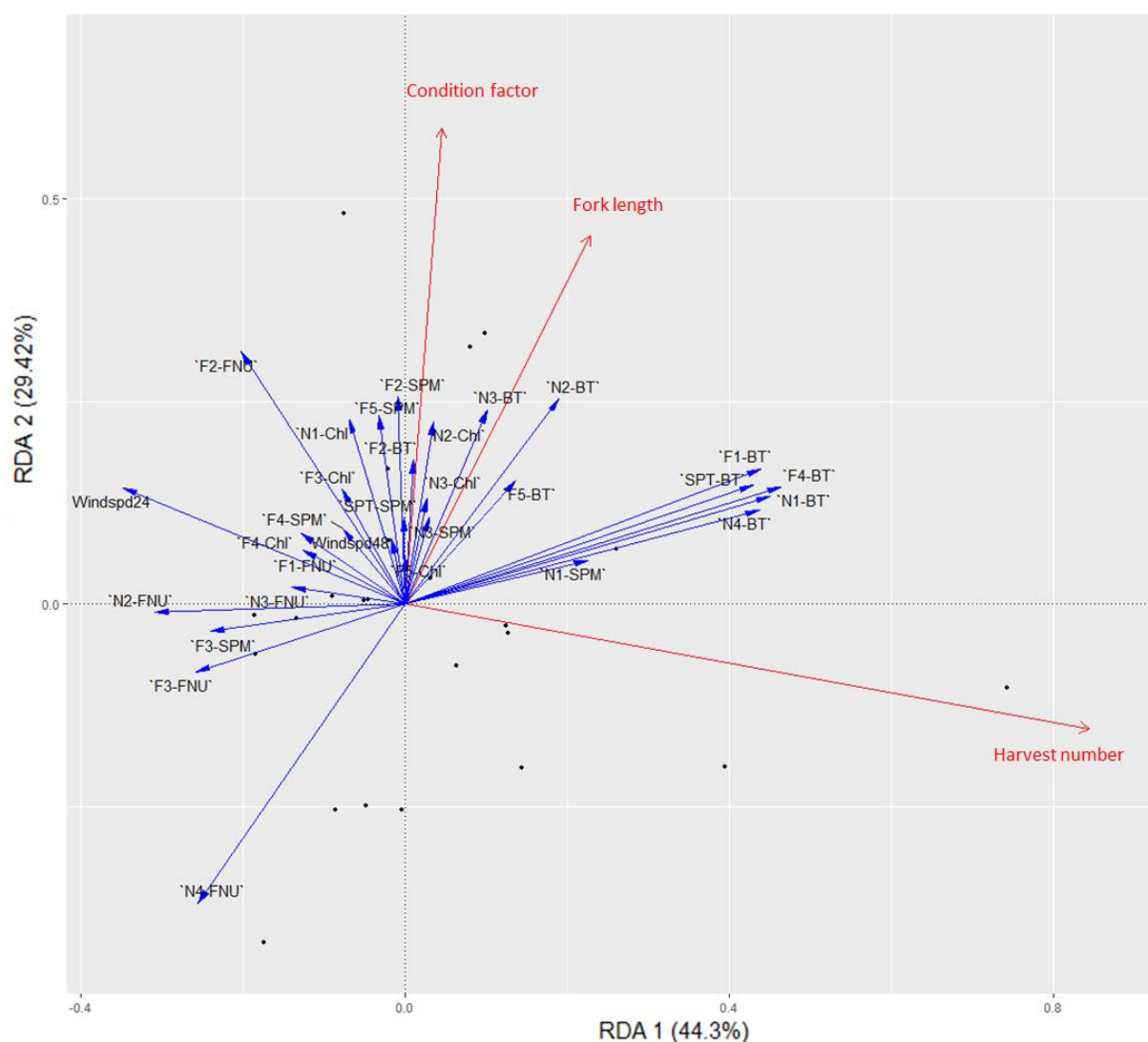


Fig. 36, Redundancy Analysis (RDA) of the biological parameters of Dolly Varden (*S. malma malma*). RDA 1 (44.3 %) and RDA2 (29.42 %) show the relation of the response variables (red arrows) on the environmental parameters of the different AOIS as explanatory variables (blue arrows). The length of an arrow reflects the contribution to explain the total variance while a small angle between two arrows represents the strength of the correlation between the two corresponding parameters. The RDA was significant ($p < 0.05$) and revealed an adjusted coefficient of determination of 0.49.

The first two axes explained 73.72% of the variability of the Dolly Varden indices. Whereas the first RDA axis (RDA1; 44.3% of the explained variability) showed a strong association with Dolly Varden harvest number, the second axis (RDA2; 29.42% of the explained variability) was correlated with the somatic parameters.

Other than on HIQ, the contribution for the explanation on the variance of the response variables was primarily provided by the parameter and with no clear distinction on the geographical position of the different AOIs. The arrow length shows that FNU (N4, F2), BT (F1, F4, N1, N4) and SPT (F2, F5) and wind speed (24 before) reflect the highest contribution to explain the variance of the model.

According to the triplot (Fig. 36), the harvest number at SPT was positively correlated with brightness temperature (F4, N1, N4, SPT and N1) as well as SPM in AOI N1. On the other hand, the arrows of the environmental parameter turbidity (F3, N3, N2, F1, F2), SPM (F3, F4, F2, F5), and wind speed direction (day of harvest and 48 hours prior) pointed in the opposite direction. Consequently, a negative relationship is observed with respect to these parameters and harvest number.

The somatic factors (condition and fork length) were strongly correlated with RDA axis 2. The arrows of both response variables revealed an association with chl-a concentration (N1, N2, N3), SPM (SPT, F2, F2, N3) and BT (F2, F5, N2). Additionally, turbidity values (N4- and F3-FNU) as well as concentration of SPM in the AOI F3 suggest a negative relationship with both somatic response variables.

Similar to HIQ, the outcome of the RDA should be interpreted with caution, as the limited number of data may cause unwanted effects and spurious interactions.

5 Discussion

The present study used remote sensing (L8 and S2) derived environmental parameters to describe the habitat use patterns of anadromous Dolly Varden during the summer months in the western Canadian Arctic, Beaufort Sea. Overall, the results provided a valuable source of information on the habitat use and distribution of the species under fluctuating environmental conditions. During ocean residence in summer, the species utilizes productive, and warmer, habitats under less turbid conditions. The Mackenzie River plume influences the physico-chemical conditions in the coastal and offshore region and spatially impacts the distribution of Dolly Varden in the Beaufort Sea depending on wind conditions.

5.1 Dolly Varden Parameters

5.1.1 Harvesting Rate

For both sites (HIQ and SPT), harvest numbers showed strong intra- and interannual fluctuations between the respective fishing days. These findings were to be expected, however, since the species is extremely mobile and experiences dynamic environmental factors (Park et al., 2020). Accordingly, spatial, and temporal distribution of ichthyofauna underlies a variety of factors, such as seasonal variation in spawning and feeding migrations (Peer & Miller, 2014), changes in food availability (e.g., Mackinson et al., 1999), inter- and intraspecific competition and predation (Ciannelli et al., 2008), and shifts of environmental factors (i.e., temperature, turbidity, and salinity) (Pennino et al., 2020). The habitat use of Dolly Varden in marine waters is subject to physical and ecological conditions (Park et al., 2020). As environmental physicochemical conditions in the Beaufort Sea fluctuate, specimens move between areas to maximize their ontogenetic fitness, leading to distinct fluctuations of spatial aggregation of individuals.

On average, higher catch numbers were recorded on HIQ, while numbers on SPT were considerably lower. Being an opportunist feeder, Dolly Varden moves spatially in the marine environment between different areas to maximize its ontological fitness (McCart, 1980). While previous studies have suggested that species inhabits milder, brackish waters nearshore and forego temporal migrations into deep, colder waters with higher salinity (Craig, 1989), Gallagher et al. (2021) showed that the marine habitat use of the species is primarily determined by foraging behaviour and physical oceanography. Furthermore, the authors hypothesize, that the warmer, brackish water plume of the Mackenzie River extends the suitable habitat to the species

and thus open the possibility to exploit a larger foraging area of higher productivity (Gallagher et al., 2021). Therefore, with the potential to maximize ontogenetic fitness in offshore areas, the results suggest that fewer specimens reside in waters in close proximity to the river delta (i.e., SPT).

Overall, month-to-month catch numbers fluctuated considerably, with the most fish harvested in July, with the lowest numbers shown for June. With the onset of ice sheet breakup in fresh and marine waters during late spring and summer, species of anadromous fish migrate to marine areas to take advantage of the increased productivity (Gross et al., 1988). However, Jonsson et al. (1997) found, that during migration- and spawning phases, absolute and relative energy losses of Atlantic salmon (*Salmo salar*) positively correlated with the individual's body length. Therefore, anadromous individuals would require a minimum level of somatic reserves to ensure downstream migration (Jonsson & Jonsson, 2002), leading to specimens with greater somatic reserves are the first to undertake the ocean migration, whereas weaker specimens need to regain energy reserves first. Furthermore, it has been documented, that the distinct populations of the different natal streams vary in their migration times by a few weeks (Kowalchuk et al., 2010). Accordingly, a reduced number of fish catches in June would be attributed to a lower abundance Dolly Varden in the Beaufort Sea in June.

However, differences in the monthly catch of Dolly Varden between sampling points also reflect differences in sampling periods and methodologies. While the catches on HIQ were documented from June to August, the records for SPT only showed catches in July and August. At Herschel Island, the total Dolly Varden catch was consistently recorded by Herschel Island Territorial Park rangers, who are stationed on the island annually by mid-June till September (Gallagher et al., 2013). The sampling on SPT was conducted by subsistence fishers, who are only present on the headland from mid-July onwards (Lowewen et al., 2019), thus resulting in a shortened sampling season at the site. The data show that fishing at both sites did not occur daily, but was heterogeneously distributed over time, with several gaps between days. On Herschel Island, fishing days in June were often recorded very infrequently. Accordingly, higher quantities of Dolly Varden may have been present at the respective sites but were not recorded due to the absence of harvest numbers.

5.1.2 Fork length and Condition factor

In terms of fork length, the comparison of the two study points showed evident differences. Considering the recordings at both sampling points in July and August, the average length of the fish caught at HIQ was 73.42 ± 21.88 mm greater. The Inuvialuit have found pronounced differences in Dolly Varden size between Herschel Island and Shingle Point, which they attribute to the different water characteristics of the two sites (Byers et al., 2010). Spatiotemporal distribution of fish populations may be influenced by ontogenetic aspects, among other factors, as individual's age and size (Gratwicke, et al., 2006). The colder and less saline waters around Herschel Island may thus not only provide suboptimal habitat conditions for smaller specimens but also may provide less shelter from predators due to less turbidity. With the proximity of SPT to the Mackenzie River, we would hypothesize that due to the strong freshwater outflow, the warmer and less saline water conditions would provide preferential habitat for younger/smaller specimens (Gadomski & Cadell, 1991). However, given the different mesh sizes of the fishing nets which have been applied at the two sampling points (SPT 3 - 3.5 inches; and HIQ 3.5 - 4 inches), it is likely that this has resulted in a bias in the length data. Mesh sizes in gill nets have been shown to act relatively selective regarding the fish size (Rudstam et al., 1984)

Dolly Varden captured in June had the longest average fork lengths which then decreased towards mid-July. As the ice cover retreats in June, anadromous individuals begin to migrate to coastal waters. Smaller individuals are at a distinct fitness disadvantage relative to their larger conspecifics because of energy-consuming migration routes which translates into increased mortality or predation (Hendry et al., 2004). Therefore, after the overwintering phase in spring, anadromous individuals would require a minimum level of somatic reserves to ensure downstream migration (Jonsson & Jonsson, 2002). Early migrating fish can thus be expected to be individuals with sufficient somatic energy reserves, osmoregulatory capabilities, and growth rates, which seek out the highly productive coastal waters for early migration to cover metabolic needs.

Furthermore, it was found that caught specimens increased in fork lengths again from mid-July toward the middle and end of August. Dutil (1986) described that time at sea for post-spawning individuals was found to be on average 3 weeks longer than for non-spawners, presumably because they required more time feeding in response to the increased energy demands associated with spawning. However, in ectotherms warming temperatures and rich feeding lead to an increase in metabolism and growth rate (Pörtner et al., 2008). Nevertheless, the exact

number of animals as well as the behavioural age distribution in marine waters at this time was not known. Whether the increased fork length in late summers can be attributed to migration patterns or somatic changes (summer growth) remains unclear in the context of this study.

Feeding during the summer season is essential for anadromous species to build up energy reserves for the winter months, which are consumed during this time for spawning and survival without replenishing reserves until the next summer (Dutil, 1986). With progression of the summer season, K showed growing values at both harvesting sites, with lowest recorded values in June and highest in August. Energy reserves are nearly depleted at this time as fish usually do not feed during the winter months due to resource scarcity, resulting in relatively low K during the early summer months (Gross et al., 1988). Summer feeding in marine waters occurs for two months and ensures that Dolly Varden increase their somatic condition and gain enough reserved for overwintering period, during which they do not feed (Gyselman, 1994). Accordingly, the findings that K increases during the summer season were expected whereby no evident atypical patterns were observed.

For July and August, the results revealed distinct differences in average condition and length between the two sampling sites (HIQ and SPT). However, both sites exhibit different physicochemical water characteristics, most likely to affect the spatial distribution of the species respective to the individual's size, somatic robustness and well-being (e.g., Hicks et al., 2014). Yet, K and length of Dolly Varden are most likely be influenced by ontogenetic changes associated with the age, size, and competitive ability of individuals (e.g., Hicks et al., 2014). However, similar to fork length such results may be related to different mesh sizes by the harvesters, as K is being derived from the specimen's fork length. Consequently, based on selective harvesting by the smaller mesh size a bias on K values for SPT cannot be ruled out.

5.1.3 Limitations

At both sampling locations, harvesting and biological sampling was primarily opportunistic and did not follow a systematic strategy. Therefore, sampling times varied widely from one day to the next mainly due to weather conditions that impacted the ability to fish. In addition, no records of fishing time and number of harvesters were available, which could provide information on CPUE (catch per unit effort), serving as a more precise metric to determine fish abundance in a given area. Furthermore, the assumption of the study was, that catches reflect the marine summer distribution of Dolly Varden in the Beaufort Sea. However, under certain atmospheric and environmental conditions (e.g., bad weather), the gear may experience a

reduced effectiveness. As a result, fewer or no fish were caught in the nets, although large quantities of fish were present.

5.2 Environmental Parameters

5.2.1 Wind speed and direction

Wind directions of moderate to fresh breezes appeared to originate from W to WNW and E to ES directions and is consistent with Hill et al. (1991) who reported that winds were predominantly from ESE and NW directions in the Beaufort Sea. In August, storms became more frequent, blowing predominantly from W to WSW at increased speeds up to 48 km/h and were similar to observations by Solomon (2005).

The wind intensity on the day of harvest as well as 48 hours prior showed a significant effect on the number of fish captured at HIQ. The influence of wind on harvest rates has been examined in other fisheries such as European plaice (*Pleuronectes platessa*) in the southern North Sea whose catches were negatively correlated with increasing northerly winds (Harden Jones et al., 1979). Alternatively, Atlantic cod (*Gadus morhua*) were found to increase under increased winds (Scholes, 1982). Wind-driven waves and associated currents can affect the distribution of fish in shallow waters (Bentounsi et al., 2018). Such atmospheric events are known to influence the physicochemical properties of aquatic ecosystems, i.e., through upwelling events, thermal changes (Williams & Carmack, 2008) and redistribution of planktonic larvae as well as phyto- and zooplankton (Sobral & Widdows 2000; Walkusz et al., 2010).

Gallagher et al. (2021) emphasise the influence of the Mackenzie plume on the summer distribution of Dolly Varden in the Beaufort Sea. The influence of wind vectors on the spread of the plume has been described by Carmack and Macdonald (2002), whereas easterly winds favour upwelling and spread the plume into the offshore regions, westerly winds push the plume against the coast towards Amundsen Gulf. Mulligan and Perrie (2019) describe that under strong winds, the Mackenzie River plume can spread up to 30 km per day into offshore waters. Furthermore, the coastal plume responds to wind events in less than a day, leading to the development of intense currents and large fluctuations in water mass properties throughout the shallow zone of the submarine delta (Mulligan & Perrie, 2019). The approximate distance of 100 km between the HIQ and the river mouth suggests that a time lag between the intensity of atmospheric forcing and the accumulation of Dolly Varden in PC is to be expected. However, the magnitude of the time lag between the occurrence of the atmospheric event and the response of the Dolly Varden relies on the initial position of the plume.

5.2.2 Sea Ice Concentration

Sea ice abundance was only observed at Herschel Island in July 2013 and 2018. During this time, the harvest rate of Herschel increased noticeably within the 20 km radius. The fork length and condition factor on these events did not show atypical patterns. The influence of the Mackenzie discharge of relatively warmer water at SPT, in general, results in earlier ice breakup in the area and a substantially longer ice-free season (Carmack & Macdonald, 2002) that likely influenced the lack of ice observed in the area among study years.

The results show that summer sea ice in the northern as well as eastern positions to Herschel Island has a significant, but weak, influence on the aggregation of Dolly Varden in PC. The impact of sea ice on the habitat use of Dolly Varden is a long-standing knowledge to indigenous subsistence fisheries. Traditional Inuvialuit knowledge documents that Dolly Varden become more easily trapped in fishing nets when sea ice moves shoreward (Harwood et al., 2012). Whereas under ice free conditions Dolly Varden disperses in greater distance to the shore (Courtney et al., 2018), previous research has shown that Dolly Varden moves on and off the coast according to sea ice movements, while feeding on pagophilic invertebrates (Benson, 2010). While this supports the suggestion that the animals reside close to sea ice for foraging, there has been further evidence to suggest that sea ice acts as a barrier to the species, which pushes specimens onshore when ice is in close proximity to the coast (Gallagher et al., 2021). Nevertheless, unlike the study by Gallagher et al. (2021), results of this study showed a very patchy ice density with a maximum areal coverage of 50 - 80%. Therefore, it cannot be said with certainty whether ice may have functioned primarily as a food source or as a migratory barrier to the species in this study.

However, further studies should be undertaken to fully understand the relationship between drifting sea ice and the distribution of Dolly Varden off the ice edge, which may help to better understand the ecology and distribution mechanisms of the species in the future.

5.3 Environmental parameters (L8 and S2)

Remote sensing derived parameters (i.e., BT, Chl-a, turbidity and SPM) showed strong differences between the sites (SPT and HIQ), with spatial and monthly variations evident throughout the sampling period. In general, most parameters showed significantly greater values for SPT than for HIQ. Such variations are primarily linked to the distance between our two study locations in the Mackenzie River Delta. The river is known for its high sediment (127×10^6 tons per year; O'Brien et al. 2006) and high nitrate load ($5.3 \mu\text{mol}$ per litre; Emmerton et al., 2008). According to Walkusz et al. (2009), the surface water characteristics transition from warm (temperatures of 10 and 12 °C), fresh (salinities of 15 and 6 psu), and highly turbid Mackenzie River waters to a relatively clear, cooler (4 - 9 °C), surface layer of higher salinity (14 to 28 psu) as it traverses from near- to offshore regions. In the absence of winds or under NW winds, incoming water masses from the Mackenzie Delta are pushed eastward along the Tuktoyaktuk Peninsula toward the Amundsen Gulf (McDonald & Yu, 2006). Under easterly wind conditions, the Mackenzie River plume extends much further west on the Canadian Beaufort Shelf (Carmack & Macdonald, 2002). It is well known that seasonal time and intensity of Mackenzie River outflow strongly influence the biochemistry of the nearshore areas (Carmack et al., 2004). The phytoplankton bloom directly relies on the influx of nutrients, sediments, and other plankton organisms, while it indirectly underlies the regulation of vertical and horizontal density gradients and the light climate (i.e., turbidity) (Carmack et al., 2004). Nevertheless, due to sufficient nutrient supply and better light climate, it becomes clear that Chl-a concentrations are higher under lower influence of the Mackenzie in the offshore regions.

The satellite-derived parameters also vary strongly from month to month. The highest values for SPM and turbidity were recorded in June with the melting of the snow and ice masses, which consistently decreased towards the end of the summer season. As inland temperatures increase starting in mid-May and June, freshwater stream discharge peaks because of melting snow in the catchments (Carmack & Macdonald, 2002). As the snow and ice melt, the high amounts of sediment and particulate matter enter the Canadian Beaufort Sea. Consequently, the particulate matter and turbidity of the plume increases during this period (Carmack & Macdonald, 2002). As summer progresses, the discharge of sediments and particulate matter decreases, resulting in substantial lower values of the parameters in July and August.

The seasonal maximum values for BT and Chl-a, unlike for SPM and turbidity, were observed in July and August. The lowest average values were recorded in June. This is expected as the highest values of solar radiation occur in June (Carmack & Macdonald, 2002) while the

maximum air temperatures are measured in July and August (Burn & Zhang, 2008). With the discharge of the Mackenzie River, high quantities of nutrients also are released into the sea. As the ice cover breaks up, the light climate at the water surface intensifies, leading to a pronounced bloom of primary production (Carmack & Macdonald, 2002). As a result of summer stratification, nutrients in the photic layer are depleted, which leads to a decline in pelagic algal production (Tremblay et al., 2008) and lower August Chl-a concentration at both study sites.

5.3.1 Limitations

A satellite image is an instantaneous representation of dynamics of the study area and is thus showing a snapshot of environmental forces at work immediately prior to the image acquisition. The combined use of Landsat-8 (16-day repeat cycle) and Sentinel-2 (10-day repeat cycle; 5-day repeat cycle with S2B satellite) provides a reasonable temporal coverage of the study period. The entire sampling period spans 630 days, and a total of 94 images were retrieved for that period. The images are therefore scattered in time and separated by varying timespans which resulted in substantial time gaps. Discrete environmental events (e.g., plankton bloom) may not have been recorded by our time series even though they might have substantial impacts on fish behaviour. Some sensors (e.g., SeaWiFS, MODIS) can overcome this issue by providing imagery on a much more frequent basis, but they are characterized by a considerably coarser resolution (~1 km/pixel). This resolution is often too coarse to resolve small-scale environmental features relevant to coastal ecology (Chen et al., 2007).

The determination of specific environmental parameters is also challenging and is highly dependent on the relevance and accuracy of the algorithms used in the process. Chl-a determination, for instance, is known to be plagued with important limitations. Because of the limited light intensity in polar waters, phytoplankton organisms have increased their cellular pigment concentration to absorb sufficient light for net growth. As a result, the organisms form dense concentrations which forces them to absorb less light per pigment unit than their counterparts in mid- low latitudes (Matsuoka et al., 2007). On the other hand, accumulation of chromophoric dissolved organic matter (CDOM) in the nearshore zones of the study area may occur because of the input from the Mackenzie River (Retamal et al., 2008; Hessen et al., 2010). Generally, CDOM compounds show similar properties to the Chl-a molecule of phytoplankton (Mitchell & Holm-Hansen, 1991) due to the strong absorption properties of the blue and reduced green wavelengths. Hence, based on satellite imagery, waters with high CDOM concentrations misleadingly appear to contain large amounts of phytoplankton (Matsuoka et al., 2007), which could have led to a bias in the results, especially for SPT.

5.4 Redundancy Analysis and Synopsis

Dolly Varden coastal fisheries are influenced by various environmental factors (temperature, turbidity, and Chl-a, wind, and ice), whereby the spatial position (AOI) of the environmental event showed different impacts on harvest number and fork length at both sites.

For both study sites (HIQ and SPT), temperature (BT) showed a positive correlation with the harvesting numbers. For instance, BT data for July showed that temperature values increased by 7 to 11 °C when influenced by the Mackenzie plume, depending on geographic location. Accordingly, SPT (measured 10 - 14°C) and HIQ (measured 8 - 10°C) were shown to have considerably higher values under plume influence compared to the rest of the western Canadian Beaufort Sea (measured 1 - 3°C). In ectotherms, ambient temperature largely determines physiological processes (e.g., metabolic- and growth rates), which are limited by optimal thermal conditions (Mark et al., 2002; Farrell et al., 2009). In the marine environment, anadromous Dolly Varden are described to inhabit waters with a salinity of < 32‰ and a temperature ranging from 0.5 to 14 °C (COSEWIC, 2010). Gallagher et al. (2021) support the results of this study by stating that Dolly Varden use the Mackenzie warmer, less saline water properties of the plume to migrate offshore, whereby the authors emphasize that preferably occupied areas showed thermal ranges from 5 - 8°C. Consequently, under the influence of the Mackenzie plume, warmer, less saline waters indicate favourable habitat conditions for this species. Relative to both fishing areas, HIQ indicates better thermal conditions for the species, suggesting higher catch rates under thermal influence of the Mackenzie plume.

Chl-a concentrations appeared to have both positive and negative effects on Dolly Varden catch rates sites. High Chl-a values in PC showed a significant positive correlation to the harvest numbers on HIQ. On the other hand, elevated Chl-a concentrations in the surrounding AOIs (F4, N1, F5, N4, and F1) had a negative effect on the harvest number. Bellido et al. (2008) found a weak but positive correlation between indicators of primary productivity (i.e., Chl-a) and abundance of pelagic primary and secondary consumers, which supports the assumption that areas with higher primary productivity are preferred by fish of higher trophic levels, such as Dolly Varden. Accordingly, anadromous salmonids aim to maximize their energetic and physiological fitness during the summer open water season (McCart, 1980). Therefore, spatial distribution of Dolly Varden in offshore region of the Beaufort is likely related to the high abundance of epipelagic zooplankton and forage fishes (Smith, 2010), which consequently would result in higher aggregations of the species in areas of increased productivity.

Additionally, a significant positive correlation between fork length of caught individuals and chl-a concentrations at fishing points and AOIs in close proximity site was found at HIQ and SPT. It can be hypothesized, that the increased prey density may have attracted specimens of greater fork length (McCart, 1980), which migrate to nearshore waters to exploit high resource availability.

Nevertheless, while primary production (Chl-a) can be derived directly from satellite imagery, there have been mixed results from extrapolating such information to secondary or tertiary trophic levels, or from deriving both spatial and temporal variability to biological activity in the given regions (Suryan et al., 2006; Block et al., 2011). However, the satellite images are an instantaneous representation of the environment, because of the heterogeneously scattered imagery, peaks in productive algal bloom may have been missed. Consequently, an apparent spatial and temporal discrepancy between secondary and tertiary consumers in response to Chl-a peaks could potentially have been overlooked in scope of this thesis (Suryan et al., 2012).

Increasing turbidity and SPM levels were found to negatively affect catches, size, and condition of Dolly Varden. While SPT had relatively constant turbidity values, increasing FNU values at PC and the nearby eastern AOIs (N4) were found to negatively influence the catches. On the other hand it can be hypothesized, that elevated turbidity in the far NE (F4) region of Herschel Island, pushed the animals to the nearshore areas, as it significantly positively correlated with in harvesting numbers on the island. Similar results were found by Gallagher et al. (2021) who state, turbid plume of the Mackenzie River strongly influences the offshore movements of Dolly Varden, as the species was suggested to avoid increased turbidity concentrations. Turbidity is well known to affect the physicochemical properties of aquatic ecosystems through shading, scattering and absorption of light, resulting in reduced dissolved oxygen and increased temperature (Bruton, 1985) or reduced light levels (Donohue & Garcia Molinos, 2009). The extent of turbidity has been found to have differential effects on marine fish communities, with respect to feeding guilds and environmental conditions (Bowmaker, 1995). Being a visual forager, light and turbidity have a strong influence on the detection of prey as well as the temporal-spatial foraging success of Dolly Varden (Henderson & Northcote, 1985; Guthrie & Muntz 1993). However, the species is described as capable of using habitat with turbidity of 1 – 146 FNU (Craig et al., 1984). Yet, values > 55 FNU have rarely been recorded around HIQ. Gallagher et al. (2021) describe clear differences in habitat use of the offshore and nearshore

areas with respect to turbidity. Although fish in the nearshore zone appear to tolerate higher levels of turbidity, catch rates decrease significantly under increasing FNU values.

While SPM was excluded for HIQ for the best fitting model, the results on SPT suggest a mixed relationship between both SPM and turbidity on catch rates, fork length and condition factor. Because of their strong absorption properties in the blue and reduced green wavelength range, CDOM particles show similar properties to the Chl-a molecule of phytoplankton. As SPT experiences more of the effects of the Mackenzie Delta plume (including e.g. a high loading of fine and coarse particles) that produce a continuous exposure to CDOM. However, in comparison to HIQ, Dolly Varden harvested in the vicinity of SPT typically exhibited reduced conditions and lengths values. With the RDA, it is clearly implied that both these factors experience an influence by the environmental parameters. Yet the influence is very small and should be taken with caution since a smaller mesh size of the fishing nets was used at SPT.

5.4.1 Limitations

The outputs of the RDA illustrate the relationships among data derived from fisheries-dependent harvest monitoring and satellite imagery. Regarding data collection, there were considerable limitations in methodology from harvest monitoring and remote sensing. There were frequent inconsistencies between day of harvest and satellite imagery. While the method of using the average harvest number ± 2 days of the satellite image may provide an estimate of the distribution and relative abundance of fish and their response to environmental conditions, it should still be considered cautiously. As a highly mobile species, Dolly Varden uses coastal areas in response to changing biological and physical environmental conditions. Although strong fluctuations were occasionally observed between fishing days, for most of the sampling period there was little variation between the individual days used for the satellite images.

6 Conclusion and Recommendation

As a species of cultural and nutritional importance of the indigenous communities residing the North American Arctic regions, findings of the study on the habitat use mechanisms of the Dolly Varden are of great importance for future management and impact assessment in the Beaufort Sea. Although numerous studies in the past have examined population dynamics of the Dolly Varden in Arctic marine waters, important details of marine distribution and influencing environmental factors remains not fully understood.

The objective of the study was to examine how the timing and harvest of Dolly Varden in the nearshore summer subsistence fishery are influenced by environmental conditions in the Beaufort Sea. In addition, it was investigated whether there was a relationship between environmental parameters and the demographic and somatic characteristics of the captured Dolly Varden. In situ biological data (catch numbers, fork length and condition) combined with satellite imagery (Landsat 8 and Sentinel 2), sea ice and wind were analysed under seasonal summer conditions (2013 – 2019) with a focus on Chl-a, SPM, turbidity and BT.

Results of the study clearly support tradition knowledge of the indigenous communities as they revealed that animal dispersal is subject to a variety of environmental mechanisms. The most important environmental drivers in dispersal mechanisms were apparently turbidity and chl-a (primary production) and temperature/salinity, which affected the accumulation of animals at the two sampling sites differently, depending on the geographical location of the respective environmental event.

According to the findings of the study, the following conclusions can be drawn:

- The environmental conditions of warmer water temperatures around HIQ and increased production levels in PC showed a significant correlation with numbers of harvested fish, suggesting increased aggregation of animals in the cove. Additionally, the presence of the plume related turbid front in the northern offshore areas (F4) was found to increase harvest. Therefore, we suggest that under exposure of increased plume related turbidity, the species seeks out for clearer water properties, including bays and coves in near shore areas. Increase in fork length under higher Chl-a concentration in PC suggest a higher concentration of larger/ older specimens to exploit the highly productive foraging ground in the area.

- The presence of sea ice in close proximity to the fishing site had a positive effect on harvest numbers as well. While Inuvialuit traditional knowledge associates this phenomenon with increased prey abundance of sympagic fauna, other studies suggest that the ice acts as a barrier and retains fish in coastal areas. Throughout this study, however, sea ice was very infrequent during the summer season, thus the driving forces causing Dolly Varden to aggregate in PC under the presence of sea ice were not clear and remains to be investigated for future studies.
- Higher chlorophyll-a levels in surrounding areas had a negative effect on aggregation of animals in Pauline Cove, apparently causing fish to migrate to more productive waters. So did an increase of turbidity levels in the cove. The results support common theories, that Dolly Varden seeks to maximize its ontogenetical fitness by occupies areas to support conditions to support the strategy in a best possible way.
- Winds appear to be major an indirect factor, as it is the primary influence physicochemical properties due to upwelling and distribution of the Mackenzie Plume in the Beaufort Sea.
- Although similar influences were found on SPT, the area is strongly influenced by Mackenzie River runoff. The high turbidity levels and concentrations of suspended particles in the water column had a visible impact on the remote sensing method readings. Whether the occupancy of smaller/ younger specimens at SPT is related to the physicochemical water properties or relies on selective harvesting methods remains to be open.

For the purpose of improving the results of this study and to be able to draw valid conclusions in the long term, greater precision in situ measurements are needed from the area under study to determine the population distribution of the animals on the best possible daily basis. It is recommended to implement standardised sampling methods, from which higher values can be derived (i.e., catch per unit effort), thereby providing more precise information on the population dynamics of Dolly Varden in the Beaufort Sea. For the future, environmental-based distribution mechanisms of the animals could be better understood thus help to design management- and conservation strategies of the species.

7 Bibliography

- Agmour, I., Bentounsi, M., Baba, N., Foutayeni, Y. E., Achtaich, N., & Aouiti, C. (March 2020). Impact of wind speed on fishing effort. *Modeling Earth Systems and Environment*, 6, 1007–1015. doi:10.1007/s40808-020-00736-7
- Alberta Society of Petroleum Geologists. (1951). Western Canada. *AAPG Bulletin*, 35. doi:10.1306/3d934166-16b1-11d7-8645000102c1865d
- Andrade, H. A. (January 2003). The relationship between the skipjack tuna (*Katsuwonus pelamis*) fishery and seasonal temperature variability in the south-western Atlantic. *Fisheries and Oceanography*, 12, 10–18. doi:10.1046/j.1365-2419.2003.00220.x
- Armitage, D., Berkes, F., Dale, A., Kocho-Schellenberg, E., & Patton, E. (August 2011). Co-management and the co-production of knowledge: Learning to adapt in Canada's Arctic. *Global Environmental Change*, 21, 995–1004. doi:10.1016/j.gloenvcha.2011.04.006
- Asplin, L., Albretsen, J., Johnsen, I. A., & Sandvik, A. D. (May 2020). The hydrodynamic foundation for salmon lice dispersion modeling along the Norwegian coast. *Ocean Dynamics*, 70, 1151–1167. doi:10.1007/s10236-020-01378-0
- Barsi, J., Schott, J., Hook, S., Raqueno, N., Markham, B., & Radocinski, R. (November 2014). Landsat-8 Thermal Infrared Sensor (TIRS) Vicarious Radiometric Calibration. *Remote Sensing*, 6, 11607–11626. doi:10.3390/rs61111607
- Bellido, J. M., Brown, A. M., Valavanis, V. D., Giráldez, A., Pierce, G. J., Iglesias, M., & Palialexis, A. (2008). Identifying essential fish habitat for small pelagic species in Spanish Mediterranean waters. In *Essential Fish Habitat Mapping in the Mediterranean* (S. 171–184). Springer Netherlands. doi:10.1007/978-1-4020-9141-4_13
- Benson, K. L., Faff, R. W., & Smith, T. (April 2010). The simultaneous relation between fund flows and returns. *Australian Journal of Management*, 35, 51–68. doi:10.1177/0312896209354217
- Bentounsi, M., Agmour, I., Achtaich, N., & Foutayeni, Y. E. (2018). The Impact of Price on the Profits of Fishermen Exploiting Tritrophic Prey-Predator Fish Populations. *International Journal of Differential Equations*, 2018, 1–13. doi:10.1155/2018/2381483

- Block, B. A., Jonsen, I. D., Jorgensen, S. J., Winship, A. J., Shaffer, S. A., Bograd, S. J., . . . Costa, D. P. (June 2011). Tracking apex marine predator movements in a dynamic ocean. *Nature*, *475*, 86–90. doi:10.1038/nature10082
- Bost, C. A., Cotté, C., Bailleul, F., Cherel, Y., Charrassin, J. B., Guinet, C., . . . Weimerskirch, H. (October 2009). The importance of oceanographic fronts to marine birds and mammals of the southern oceans. *Journal of Marine Systems*, *78*, 363–376. doi:10.1016/j.jmarsys.2008.11.022
- Bouchard, C., Geoffroy, M., LeBlanc, M., Majewski, A., Gauthier, S., Walkusz, W., . . . Fortier, L. (August 2017). Climate warming enhances polar cod recruitment, at least transiently. *Progress in Oceanography*, *156*, 121–129. doi:10.1016/j.pocean.2017.06.008
- Braga, A. M., Marques, R. C., Rodrigues, F. A., & Medeiros, F. N. (July 2017). A Median Regularized Level Set for Hierarchical Segmentation of SAR Images. *IEEE GEOSCIENCE AND REMOTE SENSING LETTERS*, *14*, 1171–1175. doi:10.1109/lgrs.2017.2702062
- Brown, R. J., Courtney, M. B., & Seitz, A. C. (October 2018). New Insights into the Biology of Anadromous Dolly Varden in the Canning River, Arctic National Wildlife Refuge, Alaska. *Transactions of the American Fisheries Society*, *148*, 73–87. doi:10.1002/tafs.10122
- Bruton, M. N. (1985). The effects of suspensoids on fish. In *Developments in Hydrobiology* (S. 221–241). Springer Netherlands. doi:10.1007/978-94-009-5522-6_16
- Burn, C. R. (May 2012). *Herschel Island Qikiqtaryuk: A Natural and Cultural History*. UNIV OF CALGARY PR. Von https://www.ebook.de/de/product/19118343/herschel_island_qikiqtaryuk_a_natural_and_cultural_history.html abgerufen
- Burn, C. R., & Zhang, Y. (April 2009). Permafrost and climate change at Herschel Island (Qikiqtaruq), Yukon Territory, Canada. *Journal of Geophysical Research*, *114*. doi:10.1029/2008jf001087
- Carmack, E. C., & Macdonald, R. W. (2002). Oceanography of the Canadian Shelf of the Beaufort Sea: A Setting for Marine Life. *Arctic*, *55*, 29–45. <http://www.jstor.org/stable/40512418>.

- Carmack, E. C., Macdonald, R. W., & Jasper, S. (2004). Phytoplankton productivity on the Canadian Shelf of the Beaufort Sea. *Marine Ecology Progress Series*, 277, 37–50. doi:10.3354/meps277037
- Chen, Q., Wang, C., Zhan, Z., He, W., Cheng, Z., Li, Y., & Liu, Z. (September 2014). Near-infrared dye bound albumin with separated imaging and therapy wavelength channels for imaging-guided photothermal therapy. *Biomaterials*, 35, 8206–8214. doi:10.1016/j.biomaterials.2014.06.013
- Chen, Z., Hu, C., & Muller-Karger, F. (July 2007). Monitoring turbidity in Tampa Bay using MODIS/Aqua 250-m imagery. *Remote Sensing of Environment*, 109, 207–220. doi:10.1016/j.rse.2006.12.019
- Ciannelli, L., Fauchald, P., Chan, K. S., Agostini, V. N., & Dingsør, G. E. (June 2008). Spatial fisheries ecology: Recent progress and future prospects. *Journal of Marine Systems*, 71, 223–236. doi:10.1016/j.jmarsys.2007.02.031
- COSEWIC. (2010). *COSEWIC assessment and status report on the Dolly Varden, Salvelinus malma malma, western Arctic populations in Canada*. Ottawa: Committee on the Status of Endangered Wildlife in Canada. Von www.sararegistry.gc.ca/status/status_e.cfm abgerufen
- Courtney, M. B., Scanlon, B., Brown, R. J., Rikardsen, A. H., Gallagher, C. P., & Seitz, A. C. (January 2018). Offshore ocean dispersal of adult Dolly Varden *Salvelinus malma* in the Beaufort Sea. *Polar Biology*, 41, 817–825. doi:10.1007/s00300-017-2246-5
- Craig, P. C. (May 1984). Fish Use of Coastal Waters of the Alaskan Beaufort Sea: A Review. 113, 265–282. doi:10.1577/1548-8659(1984)113<265:fuocwo>2.0.co;2
- Dassenakis, M., Paraskevopoulou, V., Cartalis, C., Adaktilou, N., & Katsiabani, K. (December 2011). Remote sensing in coastal water monitoring: Applications in the eastern Mediterranean Sea (IUPAC Technical Report). *Pure and Applied Chemistry*, 84, 335–375. doi:10.1351/pac-rep-11-01-11
- Department of Indian Affairs and Northern Development. (1984). *Indian and Northern Affairs Canada Annual Report 1984 1985*. Ottawa: Minister of Indian Affairs and Northern Development.

- Deschamps, P. Y., Herman, M., & Tanre, D. (March 1983). Definitions of atmospheric radiance and transmittances in remote sensing. *Remote Sensing of Environment*, *13*, 89–92. doi:10.1016/0034-4257(83)90029-9
- Dogliotti, A. I., Ruddick, K. G., Nechad, B., Doxaran, D., & Knaeps, E. (January 2015). A single algorithm to retrieve turbidity from remotely-sensed data in all coastal and estuarine waters. *Remote Sensing of Environment*, *156*, 157–168. doi:10.1016/j.rse.2014.09.020
- Donohue, I., & Molinos, J. G. (November 2009). Impacts of increased sediment loads on the ecology of lakes. *Biol Rev Camb Philos Soc.*, *84*, 517–531. doi:10.1111/j.1469-185x.2009.00081.x
- Dunton, K. H., Weingartner, T., & Carmack, E. C. (October 2006). The nearshore western Beaufort Sea ecosystem: Circulation and importance of terrestrial carbon in arctic coastal food webs. *Progress in Oceanography*, *71*, 362–378. doi:10.1016/j.pocean.2006.09.011
- Dutil, J.-D. (December 1986). Energetic Constraints and Spawning Interval in the Anadromous Arctic Charr (*Salvelinus alpinus*). *Copeia*, *1986*, 945. doi:10.2307/1445291
- Ehrlich, J., Schaafsma, F. L., Bluhm, B. A., Peeken, I., Castellani, G., Brandt, A., & Flores, H. (June 2020). Sympagic Fauna in and Under Arctic Pack Ice in the Annual Sea-Ice System of the New Arctic. *Frontiers in Marine Science*, *7*. doi:10.3389/fmars.2020.00452
- Emmerton, C. A., Lesack, L. F., & Vincent, W. F. (March 2008). Mackenzie River nutrient delivery to the Arctic Ocean and effects of the Mackenzie Delta during open water conditions. *Biogeochemical Cycles*, *22*, n/a–n/a. doi:10.1029/2006gb002856
- Farrell, A. P., Eliason, E. J., Sandblom, E., & Clark, T. D. (October 2009). Fish cardiorespiratory physiology in an era of climate change
The present review is one of a series of occasional review articles that have been invited by the Editors and will feature the broad range of disciplines and expertise represented in our Editorial Advisory Board. *Canadian Journal of Zoology*, *87*, 835–851. doi:10.1139/z09-092
- Ferrari, R., Bryson, M., Bridge, T., Hustache, J., Williams, S. B., Byrne, M., & Figueira, W. (February 2016). Quantifying the response of structural complexity and community

- composition to environmental change in marine communities. *22*, 1965–1975. doi:10.1111/gcb.13197
- Finstad, B., Nilssen, K. J., & Arnesen, A. M. (1989). Seasonal changes in sea-water tolerance of Arctic charr (*Salvelinus alpinus*). *Journal of Comparative Physiology B*, *159*, 371–378. doi:10.1007/bf00692408
- Fonseca, V. F., Vasconcelos, R. P., Gamito, R., Pasquaud, S., Gonçalves, C. I., Costa, J. L., . . . Cabral, H. N. (December 2013). Fish community-based measures of estuarine ecological quality and pressure–impact relationships. *134*, 128–137. doi:10.1016/j.ecss.2013.02.001
- Franz, B. A., Bailey, S. W., Kuring, N., & Werdell, P. J. (March 2015). Ocean color measurements with the Operational Land Imager on Landsat-8: implementation and evaluation in SeaDAS. *Journal of Applied Remote Sensing*, *9*, 096070. doi:10.1117/1.jrs.9.096070
- Fritz, M., Wetterich, S., Schirrmeister, L., Meyer, H., Lantuit, H., Preusser, F., & Pollard, W. H. (February 2012). Eastern Beringia and beyond: Late Wisconsinan and Holocene landscape dynamics along the Yukon Coastal Plain, Canada. *Palaeogeography, Palaeoclimatology, Palaeoecology*, *319-320*, 28–45. doi:10.1016/j.palaeo.2011.12.015
- Gallagher, C. P., Courtney, M. B., Seitz, A. C., Lea, E. V., & Howland, K. L. (November 2021). Ocean-entry timing and marine habitat-use of Canadian Dolly Varden: Dispersal among conservation, hydrocarbon exploration, and shipping areas in the Beaufort Sea. *Estuarine, Coastal and Shelf Science*, *262*, 107609. doi:10.1016/j.ecss.2021.107609
- Gallagher, C. P., Morrison, C. M., Lea, E. V., Halden, N. M., & Howland, K. L. (March 2019). Growth and reproductive characteristics of rarely observed resident female Dolly Varden (*Salvelinus malma malma*) in North America. *Hydrobiologia*, *840*, 189–205. doi:10.1007/s10750-019-3927-6
- Gernez, P., Doxaran, D., & Barillé, L. (May 2017). Shellfish Aquaculture from Space: Potential of Sentinel2 to Monitor Tide-Driven Changes in Turbidity, Chlorophyll Concentration and Oyster Physiological Response at the Scale of an Oyster Farm. *frontiers in Marine Science*, *4*. doi:10.3389/fmars.2017.00137
- Giardino, C., Bresciani, M., Braga, F., Cazzaniga, I., Keukelaere, L. D., Knaeps, E., & Brando, V. E. (2017). Bio-optical Modeling of Total Suspended Solids. In *Bio-optical Modeling*

- and Remote Sensing of Inland Waters* (S. 129–156). Elsevier. doi:10.1016/b978-0-12-804644-9.00005-7
- Gill, H., & Lantz, T. (October 2014). A Community-Based Approach to Mapping Gwich'in Observations of Environmental Changes in the Lower Peel River Watershed, NT. *Journal of Ethnobiology*, 34, 294. doi:10.2993/0278-0771-34.3.294
- Gouveia, N. A., Gherardi, D. F., Wagner, F. H., Paes, E. T., Coles, V. J., & Aragão, L. E. (January 2019). The Salinity Structure of the Amazon River Plume Drives Spatiotemporal Variation of Oceanic Primary Productivity. *Journal of Geophysical Research: Biogeosciences*, 124, 147–165. doi:10.1029/2018jg004665
- Grange, S. K. (2014). Technical note: Averaging wind speeds and directions. *Technical note: Averaging wind speeds and directions*. Unpublished. doi:10.13140/RG.2.1.3349.2006
- Gratwicke, B., Petrovic, C., & Speight, M. R. (July 2006). Fish distribution and ontogenetic habitat preferences in non-estuarine lagoons and adjacent reefs. *Environmental Biology of Fishes*, 76, 191–210. doi:10.1007/s10641-006-9021-8
- Gross, M. R., Coleman, R. M., & McDowall, R. M. (March 1988). Aquatic Productivity and the Evolution of Diadromous Fish Migration. *Science*, 239, 1291–1293. doi:10.1126/science.239.4845.1291
- Harden Jones, F. R., Arnold, G. P., Walker, M. G., & Scholes, P. (August 1979). Selective tidal stream transport and the migration of plaice (*Pleuronectes platessa* L.) in the southern North Sea. *ICES Journal of Marine Science*, 38, 331–337. doi:10.1093/icesjms/38.3.331
- Harper, J. R. (January 1990). Morphology of the Canadian Beaufort Sea coast. *Marine Geology*, 91, 75–91. doi:10.1016/0025-3227(90)90134-6
- Harris, L. N., Bajno, R., Gallagher, C. P., Koizumi, I., Johnson, L. K., Howland, K. L., . . . Reist, J. D. (October 2015). Life-history characteristics and landscape attributes as drivers of genetic variation, gene flow, and fine-scale population structure in northern Dolly Varden (*Salvelinus malma malma*) in Canada. (P. Morán, Hrsg.) *Canadian Journal of Fisheries and Aquatic Sciences*, 72, 1477–1493. doi:10.1139/cjfas-2015-0016

- Harrison, T. D., & Whitfield, A. K. (September 2004). A multi-metric fish index to assess the environmental condition of estuaries. *65*, 683–710. doi:10.1111/j.0022-1112.2004.00477.x
- Henderson, M. A., & Northcote, T. G. (April 1985). Visual Prey Detection and Foraging in Sympatric Cutthroat Trout (*Salmo clarki clarki*) and Dolly Varden (*Salvelinus malma*). *Canadian Journal of Fisheries and Aquatic Science*, *42*, 785–790. doi:10.1139/f85-100
- Hessen, D. O., Carroll, J., Kjeldstad, B., Korosov, A. A., Pettersson, L. H., Pozdnyakov, D., & Sørensen, K. (June 2010). Input of organic carbon as determinant of nutrient fluxes, light climate and productivity in the Ob and Yenisey estuaries. *Estuarine, Coastal and Shelf Science*, *88*, 53–62. doi:10.1016/j.ecss.2010.03.006
- Hidalgo, M., Rossi, V., Monroy, P., Ser-Giacomi, E., Hernández-García, E., Guijarro, B., . . . Reglero, P. (May 2019). Accounting for ocean connectivity and hydroclimate in fish recruitment fluctuations within transboundary metapopulations. *Ecological Applications*, *29*. doi:10.1002/eap.1913
- Hill, P. R., Blasco, S. M., Harper, J. R., & Fissel, D. B. (August 1991). Sedimentation on the Canadian Beaufort Shelf. *Continental Shelf Research*, *11*, 821–842. doi:10.1016/0278-4343(91)90081-g
- Holland, M. M., Everett, J. D., Cox, M. J., Doblin, M. A., & Suthers, I. M. (February 2021). Pelagic forage fish distribution in a dynamic shelf ecosystem – Thermal demands and zooplankton prey distribution. *Estuarine, Coastal and Shelf Science*, *249*, 107074. doi:10.1016/j.ecss.2020.107074
- Irrgang, A. M., Lantuit, H., Gordon, R. R., Piskor, A., & Manson, G. K. (June 2019). Impacts of past and future coastal changes on the Yukon coast — threats for cultural sites, infrastructure, and travel routes. *Arctic Science*, *5*, 107–126. doi:10.1139/as-2017-0041
- Jarvela, L. E., & Thorsteinson, L. K. (January 1999). The Epipelagic Fish Community of Beaufort Sea Coastal Waters, Alaska. *Arctic*, *52*. doi:10.14430/arctic912
- Jonsson, N., & Jonsson, B. (July 2002). Migration of anadromous brown trout *Salmo trutta* in a Norwegian river. *Freshwater Biology*, *47*, 1391–1401. doi:10.1046/j.1365-2427.2002.00873.x

- Kassi, J.-B., Racault, M.-F., Mobio, B., Platt, T., Sathyendranath, S., Raitzos, D., & Affian, K. (May 2018). Remotely Sensing the Biophysical Drivers of *Sardinella aurita* Variability in Ivorian Waters. *Remote Sensing of Ocean Colour*, *10*, 785. doi:10.3390/rs10050785
- Klein, K. P., Lantuit, H., Heim, B., Fell, F., Doxaran, D., & Irrgang, A. M. (November 2019). Long-Term High-Resolution Sediment and Sea Surface Temperature Spatial Patterns in Arctic Nearshore Waters Retrieved Using 30-Year Landsat Archive Imagery. *Remote Sensing*, *11*, 2791. doi:10.3390/rs11232791
- Klemas, V. (November 2013). Fisheries applications of remote sensing: An overview. *International Journal of Remote Sensing*, *148*, 124–136. doi:10.1016/j.fishres.2012.02.027
- Koenigstein, S., Mark, F. C., Gößling-Reisemann, S., Reuter, H., & Poertner, H.-O. (March 2016). Modelling climate change impacts on marine fish populations: process-based integration of ocean warming, acidification and other environmental drivers. *Fish and Fisheries*, *17*, 972–1004. doi:10.1111/faf.12155
- Kovalenko, K. E., Thomaz, S. M., & Warfe, D. M. (December 2011). Habitat complexity: approaches and future directions. *Hydrobiologia*, *685*, 1–17. doi:10.1007/s10750-011-0974-z
- Lannuzel, D., Tedesco, L., van Leeuwe, M., Campbell, K., Flores, H., Delille, B., . . . Wongpan, P. (October 2020). The future of Arctic sea-ice biogeochemistry and ice-associated ecosystems. *Nature Climate Change*, *10*, 983–992. doi:10.1038/s41558-020-00940-4
- Lantuit, H., & Pollard, W. H. (May 2005). Temporal stereophotogrammetric analysis of retrogressive thaw slumps on Herschel Island, Yukon Territory. *Natural Hazards and Earth System Sciences*, *5*, 413–423. doi:10.5194/nhess-5-413-2005
- Lantuit, H., & Pollard, W. H. (March 2008). Fifty years of coastal erosion and retrogressive thaw slump activity on Herschel Island, southern Beaufort Sea, Yukon Territory, Canada. *Geomorphology*, *95*, 84–102. doi:10.1016/j.geomorph.2006.07.040
- Lea, E. V., Gallagher, C. P., Maier, & Ayles, B. (2021). *Dolly Varden (Salvelinus malma malma) fisheries in the Inuvialuit Settlement Region and the Gwich'in Settlement Area 2009-2014 : harvest, monitoring and communications in an adaptive co-management setting*. DFO Can. Sci. Advis. Sec. Res. Doc. Ottawa: Canadian Science Advisory Secretariat (CSAS).

- Legendre, P., & Legendre, L. (2012). Numerical ecology. Oxford: Elsevier.
- Logerwell, E., Rand, K., Danielson, S., & Sousa, L. (June 2018). Environmental drivers of benthic fish distribution in and around Barrow Canyon in the northeastern Chukchi Sea and western Beaufort Sea. *Deep Sea Research Part II: Topical Studies in Oceanography*, *152*, 170–181. doi:10.1016/j.dsr2.2017.04.012
- Loseto, L. L., Hoover, C., Ostertag, S., Whalen, D., Pearce, T., Paulic, J., . . . MacPhee, S. (November 2018). Beluga whales (*Delphinapterus leucas*), environmental change and marine protected areas in the Western Canadian Arctic. *Estuarine, Coastal and Shelf Science*, *212*, 128–137. doi:10.1016/j.ecss.2018.05.026
- Loseto, L. L., Stern, G. A., Connelly, T. L., Deibel, D., Gemmill, B., Prokopowicz, A., . . . Ferguson, S. H. (June 2009). Summer diet of beluga whales inferred by fatty acid analysis of the eastern Beaufort Sea food web. *Journal of Experimental Marine Biology and Ecology*, *374*, 12–18. doi:10.1016/j.jembe.2009.03.015
- Macdonald, R. W., Solomon, S. M., Cranston, R. E., Welch, H. E., Yunker, M. B., & Gobeil, C. (January 1998). A sediment and organic carbon budget for the Canadian Beaufort Shelf. *Marine Geology*, *144*, 255–273. doi:10.1016/s0025-3227(97)00106-0
- MacGregor, J. M., & Houde, E. D. (1996). Onshore-offshore pattern and variability in distribution and abundance of bay anchovy *Anchoa mitchilli* eggs and larvae in Chesapeake Bay. *Marine Ecology Progress Series*, *138*, 15–25. doi:10.3354/meps138015
- Mackinson, S., L. Nøttestad, S., Guénette, Pitcher, T., Misund, O. A., & Fernö, A. (October 1999). Cross-scale observations on distribution and behavioural dynamics of ocean feeding Norwegian spring-spawning herring (*Clupea harengus* L.). *ICES Journal of Marine Science*, *56*, 613–626. doi:10.1006/jmsc.1999.0513
- Mark, F. C., Bock, C., & Pörtner, H. O. (November 2002). Oxygen-limited thermal tolerance in Antarctic fish investigated by MRI and ³¹P-MRS. *Am J Physiol Regul Integr Comp Physiol*, *283*, R1254–R1262. doi:10.1152/ajpregu.00167.2002
- Mitchell, B. G., & Holm-Hansen, O. (January 1991). Bio-optical properties of Antarctic Peninsula waters: differentiation from temperate ocean models. *Deep Sea Research Part A. Oceanographic Research Papers*, *38*, 1009–1028. doi:10.1016/0198-0149(91)90094-v

- Mkrtchyan, F. A., & Varotsos, C. A. (August 2018). A New Monitoring System for the Surface Marine Anomalies. *Water, Air, & Soil Pollution*, 229. doi:10.1007/s11270-018-3938-3
- Mobley, C. D. (December 1999). Estimation of the remote-sensing reflectance from above-surface measurements. *Applied Optics*, 38, 7442-55. doi:10.1364/ao.38.007442
- Montanaro, M., Gerace, A., Lunsford, A., & Reuter, D. (October 2014). Stray Light Artifacts in Imagery from the Landsat 8 Thermal Infrared Sensor. *Remote Sensing*, 6, 10435–10456. doi:10.3390/rs61110435
- Mulligan, R. P., & Perrie, W. (April 2019). Circulation and structure of the Mackenzie River plume in the coastal Arctic Ocean. *Continental Shelf Research*, 177, 59–68. doi:10.1016/j.csr.2019.03.006
- Nazeer, M., Nichol, J. E., & Yung, Y.-K. (August 2014). Evaluation of atmospheric correction models and Landsat surface reflectance product in an urban coastal environment. *International Journal of Remote Sensing*, 35, 6271–6291. doi:10.1080/01431161.2014.951742
- Nechad, B., Ruddick, K. G., & Neukermans, G. (September 2009). Calibration and validation of a generic multisensor algorithm for mapping of turbidity in coastal waters. (J. Charles R. Bostater, S. P. Mertikas, X. Neyt, & M. Velez-Reyes, Hrsg.) *Proc. SPIE 7473, Remote Sensing of the Ocean, Sea Ice, and Large Water Regions 2009, 74730H*. doi:10.1117/12.830700
- Nechad, B., Ruddick, K. G., & Park, Y. (April 2010). Calibration and validation of a generic multisensor algorithm for mapping of total suspended matter in turbid waters. *Remote Sensing of Environment*, 114, 854–866. doi:10.1016/j.rse.2009.11.022
- O'Reilly, J. E., Maritorena, S., Mitchell, B. G., Siegel, D. A., Carder, K. L., Garver, S. A., . . . McClain, C. (October 1998). Ocean color chlorophyll algorithms for SeaWiFS. *Journals of Geophysical Research*, 103, 24937–24953. doi:10.1029/98jc02160
- Pahlevan, N., Chittimalli, S. K., Balasubramanian, S. V., & Vellucci, V. (January 2019). Sentinel-2/Landsat-8 product consistency and implications for monitoring aquatic systems. *Remote Sensing of Environment*, 220, 19–29. doi:10.1016/j.rse.2018.10.027
- Pahlevan, N., Sarkar, S., Franz, B. A., Balasubramanian, S. V., & He, J. (November 2017). Sentinel-2 MultiSpectral Instrument (MSI) data processing for aquatic science

- applications: Demonstrations and validations. *Remote Sensing of Environment*, 201, 47–56. doi:10.1016/j.rse.2017.08.033
- Park, H., Watanabe, E., Kim, Y., Polyakov, I., Oshima, K., Zhang, X., . . . Yang, D. (November 2020). Increasing riverine heat influx triggers Arctic sea ice decline and oceanic and atmospheric warming. *Science Advances*, 6. doi:10.1126/sciadv.abc4699
- Pearce, T., Ford, J. D., Duerden, F., Smit, B., Andrachuk, M., Berrang-Ford, L., & Smith, T. (April 2010). Advancing adaptation planning for climate change in the Inuvialuit Settlement Region (ISR): a review and critique. *Regional Environmental Change*, 11, 1–17. doi:10.1007/s10113-010-0126-4
- Peer, A. C., & Miller, T. J. (January 2014). Climate Change, Migration Phenology, and Fisheries Management Interact with Unanticipated Consequences. *North American Journal of Fisheries Management*, 34, 94–110. doi:10.1080/02755947.2013.847877
- Pelicice, F. M., Latini, J. D., & Agostinho, A. A. (May 2014). Fish fauna disassembly after the introduction of a voracious predator: main drivers and the role of the invader's demography. *Hydrobiologia*, 746, 271–283. doi:10.1007/s10750-014-1911-8
- Pennino, M. G., Coll, M., Albo-Puigserver, M., Fernández-Corredor, E., Steenbeek, J., Giráldez, A., . . . Bellido, J. M. (July 2020). Current and Future Influence of Environmental Factors on Small Pelagic Fish Distributions in the Northwestern Mediterranean Sea. *Frontiers in Marine Science*, 7. doi:10.3389/fmars.2020.00622
- Poddar, S., Chacko, N., & Swain, D. (October 2019). Estimation of Chlorophyll-a in Northern Coastal Bay of Bengal Using Landsat-8 OLI and Sentinel-2 MSI Sensors. *Frontiers in Marine Science*, 6. doi:10.3389/fmars.2019.00598
- Pörtner, H. O. (August 2002). Climate variations and the physiological basis of temperature dependent biogeography: systemic to molecular hierarchy of thermal tolerance in animals. *Comparative Biochemistry and Physiology Part A: Molecular & Integrative Physiology*, 132, 739–761. doi:10.1016/s1095-6433(02)00045-4
- Pörtner, H., Bock, C., Knust, R., Lannig, G., Lucassen, M., Mark, F. C., & Sartoris, F. J. (October 2008). Cod and climate in a latitudinal cline: physiological analyses of climate effects in marine fishes. *Climate Research*, 37, 253–270. doi:10.3354/cr00766

- Ramette, A., & Tiedje, J. M. (February 2007). Multiscale responses of microbial life to spatial distance and environmental heterogeneity in a patchy ecosystem. *Proceedings of the National Academy of Sciences*, *104*, 2761–2766. doi:10.1073/pnas.0610671104
- Reese, D. C., Malley, R. T., Brodeur, R. D., & Churnside, J. H. (July 2011). Epipelagic fish distributions in relation to thermal fronts in a coastal upwelling system using high-resolution remote-sensing techniques. *ICES Journal of Marine Science*, *68*, 1865–1874. doi:10.1093/icesjms/fsr107
- Retamal, L., Bonilla, S., & Vincent, W. F. (October 2007). Optical gradients and phytoplankton production in the Mackenzie River and the coastal Beaufort Sea. *Polar Biology*, *31*, 363–379. doi:10.1007/s00300-007-0365-0
- Robinson, M. L., Gomez-Raya, L., Rauw, W. M., & Peacock, M. M. (August 2008). Fulton's body condition factor K correlates with survival time in a thermal challenge experiment in juvenile Lahontan cutthroat trout (*Oncorhynchus clarki henshawi*). *Journal of Thermal Biology*, *33*, 363–368. doi:10.1016/j.jtherbio.2008.05.004
- Rudstam, L. G., Magnuson, J. J., & Tonn, W. M. (August 1984). Size Selectivity of Passive Fishing Gear: A Correction for Encounter Probability Applied to Gill Nets. *Canadian Journal of Fisheries and Aquatic Sciences*, *41*, 1252–1255. doi:10.1139/f84-151
- Sarkar, U. K., Naskar, M., Roy, K., Sudeeshan, D., Srivastava, P., Gupta, S., . . . Nandy, S. K. (September 2017). Benchmarking pre-spawning fitness, climate preferendum of some catfishes from river Ganga and its proposed utility in climate research. *Environ Monit Assess*, *189*. doi:10.1007/s10661-017-6201-2
- Scholes, P. (February 1982). The effect of wind direction on trawl catches: an analysis of haul-by-haul data. *ICES Journal of Marine Science*, *40*, 81–93. doi:10.1093/icesjms/40.1.81
- Searcy, C., Dean, K., & Stringer, W. (April 1996). A river-coastal sea ice interaction model: Mackenzie River Delta. *Journal of Geophysical Research*, *101*, 8885–8894. doi:10.1029/96jc00120
- Sharples, J., Middelburg, J. J., Fennel, K., & Jickells, T. D. (January 2017). What proportion of riverine nutrients reaches the open ocean? *Global Biogeochemical Cycles*, *31*, 39–58. doi:10.1002/2016gb005483

- Sheaves, M. (September 2009). Consequences of ecological connectivity: the coastal ecosystem mosaic. *Marine Ecology Progress Series*, 391, 107–115. doi:10.3354/meps08121
- Sinitsyn, A. O., Guegan, E., Shabanova, N., Kokin, O., & Ogorodov, S. (April 2020). Fifty four years of coastal erosion and hydrometeorological parameters in the Varandey region, Barents Sea. *Coastal Engineering*, 157, 103610. doi:10.1016/j.coastaleng.2019.103610
- Sobral, P., & Widdows, J. (March 2000). Effects of increasing current velocity, turbidity and particle-size selection on the feeding activity and scope for growth of *Ruditapes decussatus* from Ria Formosa, southern Portugal. *Journal of Experimental Marine Biology and Ecology*, 245, 111–125. doi:10.1016/s0022-0981(99)00154-9
- Solomon, S. M. (December 2004). Spatial and temporal variability of shoreline change in the Beaufort-Mackenzie region, northwest territories, Canada. *Geo-Marine Letters*, 25, 127–137. doi:10.1007/s00367-004-0194-x
- Steiner, N. S., Cheung, W. W., Cisneros-Montemayor, A. M., Drost, H., Hayashida, H., Hoover, C., . . . VanderZwaag, D. L. (April 2019). Impacts of the Changing Ocean-Sea Ice System on the Key Forage Fish Arctic Cod (*Boreogadus Saida*) and Subsistence Fisheries in the Western Canadian Arctic—Evaluating Linked Climate, Ecosystem and Economic (CEE) Models. *frontiers in Marine Science*, 6. doi:10.3389/fmars.2019.00179
- Suryan, R. M., Irons, D. B., Brown, E. D., Jodice, P. G., & Roby, D. D. (February 2006). Site-specific effects on productivity of an upper trophic-level marine predator: Bottom-up, top-down, and mismatch effects on reproduction in a colonial seabird. *Progress in Oceanography*, 68, 303–328. doi:10.1016/j.pocean.2006.02.006
- Suryan, R. M., Santora, J. A., & Sydeman, W. J. (April 2012). New approach for using remotely sensed chlorophyll a to identify seabird hotspots. *Marine Ecology Progress Series*, 451, 213–225. doi:10.3354/meps09597
- Takami, T., Kitano, F., & Nakano, S. (1997). High Water Temperature Influences on Foraging Responses and Thermal Deaths of Dolly Varden *Salvelinus malma* and White-spotted Charr *Salvelinus leucomaenis* in a Laboratory. *Fisheries Science*, 63, 6–8. doi:10.2331/fishsci.63.6

- Timco, G., & Johnston, M. (2003). *Ice Regime Shipping System Pictorial Guide*. Transport Canada Report TP14044E (January 2003). National Research Council Canada. doi:10.4224/12327589
- Todd, Z. (February 2015). Fish pluralities: Human-animal relations and sites of engagement in Paulatuuq, Arctic Canada. *Cultures inuit, gouvernance et cosmopolitiques*, 38, 217–238. doi:10.7202/1028861ar
- Tremblay, J.-É., Simpson, K., Martin, J., Miller, L., Gratton, Y., Barber, D., & Price, N. M. (July 2008). Vertical stability and the annual dynamics of nutrients and chlorophyll fluorescence in the coastal, southeast Beaufort Sea. *Journal of Geophysical Research*, 113. doi:10.1029/2007jc004547
- Turner, C. K., & Lantz, T. C. (August 2018). Springtime in the Delta: the Socio-Cultural Importance of Muskrats to Gwich'in and Inuvialuit Trappers through Periods of Ecological and Socioeconomic Change. *Human Ecology*, 46, 601–611. doi:10.1007/s10745-018-0014-y
- Utne-Palm, A. C. (January 2002). Visual feeding of fish in a turbid environment: Physical and behavioural aspects. *Marine and Freshwater Behaviour and Physiology*, 35, 111–128. doi:10.1080/10236240290025644
- van de Waal, D. B., Verschoor, A. M., Verspagen, J. M., van Donk, E., & Huisman, J. (April 2010). Climate-driven changes in the ecological stoichiometry of aquatic ecosystems. *Frontiers in Ecology and the Environment*, 8, 145–152. doi:10.1890/080178
- Vanhellemont, Q. (May 2019). Adaptation of the dark spectrum fitting atmospheric correction for aquatic applications of the Landsat and Sentinel-2 archives. *Remote Sensing of Environment*, 225, 175–192. doi:10.1016/j.rse.2019.03.010
- Vanhellemont, Q., & Ruddick, K. (April 2014). Turbid wakes associated with offshore wind turbines observed with Landsat 8. *Remote Sensing of Environment*, 145, 105–115. doi:10.1016/j.rse.2014.01.009
- Vanhellemont, Q., & Ruddick, K. (October 2018). Atmospheric correction of metre-scale optical satellite data for inland and coastal water applications. *Remote Sensing of Environment*, 216, 586–597. doi:10.1016/j.rse.2018.07.015

- Walkusz, W., Paulić, J. E., Kwaśniewski, S., Williams, W. J., Wong, S., & Papst, M. H. (August 2009). Distribution, diversity and biomass of summer zooplankton from the coastal Canadian Beaufort Sea. *Polar Biology*, *33*, 321–335. doi:10.1007/s00300-009-0708-0
- Williams, W. J., & Carmack, E. C. (September 2008). Combined effect of wind-forcing and isobath divergence on upwelling at Cape Bathurst, Beaufort Sea. *Journal of Marine Research*, *66*, 645–663. doi:10.1357/002224008787536808
- Wukelic, G. E., Gibbons, D. E., Martucci, L. M., & Foote, H. P. (April 1989). Radiometric calibration of Landsat Thematic Mapper thermal band. *Remote Sensing of Environment*, *28*, 339–347. doi:10.1016/0034-4257(89)90125-9
- Zainuddin, M., Saitoh, K., & Saitoh, S.-I. (March 2008). Albacore (*Thunnus alalunga*) fishing ground in relation to oceanographic conditions in the western North Pacific Ocean using remotely sensed satellite data. *Fisheries Oceanography*, *17*, 61–73. doi:10.1111/j.1365-2419.2008.00461.x
- Zar, J. (1999). *Biostatistical analysis*. Upper Saddle River, N.J: Prentice Hall.

Appendix I, Date acquisition and sensors of images obtained

Date	Area	Sensor
27.06.2013	Herschel Island	L8 OLI /TIRS
01.07.2013	Shingle Point	L8 OLI /TIRS
06.07.2013	Herschel Island	L8 OLI /TIRS
13.07.2013	Herschel Island	L8 OLI /TIRS
15.07.2013	Shingle Point	L8 OLI /TIRS
15.07.2013	Herschel Island	L8 OLI /TIRS
07.08.2013	Shingle Point	L8 OLI /TIRS
07.08.2013	Herschel Island	L8 OLI /TIRS
09.08.2013	Shingle Point	L8 OLI /TIRS
16.06.2014	Herschel Island	L8 OLI /TIRS
23.06.2014	Herschel Island	L8 OLI /TIRS
30.06.2014	Herschel Island	L8 OLI /TIRS
02.07.2014	Shingle Point	L8 OLI /TIRS
02.07.2014	Herschel Island	L8 OLI /TIRS
11.07.2014	Shingle Point	L8 OLI /TIRS
28.08.2014	Shingle Point	L8 OLI /TIRS
10.06.2015	Shingle Point	L8 OLI /TIRS
10.06.2015	Herschel Island	L8 OLI /TIRS
05.07.2015	Shingle Point	L8 OLI /TIRS
05.07.2015	Herschel Island	L8 OLI /TIRS
12.07.2015	Herschel Island	L8 OLI /TIRS
14.07.2015	Shingle Point	L8 OLI /TIRS
21.07.2015	Shingle Point	L8 OLI /TIRS
21.07.2015	Herschel Island	L8 OLI /TIRS
13.08.2015	Herschel Island	L8 OLI /TIRS
22.08.2015	Shingle Point	L8 OLI /TIRS
25.08.2015	Shingle Point	L8 OLI /TIRS
29.08.2015	Herschel Island	L8 OLI /TIRS
28.06.2016	Shingle Point	L8 OLI /TIRS
28.06.2016	Herschel Island	L8 OLI /TIRS
13.07.2016	Shingle Point	L8 OLI /TIRS
13.07.2016	Herschel Island	S2 MSI
14.07.2016	Shingle Point	L8 OLI /TIRS
14.07.2016	Herschel Island	L8 OLI /TIRS
05.08.2016	Herschel Island	S2 MSI
06.08.2016	Herschel Island	L8 OLI /TIRS
08.08.2016	Shingle Point	L8 OLI /TIRS
08.08.2016	Herschel Island	L8 OLI /TIRS
18.08.2016	Shingle Point	L8 OLI /TIRS
14.06.2017	Herschel Island	S2 MSI
22.06.2017	Herschel Island	L8 OLI /TIRS
24.06.2017	Shingle Point	L8 OLI /TIRS

24.06.2017	Herschel Island	L8 OLI /TIRS
01.07.2017	Shingle Point	S2 MSI
01.07.2017	Herschel Island	L8 OLI /TIRS
04.07.2017	Shingle Point	S2 MSI
08.07.2017	Herschel Island	L8 OLI /TIRS
17.07.2017	Shingle Point	S2 MSI
17.07.2017	Herschel Island	L8 OLI /TIRS
18.07.2017	Shingle Point	S2 MSI
19.07.2017	Shingle Point	L8 OLI /TIRS
27.07.2017	Herschel Island	L8 OLI /TIRS
28.07.2017	Shingle Point	L8 OLI /TIRS
28.07.2017	Herschel Island	S2 MSI
02.08.2017	Herschel Island	L8 OLI /TIRS
07.08.2017	Herschel Island	L8 OLI /TIRS
04.06.2018	Herschel Island	S2 MSI
12.06.2018	Herschel Island	S2 MSI
18.06.2018	Herschel Island	L8 OLI /TIRS
21.06.2018	Shingle Point	L8 OLI /TIRS
02.07.2018	Herschel Island	S2 MSI
12.07.2018	Herschel Island	S2 MSI
14.07.2018	Shingle Point	L8 OLI /TIRS
14.07.2018	Herschel Island	S2 MSI
15.07.2018	Shingle Point	L8 OLI /TIRS
18.07.2018	Shingle Point	S2 MSI
18.07.2018	Herschel Island	S2 MSI
20.07.2018	Shingle Point	S2 MSI
22.07.2018	Shingle Point	L8 OLI /TIRS
22.07.2018	Herschel Island	S2 MSI
23.07.2018	Shingle Point	S2 MSI
23.07.2018	Herschel Island	S2 MSI
24.07.2018	Shingle Point	S2 MSI
26.07.2018	Shingle Point	S2 MSI
04.08.2018	Shingle Point	S2 MSI
12.08.2018	Shingle Point	S2 MSI
18.08.2018	Shingle Point	S2 MSI
23.08.2018	Shingle Point	S2 MSI
24.08.2018	Shingle Point	S2 MSI
29.08.2018	Shingle Point	S2 MSI
05.06.2019	Herschel Island	L8 OLI /TIRS
06.06.2019	Herschel Island	S2 MSI
19.06.2019	Herschel Island	S2 MSI
21.06.2019	Herschel Island	L8 OLI /TIRS
23.06.2019	Shingle Point	L8 OLI /TIRS
09.07.2019	Shingle Point	L8 OLI /TIRS
13.07.2019	Shingle Point	S2 MSI
13.07.2019	Herschel Island	S2 MSI
25.07.2019	Shingle Point	S2 MSI

29.07.2019	Herschel Island	S2 MSI
30.07.2019	Shingle Point	S2 MSI
30.07.2019	Herschel Island	L8 OLI /TIRS
05.08.2019	Shingle Point	S2 MSI
08.08.2019	Herschel Island	S2 MSI
20.08.2019	Shingle Point	S2 MSI
29.08.2019	Shingle Point	S2 MSI

Eidesstattliche Erklärung

Hiermit versichere ich, dass ich die vorliegende Arbeit ohne Hilfe Dritter und ohne Zuhilfenahme anderer als der angegebenen Quellen und Hilfsmittel angefertigt habe. Die den benutzten Quellen wörtlich oder inhaltlich entnommenen Stellen sind als solche kenntlich gemacht.

Potsdam, den 01.11.2021

.....

Unterschrift